Stern slamming on an offshore heavy lift vessel

A study on the loads and vibrational responses of stern slamming on a ship

Marine Technology: Ship hydromechanics

D. Noordam

Delft University of Technology

Thesis for the degree of MSc in Marine Technology in the specialisation of *Ship Hydromechanics*

Stern slamming on an offshore heavy lift vessel

A study on the loads and vibrational responses of stern slamming on a ship

by

D. Noordam

Performed at

BigLift

This thesis **MT.24/25/056.M** is classified as confidential in accordance with the general conditions for projects performed by the TU Delft.

to be defended publicly on Friday 29th of August, 2025 at 2:00 PM.

Company supervisor

Ir. A. Vreeburg	BigLift, daily supervisor

Thesis exam committee

Dr.Ir. P.R. Wellens	TU Delft, chair and supervisor
Dr.Ir. L. Pahlavan	TU Delft
Ir. M. Bockstael	TU Delft

Author details

Student number	5148766

Cover:	Brouwersgracht on DP-mode in Singapore (Modified)
Style:	TU Delft Report Style

Note: This thesis benefited from the use of free tools like Grammarly for grammar and style enhancement, and ChatGPT for idea refinement and troubleshooting during the writing process.

Preface

This thesis marks the end of my academic journey at the TU Delft. It started out as an unsure choice where I did not know if this study was the right fit for me. It turned out to be a very good choice. I grew up fascinated by big machinery from lorries to airplanes, but ships were always the things that fascinated me the most. It was a different motivation than most students who seemed to have a sailing background. The further I got in my studies the more interesting it became. Of course, with some courses more interesting than others. My bachelor thesis sparked the interest to pursue a specialisation in hydrodynamics for my masters, which in the end resulted in this thesis. I enjoyed the process from the first till the last steps, and this report hopefully solves a piece in the big puzzle, called slamming.

First I would like to thank Peter Wellens for being able to supervise me during my thesis. His knowledge about CFD methods and hydrodynamic loads really motivated me. He kept me on track when I veered off and showed me to investigate something thoroughly and do not take anything for granted.
I also would like to thank Anne Vreeburg and Joost van der Heiden for also supervising me within BigLift. They supported me and showed me the more practical side of a problem like stern slamming. Also, the freedom to formulate the research objective is much appreciated.
Also, I would like to thank Paul Bruggeman from Marin, for helping me extract more data from the strip theory software used in this thesis.
Without either support and constructive feedback, it would have been difficult to finish and improve this thesis within the timeframe.

Lastly, I would like to thank my friends, family and fellow students. The master thesis can sometimes be a bit lonely and it is good to do something else to clear your mind with friends and family and to get their support during the process.

Have fun reading! ;)

D. Noordam
Delft, August 2025

Summary

This study investigates the possibilities of stern slamming and the effects on a heavy lift vessel that is on dynamic positioning during offshore operations. When such a vessel encounters following waves the stern becomes susceptible to high-pressure impacts. These impacts could lead to whipping effects throughout the hull. These possible vibrations can lead to discomfort for the crew and for important mechanical failures of critical DP systems. This poses a risk during the offshore operations and could lead to an abortion of the operation until the slamming stops. This study focuses on identifying how slamming occurs in conditions in which a vessel can perform offshore operations and what parameters have an effect on the pressures generated by the impacts. Also, a relation between the slamming and responses is drawn to find out how certain components could fail due to the whipping effects.

The research consists of two different steps. The first is a two-dimensional incompressible Volume-Of-Fluid model in ComFLOW is used to simulate the hydrodynamic wave impacts on the stern of a heavy lift vessel. Simulations cover two irregular sea states representative of Beaufort scales 4 and 5 and a range of different drafts for the vessel from a minimum draft of 6 meters to the design draft of 8 meters. For this 2D simulation are made to ensure relative quick computation and fundamental results. Because of the 2D simulations and the vessel being stationary, only heave and pitch motions of the vessel are modelled. Also, simulations with a series of different peak wave periods are set up with and without the vessel motions to see the effect of the incoming waves and vessel motions on the impacts on the stern. Mesh refinement and grid convergence analyses are conducted to test the accuracy of the CFD model.

The second approach uses the output of the CFD model to calculate the vibrational responses due to the wave impacts on the stern. The hull of the vessel is idealised as an Euler–Bernoulli beam and decomposed into its first four bending modes. Pressure time histories extracted from the CFD simulations serve as asymmetric loading inputs to two independent vibration response solvers, a Duhamel integral formulation and the Cummins impulse response equation. Both solvers compute time-dependent modal amplitudes and reconstruct spatial velocity fields along the beam to evaluate Root Mean Square velocities at critical locations.

The results from the CFD simulation show that in both irregular sea states significant slamming impacts occur in all loading conditions of the vessel considering the selected sea states. However, the closer the vessel gets to the design draft the lower the average recorded impact pressures are. For a sea state with a H_s of 1.1 meters and a T_p of 4.6 seconds, the average impact pressure reduced from 390 kPa at a draft of 6 meters to 80 kPa for a draft of 8 meters. For a sea state with a H_s of 1.65 meters and a T_p of 5.1 seconds, the average impact pressure reduced from around 4200 kPa at a draft of 6 meters to around 250 kPa for a draft of 8 meters. However, in both sea states impacts with pressures well above the 1000 kPa were recorded on the stern. Also, lower and higher periods seem to increase the average impact pressures, likely due to steeper waves. The vessel motions in all cases reduced the average impact pressures between the 25.7% and 46.1%.

Structural response analyses show close agreement between the Duhamel and Cummins methods, with discrepancies under 2.5% arising from different treatments of memory effects. Predicted RMS velocities at the stern exceed typical comfort thresholds between 4 and 6 mm/s for impact loads around 200 to 300 kPa and can approach equipment safety limits of 18 mm/s even in moderate sea states for the higher observed load of 750 kPa or higher. This indicates that slamming induced vibrations may pose fatigue and operational risks.

Contents

List of Figures

List of Tables

Nomenclature

In here, you can find the meaning of every abbreviation used in the literature research.

Abbreviations

Abbreviation	Definition
HLV	Heavy Lift Vessel
T&I	Transport and Installation
DP	Dynamic positioning
GWM	Generalized Wagner Model
MLM	Modified Logvinovich Model
CFD	Computational Fluid Dynamics
BEM	Boundary Element method
ELP	Elementary Loading Processes
VOF	Volume Of Fluid
SPH	Smooth Particle Hydrodynamics
RAO	Response Amplitude Operator
GCI	Grid Convergence Index
RMS	Root Mean Square
FFT	Fast Fourier Transformation

1

Introduction

As global population growth accelerates and the impacts of climate change become increasingly severe, the demand for innovative and sustainable solutions has never been so high. One critical area of focus is the expansion of offshore installation projects, which offer promising opportunities to create more clean energy from offshore wind farms. On the other hand, higher oil consumption leads to more oil production from oil fields beneath the seafloor. This expansion will result in more and larger offshore projects executed with installation vessels. These vessels encounter a lot of different forces due to waves and wind.

Due to the harsh environment at sea, these vessels also encounter more extreme forces. One of those more extreme events is called slamming. Slamming is created when a structure (re)enters the water and pressure can be built up. These slamming events can occur on the bow due to high waves and motions of the vessel. A more extreme slamming event is bottom slamming where the keel of a vessel re-enters the water. Catamarans can also encounter wetdeck slamming on the deck between the two hulls of the catamaran. The last is slamming on the stern section of the vessel. This part of the vessel is relatively flat compared to the bow and is for most vessels just above the free surface. While slamming is not an unknown subject in the current academic world, the subject related to slamming on the stern of a vessel is investigated much less. For installation vessels which execute projects on site, stern slamming might pose a bigger threat to result in whipping responses than other types of slamming or extreme wave impacts.

For all types of extreme wave impacts, a lot of questions remain unanswered. Earlier research provided some preliminary insight into the relation between impact speed and pressure build-up and how structures like the hull of a vessel can react to those forces. These relations are all defined for bow or bottom slamming and not specifically for stern slamming. section 1.1 gives an overview of the research related to slamming. In section 1.2, the specific problem and parameters related to the installation vessel are identified. section 1.3 shows the main research objective based on the identified knowledge gap and section 1.4 shows why this research is relevant.

1.1. Background Information

Sailing vessels and structures at sea encounter all kinds of responses and excitations due to waves and currents of the oceans. Some excitations are more severe than others. A dangerous physical phenomenon which vessels and structures can encounter is called slamming. According to Kapsenberg, slamming can be described as an event which is characterised by a sudden, high force of relatively short duration imposed on a body. This event occurs when a body enters a fluid with a small angle between the surface of the body and the free surface [15]. These characteristics can cause the structure of the hull to vibrate violently. This response is called whipping and can significantly increase the structural loading of ships and decrease comfort for crew onboard vessels [42].

For this reason, slamming has been a topic for research for a long time. The first time slamming was investigated dates back to 1929 when Von Karman came up with analytical formulas to estimate the forces on the floats of planes landing on water [17]. Later, Wagner improved on the momentum theory. In contrast to Von Karman, Wagner used a more mathematical approach by using potential flow theory [44].

After the first analytical work performed by Wagner and Von Karman many studies have been experimentally and numerically conducted to get more insight into the phenomena. Most studies have been focusing on bow slamming of vessels since the probability of occurrence is the highest for seagoing vessels. These studies focus on examining pressures and forces on simple wedge geometries and on local and global responses of the structure. Even though the occurrence probability of stern slamming is much lower than bow slamming, the flat geometry of the stern for most vessels can cause very high impact forces when subjected to slamming [25]. This is especially the case when a vessel is stationary or encounters following waves. It is therefore important that research into stern slamming is also conducted in order to gain more knowledge about the phenomenon and the responses.

Some research has already been performed on stern slamming. Wang et al. developed a numerical method to predict slamming loads on ship hulls using non-linear time-domain strip theory and an Arbitrary-Lagrangian Eulerian (ALE) algorithm. The results showed that slamming occurs most likely at the bow and stern of the ship, and the occurrences were highest at the aft part due to the small draft and high pitch motions [45]. The next study of Wang et al. focused on the stern slamming alone of a chemical tanker in head waves using an ALE-software method. The study concluded that the pressure distributions revealed that momentum slamming, driven by rapid changes in added mass, plays a significant role in the total slamming load [46]. Mutsuda et al. investigated numerically and experimentally the occurrence of stern slamming in following seas. They concluded that slamming pressures increase at small deadrise angles especially angles lower than ten degrees. Also, the pressure was affected strongly by the waves in which maximum values were observed for wave length to ship length ratios (λ/L) close to one. The probability increased with higher significant wave heights [28].

1.2. Vessel & Problem Description

BigLift is one of the key players in the market of the heavy lift transport industry. Their fleet is capable of lifting cargo weighing more than 2000 tonnes. Since 2023 BigLift is also been a player in the offshore installation market. With the B-type vessels Brouwersgracht and Bloemgracht, BigLift performs installation projects in the offshore renewable market and offshore oil and gas markets. The B-type vessels are equipped with a DP2 system capable of keeping the vessel in place at a certain location at sea. A key benefit of utilising a heavy lift vessel (HLV) for the offshore market is that the vessel is able to transport the equipment and cargo for the installation to the spot and install it herself (T&I) rather than dedicated installation vessels which will need transportation vessels in order to supply the vessel with the equipment to be installed. This makes these types of vessels cheaper for offshore clients with less downtime.

Table 1.1: Main particulars B-type vessel

Parameter	**Value**	**Unit**
Length overall (L)	141.30	m
Breadth (B)	24.91	m
Depth (H)	12.20	m
draft (T)	8.2	m
Deadweight (DWT)	12,332	mt
Displacement (∇)	14,860	m^3

Figure 1.1: Brouwersgracht installing subsea equipment for LNG production.

Figure 1.2: B-types alongside a pipe-lay vessel for pipeline supply.

The problem with these types of vessels is that the design draft is based on the deadweight of the cargo the vessel can carry. The vessel, however, is used mainly for project cargo which is heavy to lift with cranes, but relatively light compared to the maximum deadweight of the vessel. Therefore, the vessel cannot reach the design draft even when the vessel is ballasted since the side tanks are reserved for lifting stability. Another problem for the vessels is the SPS60 code. This code is related to stability criteria and is required when more than 60 special personnel are on board for the project. The result is that the stern is mostly above the waterline creating an overhang. This overhang above the waterline is susceptible to slamming on the bottom of the stern. This can cause vibrations throughout the hull of the vessel, which can damage critical components on board the vessel. This not only results in discomfort for the crew, but also poses a risk of a mechanical failure on a vessel that is operating on DP. In order to minimise these risks, BigLift wants more knowledge about this slamming phenomenon.

The problem of an overhang of the stern of a vessel which encounters slamming even in relatively calm weather has not been investigated properly in the current literature. Typical overhang problems that can be found in the literature are related to civil structures. The main outline is that these structures do not move due to the waves they encounter and the whipping responses are not as noticeable. This is present on vessels.

1.2.1. Operational Profiles

In order to investigate the stern slamming effect on vessels, it is important to know the exact operational profiles of these vessels. This provides a better understanding of how the vessel is used and can be the cause of the slamming behaviour.

The B-type vessels are mainly designed for offshore installation and pipe-laying supply, so the two profiles of the vessel can be distinguished. The first profile is related to the offshore installation of the vessel. In this profile, the vessel is mainly handling relatively light cargo, such as transition pieces, compared to the deadweight. This means the stern of the vessel is always above the waterline. Additionally, class societies demand that for open-top conditions with offshore personnel on board for the installation, the draft of the vessel must be limited in order to account for the possibility of water leakage into the hull. BigLift only has one stability loadline for these operations with special personnel on board, so even with the hatch covers closed, the vessel needs to comply with the open-top notation. Therefore, the maximum draft for the B-types is set at 7.5 meters. This is lower than the design draft of 8.2 metres and always results in the stern being above the waterline. During this operation, the vessel is susceptible to slamming events on the stern.

The second profile is based on pipe-laying supply. Before the load-out procedure of the pipes to the pipe-laying vessel, the B-types are fully loaded and are at or even above the design draft. This means the stern is submerged, and the risk of slamming events on the stern is minimal to none. During the load-out, the B-types do not need to comply with the open-top notation. However, as the load-out proceeds, the vessel becomes much lighter, and the draft decreases. The design draft cannot be reached by ballasting. This results in the stern moving above the waterline, and from that moment on, the vessel can encounter slamming on the stern during the load-out.

1.3. Research Questions & Objective

The introduction showed that slamming is a big problem for ships. Especially with a changing climate, the weather gets more extreme which can lead to more and more extreme slamming. While most studies on slamming look at bow or bottom slamming, only a few look at stern slamming in general. Stern slamming on stationary vessels is an unknown subject, while for vessels stationary by anchor or DP, stern slamming creates resonance of the hull which induces a higher risk of possible mechanical failure. This emphasises the need to further study the fundamental principles behind slamming on the stern of a vessel.

Based on the identified knowledge gap, the following research question can be defined:

What is the behaviour of stern slamming and what parameters have an influence on the occurrence and how does this load translate to vibrational responses on a heavy lift vessel during offshore operations?

To answer this research question, the following sub-questions are defined:

- What is the general behaviour of water hitting the stern from underneath?
- What is the influence of vessel motions and waves on slamming?
- How do different loading conditions of the vessel affect the slamming on the stern?
- What responses are created by slamming on the stern and how does it transmit through the hull?
- To what extent can stern slamming be mitigated or the responses of slamming be reduced during operations?

The main objective for this study follows from the research question defined earlier and sounds like the following:

”To create a general CFD and numerical setup that accurately captures the dynamics of the structure and slamming loads on the stern of a stationary installation vessel.”

The study is focused on the B-type vessels commercially run by BigLift. The general hull and parameters of these vessels are used as the input to conduct this study. While results will be applicable to the B-type vessels it can be extrapolated to similar installation vessels from other companies since their overall design of the hull and especially the stern is very similar. For other types of vessels which are susceptible to stern slamming, like cruise ships, this study is not suitable.

While slamming in sailing conditions still can occur, the likelihood of a slamming event on the stern in these conditions is much lower. Therefore, sailing conditions in following seas are not considered in this study. Only conditions in which the vessel is stationary via DP, anchor or other methods.

Slamming is also a critical condition for the structural integrity of a vessel. Impact loads like slamming can deform plates and can affect the fatigue life cycle of a vessel. However, the main objective of this study is to look at the hydrodynamic principles behind slamming on the stern. Therefore, fatigue assessments are outside the scope of this study.

Slamming is mainly caused by waves hitting the vessel and motions causing the vessel to hit the free surface at re-entry. With waves, it is possible that breaking waves could hit the vertical aft section of a vessel which causes slamming. However, engineers and crew of BigLift mentioned that ’white capping’ as it’s called, is not the reason behind the slamming events. It was noticed in relatively calm weather and breaking waves do not occur often in such conditions. Breaking waves are therefore also not considered in this study.

1.4. Relevance & Significance

With the ever-growing offshore wind market, the demand for offshore installation is increasing. However, reports show that the supply of offshore installation vessels cannot keep up with the demand from clients. This is also expected in the future. This can cause project delays and artificially high prices to keep the demand under control. It is, therefore, important that the existing fleet can operate as efficiently as possible with minimal downtimes [7]. Stern slamming is seen as a high risk if heavy lift vessels operate on DP since the equipment required for dynamic positioning is very sensitive. This requires vessels to abort the project until the weather changes. A better understanding of the phenomenon will enable engineers to better predict the possible risks and apply mitigation techniques to minimise downtime. This will result in the existing fleet better serving the demand of the market.

Slamming is also perceived as dangerous for the structure of the vessel. Official reports concluded that the Estonia sank due to losing the bow visor as a result of severe slamming. In 2013, the MOL Comfort broke in two. While the official reports concluded that there was a weakness in the bottom panel of the hull, there was also a lot of uncertainty regarding the sea state parameters. The conditions were not perceived as dangerous by the crew at the time of the accident, but still, the design load was possibly exceeded. Although slamming was not directly linked to the accident, it was recommended that whipping effects due to slamming should be included in future load cases [16]. These accidents show that slamming is also a danger to the whole ship itself. Understanding when slamming can occur could prevent such scenarios from happening in the future.

1.5. Thesis Outline

This report is made up of eight chapters. In chapter 2, the already known and available techniques that can be used to analyse slamming and the responses are presented and explained. In chapter 3, the methodology of the hydrodynamic part is shown. This chapter dives into how the CFD model is made and how all inputs are calculated. Chapter 4 shows how the structural model is made to calculate the responses due to the hydrodynamic load from the CFD model. Chapter 5 shows and explains all of the results from the CFD model. It also shows how the model is verified. Chapter 6 show the results and validation of the structural model. In chapter 7 the approach and results are critically reviewed and discussed. Chapter 8 explains how the research questions can be answered from the results of both models and a conclusion can be drawn. Lastly, chapter 9 explains what can be done in future work to optimise and further research stern slamming on heavy lift or installation vessels.

Also, in the appendix some additional information is given about the validation of the structural model. Also, more results of the CFD and the structural model are given.

2

Literature research

2.1. Radiation Diffraction Theory

Radiation diffraction theory is a fundamental concept in marine engineering, particularly in the analysis of wave interactions with marine structures [14, 29]. The following equation shows the potentials consisting of the incoming wave potential (Φ_w), the diffraction potential (Φ_d) and the radiation potential (Φ_r). Normally, these potentials exist for all six degrees of freedom, but for this specific problem vessels can move in three degrees of freedom.

$$\Phi(x,y,z,t) = \Phi_w + \Phi_d + \Phi_r \tag{2.1}$$

An example of the incoming wave potential of deep seas can be found in equation (2.2) and for shallow water in 2.3.

$$\Phi_w(x,y,z,t) = \frac{\zeta_a g}{\omega} e^{kz} \sin\left(kx\cos\mu + ky\sin\mu - \omega t\right) \tag{2.2}$$

$$\Phi_w(x,y,z,t) = \zeta_a \frac{g}{\omega} \cdot \frac{\cosh k(h+z)}{\cosh kh} \cdot \sin\left(kx\cos\mu + ky\sin\mu - \omega t\right) \tag{2.3}$$

The pressures, and consequently the resulting forces and moments, can be determined using the linearised Bernoulli equation. After a series of mathematical derivations the following equation is obtained, which describes the motion of floating vessels. The incoming and diffracted wave potentials give rise to the exciting forces, namely the Froude-Krilov force (F_{FK}) and the diffraction force (F_D). Additionally, the radiation forces which result from the vessel's motion are characterised by the added mass matrix (A) and the damping matrix (B). The matrices and vectors normally have a dimension of six, but due to the fact of the vessel acting on DP three directions of motion will be zero. Therefore, in this problem the matrices will have a dimension of three.

$$(\mathbf{M}+\mathbf{A})\ddot{\mathbf{x}} + \mathbf{B}\dot{\mathbf{x}} + \mathbf{C}\mathbf{x} = \mathbf{F}_{FK} + \mathbf{F}_D \tag{2.4}$$

Note that the forces in this equation are harmonic and therefore it is safe to assume that the responses are harmonic as well. This allows for the RAO's of the vessel to be defined from which the eventual accelerations of the vessel can be calculated. This is important to describe the motions of the vessel in all models. Slamming forces are not harmonic and highly non-linear. However, it can be assumed that slamming forces do not contribute much to the motions of the vessel due to the high inertia of the vessel.

2.2. Wave Theory

In order to understand the behaviour of slamming on the stern, a close look needs to be taken at the theory of waves and wave spectra. Waves cause the vessel to encounter periodic loads on the hull. This causes the vessel to move in all six degrees of freedom dependent on the waves encountered by the vessel. Waves are also the main reason why the vessel encounters more severe loads like slamming.

2.2.1. Regular Waves

The easiest way to theoretically describe waves is to assume that waves encountered in the environment are regular. When assuming regular waves, the wave can be described as a simple cosine wave with an amplitude ζ_a. A formulation can be seen below. Note that this is for a wave moving into the positive x-direction

$$\zeta(t) = \zeta_a \cos kx - \omega t + \epsilon \tag{2.5}$$

In this formulation k is the wave number and ω is the circular wave frequency. These values can be calculated with wave parameters wave length λ and the wave period T seen in the formulas below.

$$k = \frac{2\pi}{\lambda} \quad \text{and} \quad \omega = \frac{2\pi}{T} \tag{2.6}$$

For a wave moving in the opposite direction (moving in the negative x-direction) can be given by changing the minus for a plus in equation (3.2).

When a regular wave encounters a vertical wall like the stern of a hull, the wave gets reflected to the opposite direction. This means two waves which can be described by equation (3.2) can be added together. Because in the theory the amplitude and speed of the reflected wave are assumed to be equal to the incoming wave, the two waves form a standing wave. These waves seem to have no propagation speed, but only change in amplitude over time at every location [14].

2.2.2. Irregular Waves

Regular wave theory provides a simplistic model, which is easy to calculate with, on the real world scenario. However, the surface of an ocean looks far more complicated than some cosine waves. Wave parameters like the wave length and period change continuously over time. That is because at sea different types of waves interact. A more comprehensive theory can be applied by using irregular waves.

Irregular waves can be described by applying linear superposition of different wave components moving in the same direction. This can already be done with two different wave components. This is shown in the figure below.

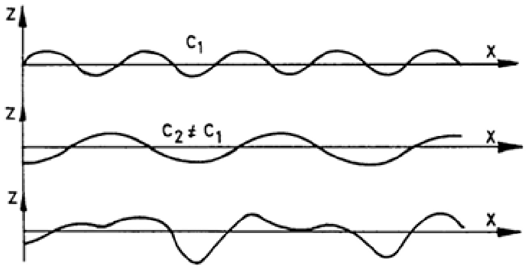

Figure 2.1: Linear superposition of different wave components resulting in an irregular wave. [14]

Although two wave components are enough to get an irregular wave, applying more components will yield a more realistic model to the real scenario at sea. To find the amplitude over time for irregular waves the sum of each component can be taken, which is shown below in 3.3.

$$\zeta(t) = \sum_{n=1}^{N} \zeta_{a_n} \cos(k_n x - \omega_n t + \varepsilon_n) \tag{2.7}$$

Because multiple wave components are added using linear superposition, it will be difficult to calculate with analytical or numerical procedures since they require fixed wave parameters. By applying statistics these wave parameters can still be found. By using a probability density function on wave data the probability for certain threshold can be determined using the following formula.

$$P\{H > a\} = \int_a^\infty f(x)dx \tag{2.8}$$

Other methods including finding the mean values and significant values of wave parameters such as the wave height. Note that slamming is an extreme scenario [14]. Therefore, peak values is the range within slamming can occur and is the limiting factor. Averaging out values could depict a better picture than the reality since the peak values will be filtered.

2.2.3. Wave Spectra

Irregular waves consist of a superposition of multiple components with different periods as can be seen in figure 2.1. This means that waves at sea consist of all kinds of different frequencies. To describe this wave energy spectra are used. Wave energy spectra describe the distribution of wave energy over a range of frequencies. Some frequencies are more dominant on the ocean which contain more energy and that results in a peak at those frequencies. The spectra are derived from statistical analysis of wave records.

To better understand the distribution of wave energy, the concept of moments of the spectrum is introduced. The n-th moment, m_n, is mathematically defined as:

$$m_n = \int_0^\infty f^n S(f)\, df. \tag{2.9}$$

These moments encapsulate important wave properties. For instance, the moment at zero, m_0, represents the total wave energy, while the first moment, m_1, is related to the mean energy frequency. Higher-order moments provide additional insights into the spectral shape and its impact on wave characteristics.

A particularly significant parameter derived from the spectrum is the significant wave height , H_s. This is a widely used measure of wave intensity, representing the average height of the highest one-third of waves in a given sea state. It is computed using the zeroth moment as:

$$H_s = 4\sqrt{m_0}. \tag{2.10}$$

The significant wave height is critical for the design of offshore structures, as it provides a reliable measure of the most impactful waves they are likely to encounter.

Another key parameter is the mean wave period, T_m, which gives an estimate of the average time interval between successive wave crests. It is determined from the ratio of the zeroth moment to the first moment:

$$T_m = \frac{m_0}{m_1}. \tag{2.11}$$

The mean wave period helps describe the temporal characteristics of the sea state and is essential for predicting wave-induced motions and loads on structures.

Several theoretical models of wave energy spectra have been developed to describe real sea conditions. One of the oldest wave spectra was found by Bretschneider. This spectrum is suited for open sea areas. The formula for this spectrum is shown below.

$$S_\zeta(\omega) = \frac{173 H_{1/3}^2}{T_1^4}\omega^{-5} \cdot exp\left(\frac{-692}{T_1^4}\omega^{-4}\right) \tag{2.12}$$

Among the most prominent is the Pierson-Moskowitz spectrum, which characterises a fully developed sea. Its mathematical form is given by:

$$S(f) = \frac{\alpha g^2}{(2\pi)^4 f^5} \exp\left(-\beta\left(\frac{f_p}{f}\right)^4\right), \tag{2.13}$$

where α and β are empirical constants, g is the gravitational acceleration, and f_p is the peak frequency of the spectrum. This model assumes that the sea has had sufficient time and distance to reach equilibrium, where wave energy input from the wind balances dissipation [14, 27].

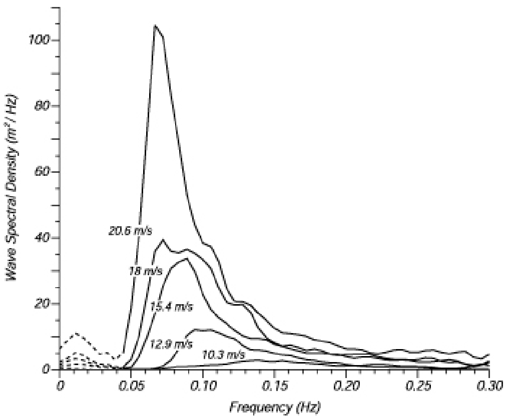

Figure 2.2: Wave spectral density of a Pierson-Moskowitz spectra. [27]

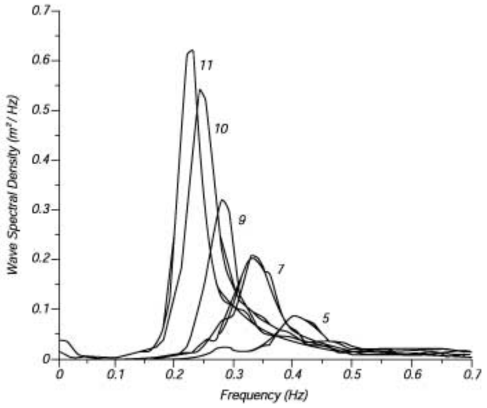

Figure 2.3: Wave spectral density of a JONSWAP spectra. [11]

For seas that are not fully developed, the JONSWAP spectrum is often used. It builds on the Pierson-Moskowitz model by introducing a peak parameter, γ, to account for fetch-limited conditions [11]. The JONSWAP spectrum is expressed as:

$$S(f) = S_{PM}(f) \cdot \gamma^{\exp\left(-\frac{(f-f_p)^2}{2\sigma^2 f_p^2}\right)}, \tag{2.14}$$

where $S_{PM}(f)$ is the Pierson-Moskowitz spectrum, and σ is a parameter that controls the spectrum's width near the peak frequency [14].

Understanding wave spectra is of great importance for this thesis. Understanding when slamming occurs and how it occurs heavily depends on the waves that the vessels encounter. Since the B-types are stationary at sea, wave spectra will be a useful tool in the calculations for the loads on the stern structure of the vessels.

2.3. Hydrodynamic Analysis Methods

The problem depicted in chapter 1 can be solved with several methods. One way to get answers is via analytical methods. The problem is modelled with basic equations which are solvable by hand. This often gets quick answers, but with a relative big uncertainty. Hydrodynamic problems and theory are often too complex to describe with simple equations to compute analytically. It often requires computational or experimental methods to get valid results. This section will dive into the possible methods that can be used for this research.

2.3.1. Analytical Methods

As described in the introduction of the literature study, the first studies performed on slamming induced pressures and forces were conducted by Von Karman. However, his study was related to the impact of the water on the floaters of water planes. Nonetheless, the principle is the same for slamming on the hull of ships. For this case, Von Karman used a simple wedge geometry and found a relation for the maximum pressure on the wedge with a certain deadrise angle. His formula can be seen below [17].

$$p_d^{max} = \frac{\pi}{2}\frac{\rho_w V^2}{tan(\beta_d)} \tag{2.15}$$

The basic analytical method for the momentum theory was later improved by Wagner. Potential theory was developed to carry out a calculation to find a solution to a wedge impact on the water surface. The biggest improvement of Wagners formula is that it incorporates the pile up effect of water. His formula is shown below. Note that the formula found by Wagner is a factor $\frac{\pi}{2}$ times higher than the relation found by Von Karman due to the contribution of the pile up effect. [15, 44].

$$p_d^{max} = \frac{\pi}{2}^2 \frac{\rho_w V^2}{tan(\beta_d)} \tag{2.16}$$

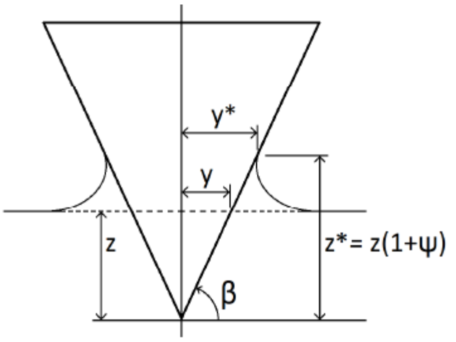

Figure 2.4: Schematic view of a wedge with pile up effect contribution from Wagner. [16]

2.3.2. Numerical Methods

There are many different numerical methods to solve hydrodynamical problems since those problems are often too complex for simple analytical methods. Since slamming is one of those complex hydrodynamic problems, it is essential that for this thesis numerical calculations are performed. In this section an outline will be given of the current state of the art numerical methods to solve slamming problems.

Boundary Element Method

The boundary element method is a numerical computational method based on potential theory for solving linear partial differential equations which have been formulated as integral equations. Boundary element methods or BEM for short are developed to study two-dimensional impacts on structures by Zhao and Faltinsen [50]. BEM solvers are able to generate good solutions while minimising computational power. This is valid while the assumptions that are made in the BEM are true [15]. At the initial contact of the body at the free surface of the fluid, there is a numerical problem shown by Ogilvie [31]. The velocity potential is discontinued causing an infinite large pressure. To overcome this, the fluid should be compressible in the BEM solver to prevent such occurrence.

Although BEM solvers are not the most common methods for research into slamming, they are used in various slamming studies. Lin and Ho [23] studied the influence of water depth on the total slamming pressure acting on a rigid wedge. They used a BEM solver to solve the following boundary value problem based on Green's second identity.

$$2\pi\phi_i = \int_L \left(G\frac{\delta\phi}{\delta n} - \phi\frac{\delta G}{\delta n} \right) dL \tag{2.17}$$

In equation (2.17) G stands for the Green's function which a BEM is able to solve. The flow field for this boundary problem is described as the following.

$$\nabla^2\phi = 0 \tag{2.18}$$

These equations are governing to analyse the slamming with the help of BEM solvers. Studies conducted by Sun [39], Sun and Faltinsen [40] and Xiao and Batra [47] used the equations of the flow field and Green's second identity in the BEM to solve the wedge tests.

Computational Fluid Dynamics

Computational fluid dynamics is a method that uses numerical analysis to solve complex problems regarding fluid flows. While BEM methods are based on potential theory, CFD is in almost all cases based on the Navier-Stokes equations, which define single-phase fluid flows. A distinction can be made for the conditions of the fluid. In CFD, fluid can be compressible and incompressible. Some fluids may experience a change in density when subjected to a pressure variation. For these applications, CFD analysis with a compressible flow is better suited to represent the reality. This extra variable increases the computing time of such problems.

In order to know which fluid properties are best suited for wave impacts such as slamming Lafeber et al. introduced Elementary Loading Processes (ELP). Lafeber et al. identified three different ELP's. The different loadings consist of direct impact, building jet along the surface of a structure and compression of entrapped gas. The jet contribution is the most common loading and describes also best the loading due to wave slamming. This loading is the only one which can numerically be described with an incompressible flow [22, 8].

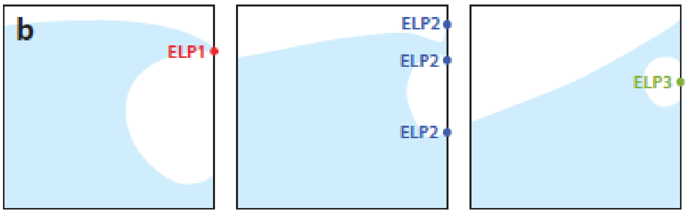

Figure 2.5: Representation of different ELP's described by Lafeber et al. [22]

Because the fluid can be described by an incompressible flow, the Navier Stokes equations for the CFD can be found. These equations for a single phase flow shown in equations (2.19) and (2.20) are governing equations based on the two principles which are that mass is conserved and the momentum is conserved [1].

$$\nabla \cdot \mathbf{u} = 0 \tag{2.19}$$

where $u = (u, v, w)$ is the three-dimensional velocity vector. ∇ is the gradient operator.

$$\frac{\partial \mathbf{u}}{\partial t} + \mathbf{u} \cdot \nabla \mathbf{u} = -\frac{1}{\rho} \nabla p + \frac{1}{\rho} \nabla \cdot \tau + \mathbf{F} \tag{2.20}$$

In this equation, the density is ρ, the pressure is denoted by p, the dynamic viscosity is denoted by μ and the F represents the external forces.

Next to a single phase flow, a two phase flow exists and can be computed. Where a single phase flow only consists of an incompressible fluid, a two phase flow also consists of a compressible gas. A two phase flow can be described with the following governing equations shown in 2.21 and 2.22 [43].

$$\frac{\partial \rho}{\partial t} + \nabla \cdot (\rho \mathbf{u}) = 0 \tag{2.21}$$

$$\frac{\partial (\rho \mathbf{u})}{\partial t} + (\mathbf{u} \cdot \nabla)(\rho \mathbf{u}) + \rho \mathbf{u} \nabla \cdot \mathbf{u} + \nabla p - \nabla \cdot \tag{2.22}$$

Both the single phase and two phase Navier-Stokes equations are very complex. Under some conditions, these equations can be simplified to Euler equations. These equations are shown below.

$$\frac{d\rho}{dt} = -\rho \nabla \cdot \mathbf{u} \tag{2.23}$$

$$\frac{d\mathbf{u}}{dt} = -\frac{1}{\rho} \nabla p + \mathbf{g} \tag{2.24}$$

The key condition has to do with the viscosity of the fluid. The Navier-Stokes equations include a term for viscosity, which is inversely proportional to the Reynolds number. When the Reynolds number is very high, indicating that inertial forces dominate over viscous forces, the viscosity term becomes negligible. This simplification leads to the Euler equations, which describe inviscid flow [10, 9]. The type of boundary conditions plays a crucial role. For instance, the no-slip boundary condition, which requires the fluid velocity to be zero at the boundary, is a significant factor in the Navier-Stokes equations. However, in cases where slip or other boundary conditions are applied, the equations can be simplified [10]. In convection-dominated flows, where the effects of viscosity are minimal, the Navier-Stokes equations can also be approximated by the Euler equations. This is particularly relevant in high-speed flows where the Mach number is high, and the flow is primarily governed by convective terms [20, 21]. Certain symmetries or specific flow conditions can also allow for the simplification of the Navier-Stokes equations to the Euler equations. For example, potential flows and inviscid rotational motions are scenarios where the Euler equations can be applied effectively [34, 35].

There are also practical implications why a simplification of the Navier-Stokes equations to the Euler equations is relevant. Stability conditions derived for the Euler equations can often be applied to the Navier-Stokes equations in the limit of high Reynolds numbers. This is useful to estimate time steps or Courant-Friedrichs-Lewy (CFL) numbers to ensure stable computations [20, 21].

There are different CFD methods and packages that can be applied for a hydrodynamic problem. Most CFD methods use a Cartesian grid to discretize the flow. This method, also called Volume Of Fluid (VOF) solves the governing equations with corresponding conditions for every cell. Cell labelling is enabled to distinguish between cells of different characters. First, the cells that are completely blocked by geometry are called boundary cells noted with a B in figure 2.6. These cells have a volume aperture of zero. Fluid aperture is a value between zero and one which describes how much fluid is in each cell at any given time step. Then the cells that are empty, but have the possibility of letting fluid flow in, are labelled empty with an E. The adjacent cells which contain fluid will form the free surface of a fluid and are surface cells noted with S. The remaining cells are labelled as fluid cells noted with an F. Cells do not have to be completely filled with fluid to be labelled as a fluid cell [1, 19, 26].

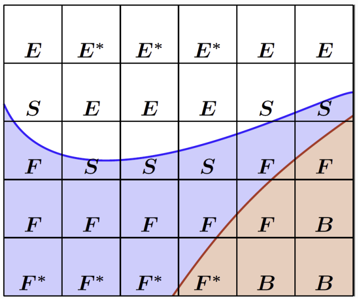

Figure 2.6: Representation of a cell labelling in ComFLOW. [1]

An other method is using a Smooth Particle Hydrodynamics (SPH) model in a CFD simulation. The conventional SPH method was developed to address hydrodynamics problems, where the governing equations are expressed in strong form as partial differential equations involving field variables such as density, velocity, and energy. The formulation of SPH involves two key steps. The first is kernel approximation, which represents a function and its derivatives in integral form using a smoothing kernel function and its derivatives. This step allows continuous quantities to be approximated effectively. The second step, known as particle approximation, discretises the computational domain into a set of particles that represent the initial conditions of the problem. Field variables for each particle are then approximated through a summation of values from neighbouring particles. Together, these steps provide a robust framework for numerically solving fluid dynamics problems. The fundamental principle of SPH is to approximate physical quantities using an integral approximation. This approximation is then discretized to obtain a set of equations that can be solved numerically.[24, 36].

$$\phi(\mathbf{r}) = \int_{\Omega} \phi(\mathbf{r}') W(\mathbf{r} - \mathbf{r}', h) d\mathbf{r}' \tag{2.25}$$

where W is the kernel function, h is the smoothing length, $\mathbf{r}$ is the focused position vector, Ω is the referenced area with a radius h to evaluate the interaction between particles and $\mathbf{r}'$ is the neighbouring position vector. This equation can be expressed in a discrete form as the following.

$$\phi(\mathbf{r}_i) = \sum_j \phi(\mathbf{r}_j) W(\mathbf{r}_i - \mathbf{r}_j, h) V_j, \tag{2.26}$$

A few conditions should be met. The first one is the normalization condition. This is shown below. This condition is also called the unity condition since the integration of the smoothing function produces the unity.

$$\sum_j W(\mathbf{r}_i - \mathbf{r}_j, h) \approx 1. \tag{2.27}$$

The second condition is the Delta function property that is observed when the smoothing length approaches zero. The third condition which should be met is the compact condition. Both conditions are shown below respectively [24].

$$\lim_{h \to 0} W(\mathbf{x} - \mathbf{x}', h) = \delta(\mathbf{x} - \mathbf{x}') \tag{2.28}$$

$$W(\mathbf{x} - \mathbf{x}', h) = 0 \quad \text{when} \quad |\mathbf{x} - \mathbf{x}'| > \kappa h \tag{2.29}$$

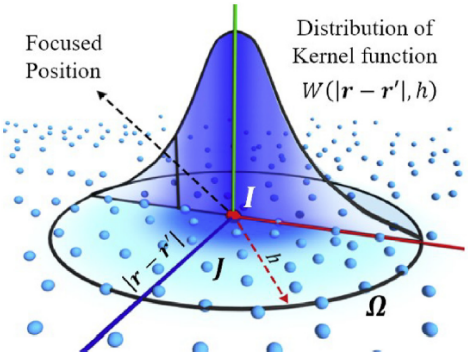

Figure 2.7: A visualisation of the fundamental theory behind a smooth particle hydrodynamic method. [28]

The SPH method is numerically very robust since it is meshless. However, CFD methods are quite computer intensive and need parallelization on a large number of processors to get reasonable performance, but SPH is even worse in this respect. The solver is quite fast since no large matrices need to be inverted, each particle only interacts with its close neighbours, but the time step is very small because compressibility is used for time stepping [15, 16]. All CFD methods require significant computing time for computers. They need parallelization and large processors in order to analyse a case in a reasonable time and even that time could get up to multiple days. The SPH method is even worse in this respect. The solver is quite fast since it does not have to invert matrices like the VOF method. Each particle only interacts with the neighbouring particles in close proximity as seen in figure 2.7. However, the time step with SPH must be very small because compressibility is used for time stepping [15]. This compromises the reasonably fast solver of the SPH method and makes that both methods are just as good or bad performance wise.

The described methods of SPH and VOF types of CFD are the most common types of CFD used to analyse slamming behaviour of vessels and other offshore structures. It is not the case that either one is much better than the other method for studies on slamming. Xie et al. used a volume of fluid CFD method based on incompressible Navier-Stokes equations to analyse the impact pressures on the bow of a hull. These loads were further used to analyse the structural integrity with FEM. For the slamming loads, the grid convergence of the CFD method was studied. The writers concluded that the ratio of the mesh to the bow flared section should be less than 0.004 to capture peak pressure [48]. Cheng et al. used a SPH method to analyse slamming on the hull of a vessel. The model used by the writers assumed weak compressibility and viscosity effects are ignored due to large Reynolds numbers of the water entry. Therefore, the Navier-Stokes equations are simplified to Euler equations. The results showed that when the structure enters the water, the keel is subjected to the maximum pressure. The CFD results in this study were validated by a BEM method [6].

2.4. Hydro-elastic Structural Responses

Slamming pressures and forces are very impulsive of nature. The impulsive forces on the hull can excite the vessel and cause vibrations. The transient vibrational response of the hull due to slamming is called whipping. Whipping is a high frequency structural response [42]. When a vessel undergoes whipping responses it can have significant impact on the structural integrity of the hull and fatigue life of the vessel.

To describe the whipping of a vessel using a beam model, several analytical methods can be employed. These methods often integrate various theories and computational techniques to accurately capture the complex interactions between the vessel's structure and the hydrodynamic forces acting upon it.

2.4.1. Euler-Bernoulli Beam Theory

The Euler-Bernoulli beam theory is a fundamental concept in structural and mechanical engineering, used to describe the behaviour of slender beams under various loading conditions. This theory is based on several key assumptions and provides a simplified model for analysing beam deflections and stresses.

The material of the beam is assumed to be isotropic and elastic, meaning it has uniform properties in all directions and returns to its original shape after the removal of loads. Cross-sections of the beam, which are initially plane and perpendicular to the neutral axis, remain plane and perpendicular to the neutral axis after deformation. The theory assumes that shear deformation is negligible, which is valid for long and slender beams but not for short or thick beams where shear effects are significant[37, 38].

The Euler-Bernoulli beam theory is governed by the following differential equation for beam deflection $w(x)$:

$$\frac{d^2}{dx^2}\left(EI\frac{d^2w}{dx^2}\right) = q(x) \tag{2.30}$$

In this formula E is the modulus of elasticity of the material. $q(x)$ is in this case the distributed load per unit length and $w(x)$ is the deflection of the beam at position x. The solution to the differential equation depends on the boundary conditions, which can vary based on the beam's support configuration. For vessels it is common that the beam representation is that of a free-free beam.

- **Simply Supported Beam**: $w(0) = 0$ and $w(L) = 0$ (deflection is zero at supports).
- **Cantilever Beam**: $w(0) = 0$ and $\frac{dw}{dx}(0) = 0$ (deflection and slope are zero at the fixed end).
- **Clamped-Clamped Beam**: $w(0) = 0$, $w(L) = 0$, $\frac{dw}{dx}(0) = 0$, and $\frac{dw}{dx}(L) = 0$ (deflection and slope are zero at both ends).
- **Free-Free Beam**: $\frac{d^2w}{dx^2}(0, L) = 0$ and $\frac{d^3w}{dx^3}(0, L) = 0$ (Bending moments and shear forces are zero a t both ends)

The Euler-Bernoulli beam theory is widely used in the analysis of structures such as bridges, buildings, and mechanical components like beams in machinery and aircraft. However, the theory is not suitable for beams where shear deformation is significant, such as short or thick beams. In such cases, the Timoshenko beam theory, which accounts for shear deformation, is more appropriate [13].

Extensions of the Euler-Bernoulli theory to include gradient elasticity can address inconsistencies related to shear strain and stress, providing more accurate models for certain materials and conditions. For visco-elastic materials, modifications to the Euler-Bernoulli theory, such as incorporating fractional constitutive laws, are necessary to capture the material's behaviour accurately [32].

2.4.2. Timoshenko Beam Theory

The Timoshenko beam theory is an extension of the classical Euler-Bernoulli beam theory, incorporating the effects of shear deformation and rotary inertia, which are particularly significant in short beams and high-frequency vibration scenarios. This theory is essential for accurately predicting the dynamic behaviour of beams under various loading conditions, including whipping, which involves rapid and large amplitude oscillations [4, 18, 49].

Unlike the Euler-Bernoulli theory, which assumes plane sections remain plane and perpendicular to the neutral axis, the Timoshenko theory accounts for shear deformation, making it more accurate for short and thick beams. The Timoshenko beam theory also includes a rotary inertia factor. This factor considers the rotational effects of the beam's cross-section, which become significant at higher frequencies [3]. Another key assumption of this beam theory is the coupling of bending and shear deformations. The Timoshenko beam theory introduces a coupling coefficient, often referred to as the Timoshenko coefficient. This coefficient links bending and shear deformations. It is derived based on the shear deformation distribution within the cross-section of the beam [30].

The governing equations for the Timoshenko beam theory can be found below:

$$\frac{\partial^2 w}{\partial t^2} + \frac{EI}{\rho A}\frac{\partial^4 w}{\partial x^4} - \frac{GA}{\rho A}\frac{\partial^2 \theta}{\partial x^2} = 0 \tag{2.31}$$

$$\frac{\partial^2 \theta}{\partial t^2} + \frac{EI}{\rho I}\frac{\partial^2 \theta}{\partial x^2} - \frac{GA}{\rho I}\left(\frac{\partial w}{\partial x} - \theta\right) = 0 \tag{2.32}$$

The top equation is the transverse displacement equation of a Timoshenko beam. In this equation (w) is the transverse displacement, (E) is the Young's modulus, (I) is the moment of inertia, (ρ) is the density, (A) is the cross-sectional area, (G) is the shear modulus, and (θ) is the rotation due to bending. The second equation is the rotary equation. In this equation (θ) is the rotation angle, and other symbols have the same meaning as the top equation.

Like the Euler-Bernoulli beam theory the same boundary conditions can be adopted in order to find the solutions. The boundary conditions again depend on the type of beam model that is adopted for the specific problem.

2.4.3. Hydro-elastic Coupling Method

In order to get a good estimate of the structural responses due to hydrodynamic loads, like slamming, it is preferred to make a coupled model with the hydrodynamics and structures. A coupled model to analyse bow flare slamming and the responses on the vessel is made by Tuitman [42].

In his research he used two models, a structural model and a hydrodynamic model. The structural model is formulated in modal coordinates, with flexible mode shapes obtained either from a finite element model of the ship structure or from a simplified 1D beam model. This formulation enables the rigid-body motion and the elastic vibration of the ship hull to be solved simultaneously.
On the hydrodynamic side, a BEM model to compute linear diffraction and radiation forces is applied. Slamming loads were incorporated via impact models like the Generalised Wagner Model (GWM) and the Modified Logvinovich Model (MLM), which are enhanced versions of the original Wagner equation.

The model is coupled via a two-way coupling. This ensures that the model during the computations alters the effect the structural whipping has on the hydrodynamics and motions of the vessel. Full-scale and model scale validations demonstrated that the coupled model predicts motion responses, bending moments, and stress with good agreement to measurements on the same hull. The study found that slamming-induced whipping could increase ultimate bending moments by about 20% and reduce fatigue life predictions by up to 40% for container ships. These results showed that slamming loads play a crucial role in determining the structural design of the hull of the vessel.

3

Methodology of ComFLOW

The methodology consists of two parts that are needed to answer the research questions, as described in the introduction. Slamming is a structural response to a hydrodynamic load. Therefore, a hydrodynamic model and a structural model are needed to translate the load into vibrational responses. The hydrodynamic model is built using ComFLOW to simulate the slamming events on the stern due to waves.

This chapter explains how exactly the model in ComFLOW is set up. It explains what the input and output of the model are. It also explains how the input is determined and calculated and what kind of simplifications are used to ensure an effective, yet accurate CFD model.

3.1. ComFLOW Set-up

The system to model in this study is the vessel on dynamic positioning at sea with following waves with respect to the vessel. The objective of this study is to analyse the behaviour and responses of slamming on the stern of the vessel. Therefore, only the aft part of the hull is modelled in ComFLOW. The system in ComFLOW is a 2D representation of the real system. This has some limitations since the system in ComFLOW misses a dimension compared to the actual scenario. This simplification is further elaborated below.

3.1.1. In- and Output of the System

In order to correctly set up ComFLOW, different parameters need to be defined as input to the CFD model to simulate the behaviour. These input values can be separated into hydrodynamic input and operational input values. The main hydrodynamic input values are the wave parameters. In ComFLOW, you have the option to calculate the motions via ComFLOW itself or as an input to the model. In this study, it is chosen to calculate the motions themselves and provide them as input into the model. How the hydrodynamic input values are calculated and determined can be found in section 3.2.

Operational input values are important in order to draw a conclusion on what has an effect on the slamming on the stern. Parameters like draft and trim can be altered for different simulations to see the output. Only a change in draft is considered due to limitations of the trim during offshore operations. This is further explained in chapter 5. In figure 3.1, a schematic representation is shown of all the input values and the output of the CFD model.

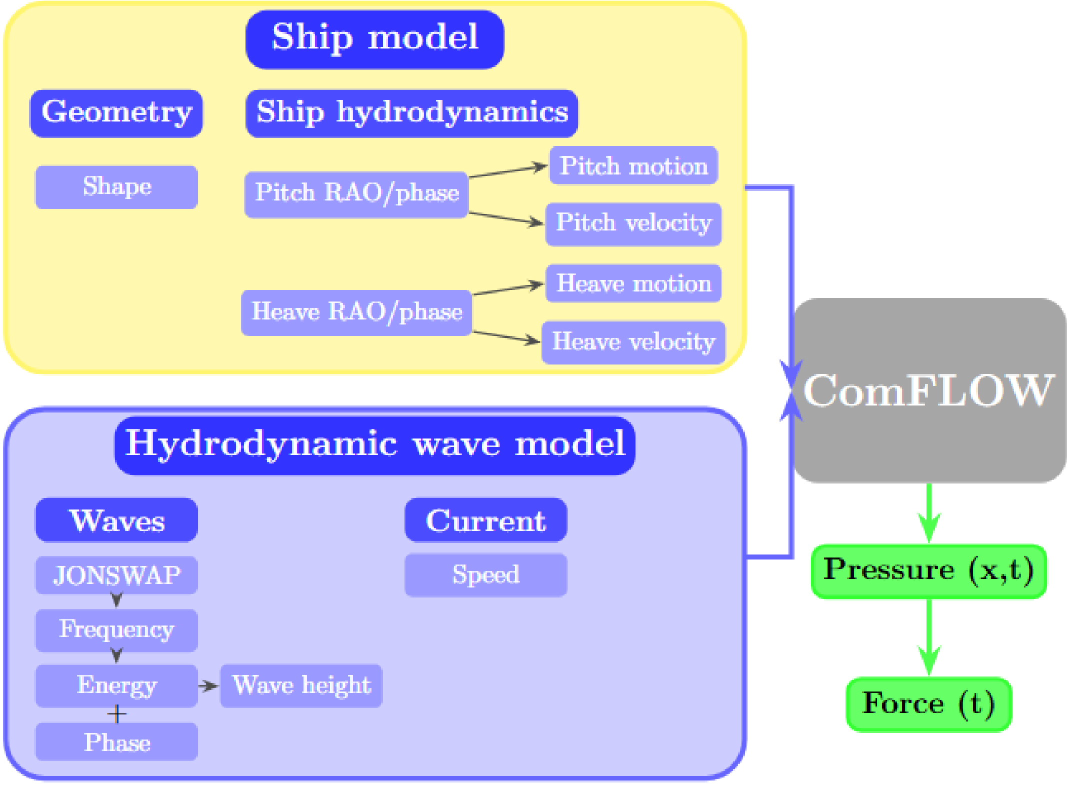

Figure 3.1: A representation of all the input into the CFD model and what the the CFD model calculates.

3.1.2. Domain Set-up

Computational Domain

In order to set up the system and correctly provide the in- and output of the system described in section 3.1.1, the domain must be correctly modelled in ComFLOW. In figure 3.2 a sketch of the ComFLOW set-up is given.

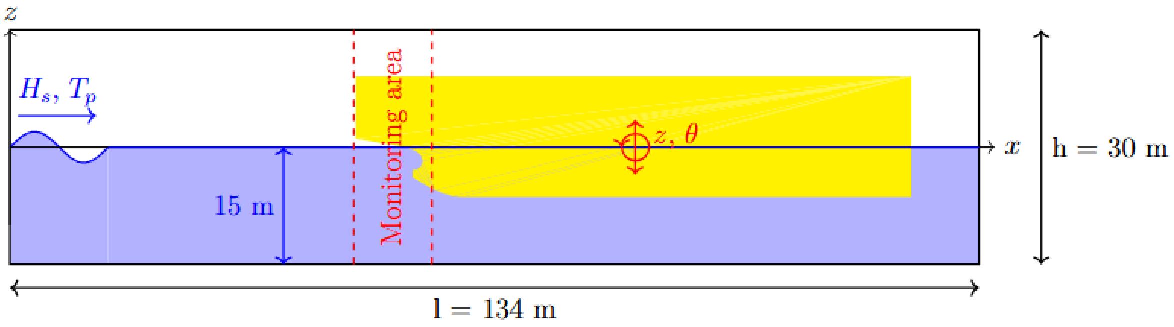

Figure 3.2: A schematic representation of the set-up made in ComFLOW.

For this specific problem, only the aft part of the vessel is necessary to model the slamming behaviour since the motions of the vessel are given as an input parameter in ComFLOW. Therefore, the geometry of the hull that is loaded is only related to the aft part of the B-types since the front does not matter in this study. Also, appendages are neglected in the geometry. It is chosen to model on true size which means that the geometry has a length of 70.8 meters and a height of 12.2 meters. To correctly fit the geometry in the domain of ComFLOW, the domain has an overall length of 134 meters, a height of 30 meters and a width of one meter. This is chosen to get the pressures and forces per unit width. The geometry, therefore has a width of one meter as well. Below in the table, the dimensions of the vertices are shown.

Table 3.1: The position of the vertices of the computational domain in meters

x_{min}	x_{max}	y_{min}	y_{max}	z_{min}	z_{max}
-10.000	124.000	-0.500	0.500	-15.000	15.000

The simulation requires a two-phase flow of an incompressible fluid. The domain is 50% filled with water and air, which ensures that the depth of the water in the simulation is set to 15 meters.

Boundary Conditions

The boundary conditions need to be carefully applied to ensure a correct simulation. The inflow field of the domain needs to be able to generate the irregular waves, but also absorb the reflected wave coming from the hull. The best option in ComFLOW is a General Absorbing Boundary condition (GABC). This boundary condition absorbs the reflected wave thus prevents the wave from being reflected again on the inflow field.

However, simply applying this boundary condition is not good enough to ensure stable simulations. The GABC can be tuned to ensure the boundary absorbs most of the reflected wave. One way of tuning the GABC is by calculating the a_0 coefficient. This can be done using the following equation.

$$a_0 = \sqrt{\frac{\tanh k_p h}{k_p h}} \tag{3.1}$$

In this equation k_p equals the wave number of the peak frequency of the spectrum. For the condition where Hs is 1.1 meters and T_p is 4.6 seconds, the a_0 coefficient is equal to 0.65. For the condition where Hs is 1.65 meters and T_p is 5.1 seconds, the a_0 coefficient can also be set to 0.65 since the difference between the sea states is small enough.

Another method to ensure that the GABC is stable and robust is to set the distance between the inflow field and the point where the wave is reflected equal to the peak wave length or a multiple of that length. This is done because the wave top is then always around the inflow field, ensuring stable inflow.

Besides the inflow field, a domain also requires an outflow field. This is placed at the end of the simulation at x equals 124 meters. This boundary condition is a Neumann outflow condition. The velocity, pressure and water height in the exterior of the domain are approximated using constant extrapolation.

Due to computational limitations, the water depth is set at 15 meters. This causes shallow water behaviour, but the vessel mostly operates in deeper water. To ensure that the water does not create unwanted shallow water effects due to the boundary layer of the bottom, a no-slip condition is placed at the bottom of the domain.

Measurement Instruments

The pressure exerted by the water on the hull must be measured in ComFLOW. This can be achieved by applying virtual pressure sensors on the hull in the form of monitoring points. The points locally measure the velocity, position and pressure at that point. These points are also set to move according to the pre-described motions of the hull.

To capture the slamming behaviour a series of monitor points are placed from the transform at $x = 44$ till $x = 52$. This allows the sensors to capture the distribution of the pressure along the length of the stern as well. Finally, rows with spacing of $y = 0.25$ along the width of the hull are placed to see the distribution of the pressure in the y-direction. The monitoring points are placed on the inclined part of the stern between the transom and the propeller shaft in the refinement area seen in figure 3.3

Computational Grid

ComFLOW is a volume of fluid type of CFD, so the domain is discretised into grid cells. It is important to make sure that the grid size is well chosen since accuracy and computation time are dependent on the size of the grid cells. ComFLOW has the option to define regions where the grid is locally refined.

For the setup of this research, it is important to minimise the computation time of each simulation. Since the number of calculations is reduced and the CFL limit is dependent on the grid size, it is chosen to get a base grid which has 680 cells along the length and 150 cells along the height. The section underneath the stern is of most interest for the problem, so a local refinement is placed there which reduces the local grid size by a factor of two. The same refinement is placed along the free surface of the domain. A representation of the computational grid can be seen in figure 3.3

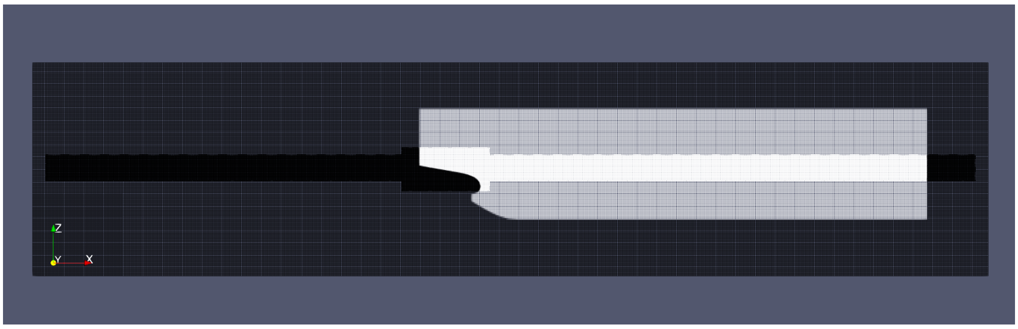

Figure 3.3: Here the computational grid of the ComFLOW simulation is shown. The white part represents the hull and the black part the two-phase flow. The brighter spots are local mesh refinement areas.

3.2. Hydrodynamics

Wave Modelling

In ComFLOW, there are multiple ways to model the incoming waves. Regular waves can be modelled using a Rienecker Fenton solver or the Airy wave theory which calculates the wave in the time domain using the following equation.

$$\eta(t) = \zeta_a \cos \omega t - kx + \phi \tag{3.2}$$

Regular waves provide the simplest way to model a wave for modelling. However, at sea, waves never consist of a single wave component with one frequency, but consist of a spectrum of frequencies. Because HLVs work offshore, irregular waves are more accurate to represent the actual sea state that a HLV can encounter. Also, a regular wave might result in a steady-state solution which might underestimate slamming events since they are highly non-linear. The wave elevation of an irregular wave can be modelled using the following equation:

$$\zeta(t) = \sum_{i=1}^{N} \zeta_{a_i} \cos(k_i x - \omega_i t + \varepsilon_i) \tag{3.3}$$

Equation (3.3) takes the sum of each chosen wave component and superimposes them in order to get the total. Choosing two different waves will already result in an irregular wave, but a higher order of wave components is beneficial. To calculate the wave components, a wave spectrum must be calculated first. This spectrum covers the energy density and distribution for different types of sea. For undeveloped seas, a JONSWAP spectrum is calculated using equations (3.4) to (3.6).

$$S_\zeta(\omega) = \frac{320 \cdot H_s^2}{T_p^4} \cdot \omega^{-5} \cdot \exp\left\{-\frac{1950}{T_p^4} \cdot \omega^{-4}\right\} \cdot \gamma^A \tag{3.4}$$

Where,

$$A = \exp\left\{-\left(\frac{\omega/\omega_p - 1}{\sigma\sqrt{2}}\right)^2\right\} \tag{3.5}$$

$$\omega_p = \frac{2\pi}{T_p} \tag{3.6}$$

$$\sigma = \begin{cases} 0.07, & \text{if } \omega < \omega_p \\ 0.09, & \text{if } \omega > \omega_p \end{cases}$$

The value of γ is set at 3.3, which is most common for a JONSWAP spectrum. For developed seas, a Brettschneider spectrum is calculated using the following equations (3.7) and (3.8):

$$S_\zeta(\omega) = \frac{173 \cdot H_s^2}{T_1^4} \cdot \omega^{-5} \cdot \exp\left(\frac{-692}{T_1^4 \cdot \omega^4}\right) \tag{3.7}$$

$$T_1 = 0.772 \cdot T_p \tag{3.8}$$

Since operations are for most of the time relatively close to a shore and not on the open ocean, it is assumed that an undeveloped sea is the most probable to occur. Also, the JONSWAP spectrum is a scientifically and industry-wide applied spectrum for calculations.

It can be seen from equations (3.4) to (3.6), that the spectrum is dependent on the significant wave height (H_s) and peak period (T_p). These values need to be chosen according to weather parameters where stern slamming poses a problem for the vessels. According to the crew, they noticed slamming mostly during Beaufort 4 and 5 winds. Based on the literature, a relation between wind speeds and wave height and period can be found. From the table below it can be found that for wind speeds correlated to Beaufort 4 and 5 scales, the significant wave height and wave period in undeveloped seas are equal to the following table [14].

Table 3.2: The relation between wind speeds and significant wave height and wave period for undeveloped seas [14]

Wave Spectrum Parameters Estimates					
Scale of Beaufort	Wind Speed at 19.5 m above sea (kn)	North Sea Areas (JONSWAP)			
		H_s (m)	T_1	T_2	γ (-)
1	2.0	0.50	3.50	3.25	3.3
2	5.0	0.65	3.80	3.55	3.3
3	8.5	0.80	4.20	3.90	3.3
4	13.5	1.10	4.60	4.30	3.3
5	19.0	1.65	5.10	4.75	3.3
6	24.5	2.50	5.70	5.30	3.3
7	30.5	3.60	6.70	6.25	3.3
8	37.0	4.85	7.90	7.35	3.3
9	44.0	6.10	8.80	8.20	3.3
10	51.5	7.45	9.50	8.85	3.3
11	59.5	8.70	10.00	9.30	3.3
12	> 64.0	10.25	10.50	9.80	3.3

Based on table 3.2 it can be found that in order to find the JONSWAP spectrum for seas with Beaufort 4 and 5 scales, a significant wave height (H_s) and a wave period (T_1) of 1.1 meters to 1.65 meters and 4.6 seconds to 5.1 seconds can be taken respectively. To analyse the effect of the peak wave period of the spectrum on stern slamming, the wave periods of (T_2) are also taken in separate simulations. To have a complete overview two higher values for the peak wave periods and one lower peak wave period are chosen to see the effect over a broader range. The influence of the wave period is only studied using one sea state of H_s = 1.65 meters. The values for all peak wave periods are shown in the table below.

Table 3.3: An overview of all peak wave periods used in the ComFLOW simulations

	Peak wave height (m)	
Peak wave period (s)	H_s = 1.1	H_s = 1.65
T_{l2}	-	4.4
T_l	-	4.75
T_1	4.6	5.1
T_h	-	5.45
T_{h2}	-	5.8

By filling in the values of H_s and T_1 in equations (3.4) to (3.6) for the initial simulations, the following results for the JONSWAP spectrum at Beaufort 4 and 5 are yielded.

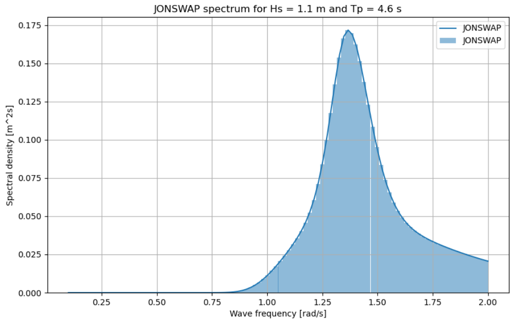

Figure 3.4: The JONSWAP spectrum for a H_s = 1.1 meters and a T_p = 4.6 seconds which represents a wind condition related to Beaufort 4.

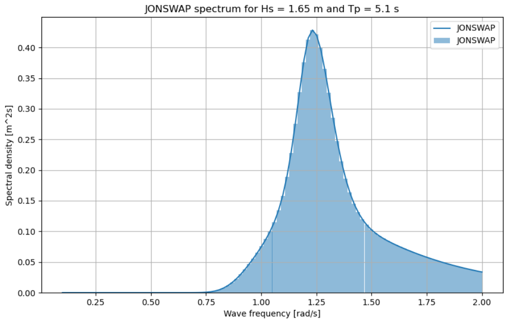

Figure 3.5: The JONSWAP spectrum for a H_s = 1.65 meters and a T_p = 5.1 seconds which represents a wind condition related to Beaufort 5.

Since ComFLOW requires a pre-defined set of values for each wave component, the wave spectrum needs to be discretised. In figures 3.4 and 3.5 it can be seen that the spectra are discretised in 100 individual wave components. This value is chosen to ensure a sufficient discretisation of the spectra without making sure the simulations don't become too slow. ω is cut off at a frequency of 2 $\frac{rad}{s}$ since higher frequencies do not contribute to the motions of the vessel. Due to the range of the wave frequency being capped at 2 $\frac{rad}{s}$ and discretised at a hundred components, $\delta\omega$ is equal to:

$$\delta\omega = 0.019\frac{rad}{s} \tag{3.9}$$

ComFLOW needs, in order to create irregular waves, values of the inflow angle of the waves with respect to the orientation of the vessel (β), the wave number (k), the amplitude of the wave (ζ) and a phase for the wave (ϵ) for each wave component. The inflow angle of all wave components is zero since the simulations are in 2D and only following wave conditions are considered in this research. The amplitude of each wave component can be calculated using the following equation:

$$\zeta_a = 2\sqrt{S_\zeta(\omega_{mid}) \cdot \delta\omega} \tag{3.10}$$

In equation (3.10), S_ζ is calculated using equations (3.4) to (3.6) where ω is taken as the middle for each bar in the discretisation of the spectra. This is calculated for each wave component using the following equation:

$$\omega_{mid,i} = \frac{\omega_{min,i} + \omega_{max,i}}{2} \tag{3.11}$$

The way to calculate the wave number of all wave components (k) is dependent on the water depth. In most seas, the water depth is high enough to assume an infinite water depth which makes the computations of the wave number less complicated. Based on real offshore operations, this can be assumed. However, in the ComFLOW domain, explained in section 2.2.1, the water depth is set at 15 meters to minimise computation time. Therefore, the water behaves as shallow water and the wave number needs to be calculated using the shallow water dispersion relation shown in equation (3.12).

$$\omega_{mid,i} = k_i g \sqrt{\tanh k_i h} \tag{3.12}$$

As can be seen from equation (3.12), the function is a transcendental equation because it involves the hyperbolic tangent function making it impossible to solve the wave number algebraically. Since the wave number appears both inside and outside the hyperbolic function, it must be solved numerically. Using an initial guess based on the deep water dispersion relation. the wave number for each wave component can be solved numerically.

The last component which needs to be pre-defined in ComFLOW to create irregular waves is the phase (ϵ_i). The phase only says something about the shift to the left or right for each component. Since a sea has infinite solutions for each wave component, a random series can be taken to translate a spectrum in the frequency domain to an irregular wave in the time domain.

With all the described values being calculated for each wave component, the timetrace of each wave can be described using equation (3.2). By taking the sum for all waves using equation (3.3) the time-trace for an irregular wave can be calculated for both wind conditions.

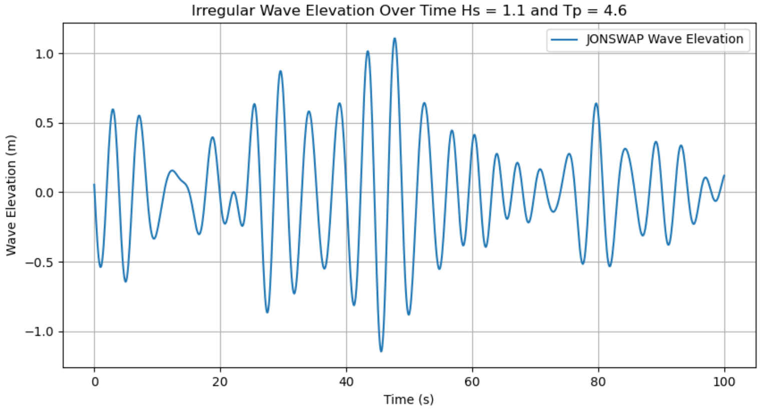

Figure 3.6: Irregular wave elevation for a Beaufort 4 condition with H_s = 1.1 meter and a T_p = 4.6 seconds.

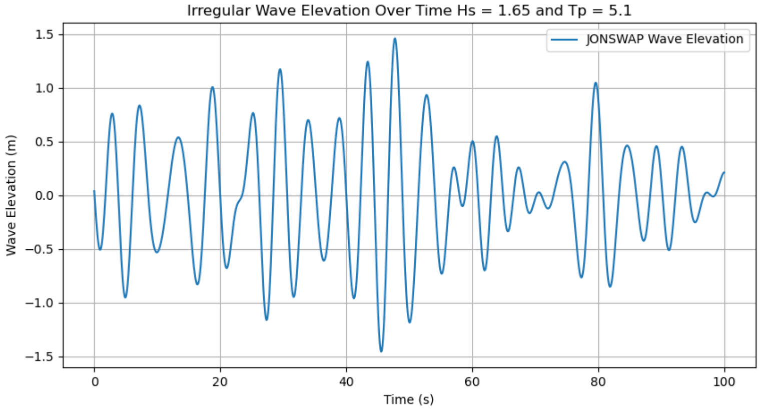

Figure 3.7: Irregular wave elevation for a Beaufort 5 condition with H_s = 1.65 meter and a T_p = 5.1 seconds.

The results of the wave elevation shown in figures 3.6 and 3.7 form a basis to calculate the motions of the vessel in these conditions.

Vessel Motions

Just like the wave elevation, the motions of an object like the vessel can be provided as input into ComFLOW. ComFLOW can determine the motions of an object in multiple ways. You either describe the motion itself or let ComFLOW calculate the motions based on the wave elevation the object encounters. The last option will cost extra computations per timestep, thus making the simulation duration longer. Therefore, it is opted to go for pre-described motions as input into the simulations.

ComFLOW has a few pre-programmed options to describe the motions of an object. In ComFLOW, you can opt for a constant and accelerated motion or a sinusoidal motion. However, due to irregular waves, the motions of the vessel will also be highly non-linear. Therefore, the best option is a motion via a timetrace. With this option, ComFLOW requires for every timestep the translation in x-, y- and z-directions and the rotation angles of roll, pitch and yaw. In 2D, only surge, heave and pitch have an effect so all other motions are considered zero. Due to the assumption of the vessel being stationary on dynamic positioning, surge is also considered to be zero. The heave and pitch motion for each wave component can be calculated using equations (3.15) and (3.16).

$$z(t) = \sum_{i=1}^{N} RAO_{z,i} \cos(\omega_{mid,i} t + \varepsilon_i) \tag{3.13}$$

$$\theta(t) = \sum_{i=1}^{N} RAO_{\theta,i} \cos(\omega_{mid,i} t + \varepsilon_i) \tag{3.14}$$

It also needs the linear velocities in x-, y- and z-directions and angular velocities of roll, pitch and yaw. The velocities can be calculated by taking the derivative of the displacements. Since only heave and pitch displacements are non-zero, only heave and pitch velocities are considered.

$$\dot{z}(t) = \frac{\delta z(t)}{\delta t} \tag{3.15}$$

$$\dot{\theta}(t) = \frac{\delta \theta(t)}{\delta t} \tag{3.16}$$

In these equations, the RAO (Response Amplitude Operator) is a transfer function that shows the response of the vessel in the frequency domain of the waves. These RAOs are calculated for every design condition of the vessel using Shipmo. Shipmo is a strip theory solver from Marin. By filling in all $\omega_{mid,i}$ and ϵ_i from figures 3.4 and 3.5 and phase RAOs respectively, the following heave and pitch motion is calculated.

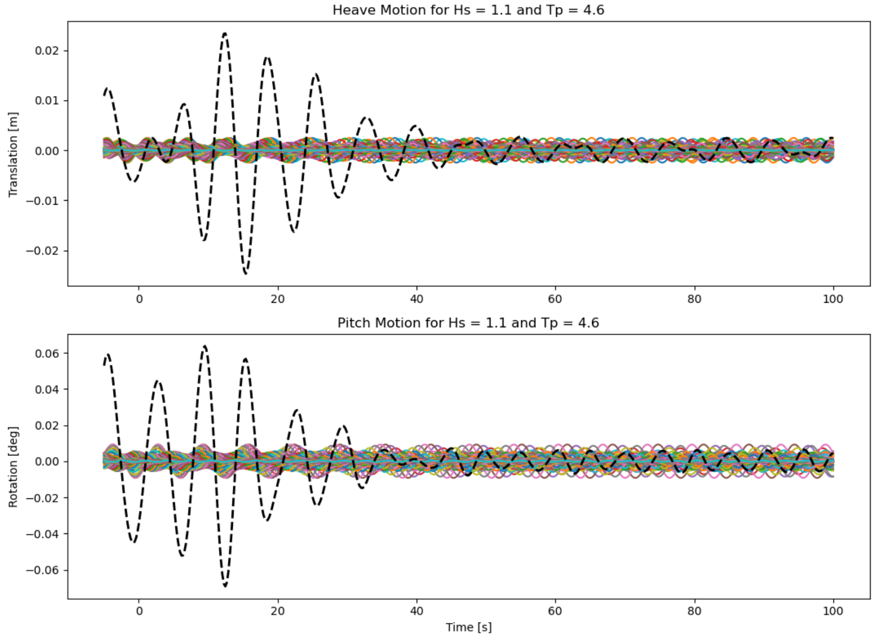

Figure 3.8: Non-linear heave and pitch motion for a Beaufort 4 condition with H_s = 1.1 meter and a T_p = 4.6 seconds. The dotted line represents the superposition and the coloured lines the individual components.

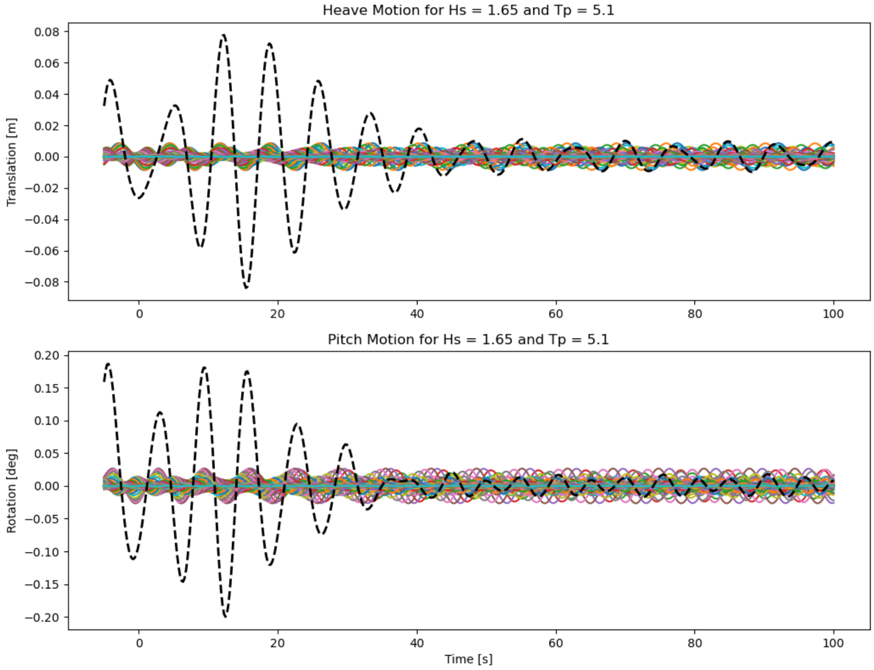

Figure 3.9: Non-linear heave and pitch motion for a Beaufort 5 condition with H_s = 1.65 meters and a T_p = 5.1 seconds. The dotted line represents the superposition and the coloured lines the individual components.

Although figures 3.8 and 3.9 show the non-linear motions of the vessel in both sea states, the motions need to be altered for the timetrace since the figures show the motion in the time domain of the vessel. Because the wave is initialised at the $x = 0$ boundary in the ComFLOW domain, it takes time before the motions of the vessel are actually initialised in the ComFLOW time domain. Since the RAOs of the vessel act around the CoG (Centre of Gravity) of the vessel, the time it takes for the wave to reach the CoG needs to be calculated first. During this time, the timetrace must return zero translation and

velocity.
To calculate the time it takes for the wave to reach the CoG, the group velocity of the wave must be calculated. First, the wave velocity must be known. This can be calculated using equation (3.17). After that value is known, the group velocity of the wave can be calculated using equation (3.18).

$$c_i = \sqrt{\frac{g}{k_i} \tanh k_i h} \tag{3.17}$$

$$c_{g,i} = \frac{1}{2} c_i \left(1 + \frac{2k_i h}{\sinh 2k_i h}\right) \tag{3.18}$$

As both equations show, the velocities are dependent on the values of all wave components. This means that some wave components reach the x-position of CoG faster than other wave components. Since low frequencies are faster, they are the first to reach the vessel and have a bigger influence on the motions of the vessel. This is due to the RAOs being highest for lower frequencies. Therefore, it is chosen that the time it takes for the whole irregular wave to reach the x-position is the time it takes the fastest wave component to reach that value. The time it takes is calculated using the following equation.

$$t_{delay} = \frac{x_{CoG}}{c_{g,i}} \quad \text{, where} \quad x_{CoG} = 126.37m \tag{3.19}$$

If the motions are forced to be zero before the time the fastest wave component reaches the x-position of CoG, there will be a sudden increase in motions. This could lead to numerical errors since the velocity is the derivative of the displacement of both motions. To counteract that, a function is added to equations (3.15) and (3.16) that slowly introduces the full motions. Although this causes a discrepancy between what actually happens, it makes sure that the simulation remains stable. The following equation is used to slowly introduce the motions in the ComFLOW time domain.

$$envelope = \frac{1}{2}\left(1 + \tanh \frac{t - t_{delay}}{t_{transition}}\right) \quad \text{, where} \quad t_{transition} = 1s \tag{3.20}$$

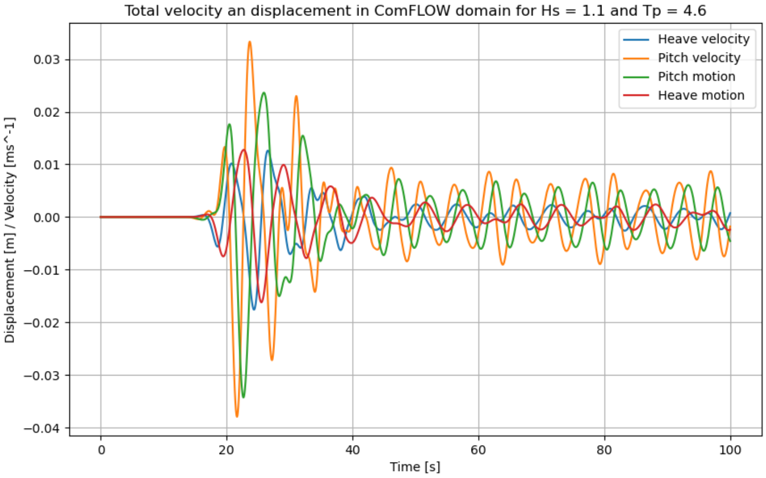

Figure 3.10: Total pitch and heave displacements and velocities in the ComFLOW domain for a Beaufort 4 condition with H_s = 1.1 meter and a T_p = 4.6 seconds.

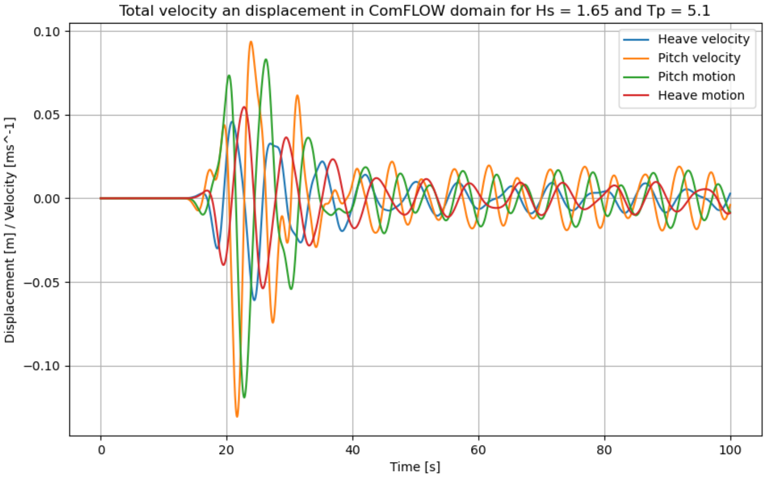

Figure 3.11: Total pitch and heave displacements and velocities in the ComFLOW domain for a Beaufort 5 condition with H_s = 1.65 meter and a T_p = 5.1 seconds.

3.3. Simplifications of the Model

Simplifications were made in the setup of the ComFLOW simulations to ensure that the simulations capture the general behaviour while preventing long computational times.

The biggest simplification that is made in the CFD simulations is the choice to analyse in 2D instead of 3D. One of the main reasons for this choice is minimising the computational time for each simulation. Adding an extra dimension to the simulation significantly bumps up the total number of grid cells in the domain. Therefore, due to the number of simulations and no access to the Delft cluster, it is beneficial to reduce running time. 2D simulations significantly reduced the total number of grid cells compared to 3D simulations while still being able to accurately capture the slamming behaviour.
This simplification does mean that water is unable to dissipate in the y-direction in the simulation. This means that water is more enclosed and pressure can build up higher than in 3D simulations. Studies show that on average the difference in pressure build-up of slamming in both types of simulations is a 10 to 20% difference.

Another simplification inherent in 2D simulations is that only following waves with an inflow angle of zero degrees are modelled. Other inflow angles in following wave conditions can not be modelled even though these angles can also provide slamming responses on the stern. However, even if 3D simulations had been performed, it would be hard to simulate other inflow angles due to the reflection of the boundaries of the domain. This would mean results are harder to quantify and physics would need to be managed more carefully.

Another simplification is the fact that for the motions only heave and pitch are considered. True scenarios require all six degrees of freedom to properly analyse the motions. Since the simulations are performed in 2D sway, roll and yaw are unable to be modelled. This simplification is valid since those motions will have less of an effect on the slamming responses than heave and pitch. Surge is set to be zero due to the assumption of the vessel acting on dynamic positioning.

Another simplification is that the hull of the vessel is assumed to be a rigid body. Therefore, bending and shear of the structure and their effect on the hydrodynamics are not taken into account. The results are completely based on one-way coupling.

4

Methodology of Structural model

The second model is the structural model. This model is needed to define the responses of the vessel due to the slamming loads since a hydrodynamic model does not answer this. The structural model is solved using semi-analytical and numerical methods. It uses the results from the hydrodynamical model as input to the system.

4.1. Hydro Elastic Model

One of the biggest problems with regard to slamming is the structural responses of the vessel. The vessel is said to vibrate across the whole length of the hull when the vessel encounters the following wave conditions. Since the accommodation of the vessel is at the front, the hull faces global responses. Since CFD results only say something about the hydrodynamic loads on the vessel, a structural model is needed to study vibrational responses of the hull.

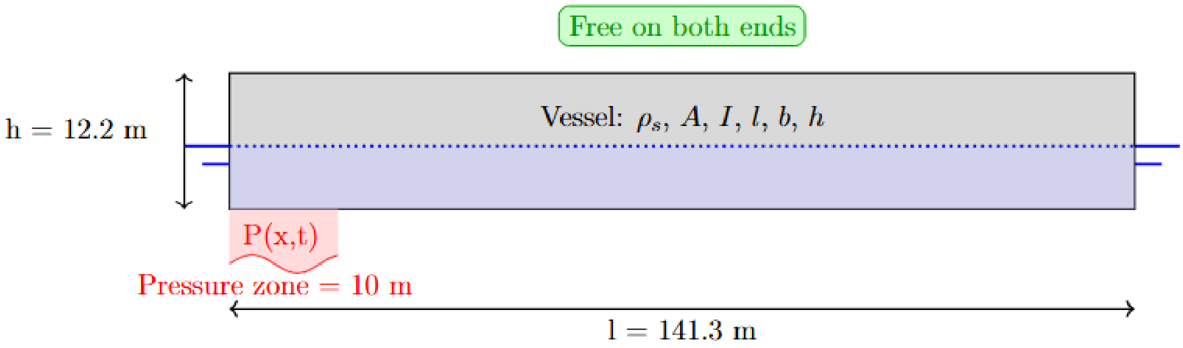

Figure 4.1: A schematic representation of the vessel modelled as a free-free Euler-Bernoulli beam. It is partly submerged and the transient load is applied on the first 10 meters, approximately the length of the stern.

In order to find how the vessel responds to the hydrodynamic loads created by slamming on the stern, a semi-analytical model in the form of an Euler-Bernoulli beam can be derived. In this case, the hull can be seen as a beam model which is free on both ends. The general equation of an Euler-Bernoulli beam can be found below.

$$EI\frac{\partial^4 w(x,t)}{\partial x^4} + \rho A\frac{\partial^2 w(x,t)}{\partial t^2} = q(x,t) \tag{4.1}$$

In equation (4.1), EI are stiffness properties of the beam, thus in this case related to the structural properties of the hull. ρA is the mass of the beam per unit length. $w(x,t)$ is the deflection as a function of space and time. At last, $q(x,t)$ is a distributed transient load on the beam. Because the beam must represent the hull of the vessel, some structural properties must be related to the vessel. These values are based on structural calculations from the newbuilding phase of the vessel and can be found in table 4.1.

Table 4.1: Main structural properties of the B-type vessel

Parameter	**Value**	**Unit**
Length overall (L)	141.30	m
Width (B)	24.91	m
Moment of Inertia (I)	44.1	m^4
Young's modulus (E)	210	GPa
Density of steel (ρ_s)	7850	$\frac{kg}{m^3}$
Lightweight (LWT)	8757	mt

4.1.1. Modal Analysis

As can be seen in equation (4.1), the equation is dependent on a spatial part and a time part. To solve the dynamic Euler-Bernoulli beam equation, a modal decomposition approach is used. The beam is assumed to vibrate in its natural flexural modes, and the total response is expressed as a linear combination of mode shapes weighted by time-dependent modal amplitudes. This reduces the governing partial differential equation to a set of uncoupled second-order ordinary differential equations which represent the modes. By taking the superposition of all these differential equations the total deflection over time and space can be found. The deflection $w(x,t)$ of the beam is approximated as:

$$w(x,t) = \sum_{n=1}^{N} \psi_n(x) q_n(t) \tag{4.2}$$

In equation (4.2), $\psi_n(x)$ are the mode shapes for each natural frequency and $q_n(t)$ are the time-dependent modal coordinates. The mode shapes follow the general form:

$$\psi_n(x) = A\sinh(\beta_n x) + B\sin(\beta_n x) + C\cosh(\beta_n x) + D\cos(\beta_n x) \tag{4.3}$$

Knowing that for a beam that is free on both ends the following boundary conditions $\frac{d^2\phi}{dx^2}(0,L) = 0$ and $\frac{d^3\phi}{dx^3}(0,L) = 0$ apply. Applying the free-free boundary conditions to the general solution yields the following matrix system:

$$\begin{bmatrix} 0 & -\beta^2 & 0 & \beta^2 \\ -\beta^3 & 0 & \beta^3 & 0 \\ \beta^2\sin(\beta L) & -\beta^2\cos(\beta L) & \beta^2\sinh(\beta L) & \beta^2\cosh(\beta L) \\ -\beta^3\cos(\beta L) & \beta^3\sin(\beta L) & \beta^3\cosh(\beta L) & \beta^3\sinh(\beta L) \end{bmatrix} \begin{bmatrix} A \\ B \\ C \\ D \end{bmatrix} = \begin{bmatrix} 0 \\ 0 \\ 0 \\ 0 \end{bmatrix}$$

For a non-trivial solution $[A,B,C,D]^T \neq 0$, the determinant of the coefficient matrix must vanish. This yields the characteristic equation:

$$\cos(\beta L)\cosh(\beta L) = 1 \tag{4.4}$$

Solving equation (4.4) yields an infinite amount of values for β. All represent a natural eigen mode of the beam. Applying the boundary conditions also results in the following equation for the mode shape.

$$\psi_n(x) = \sinh(\beta_n x) + \sin(\beta_n x) + C_n[\cosh(\beta_n x) + \cos(\beta_n x)] \tag{4.5}$$

where,

$$C_n = \frac{\sin(\beta_n L) - \sinh(\beta_n L)}{\cosh(\beta_n L) - \cos(\beta_n L)} \tag{4.6}$$

These equations yield the following first ten mode shapes for an Euler-Bernoulli beam that is free on both ends of the beam.

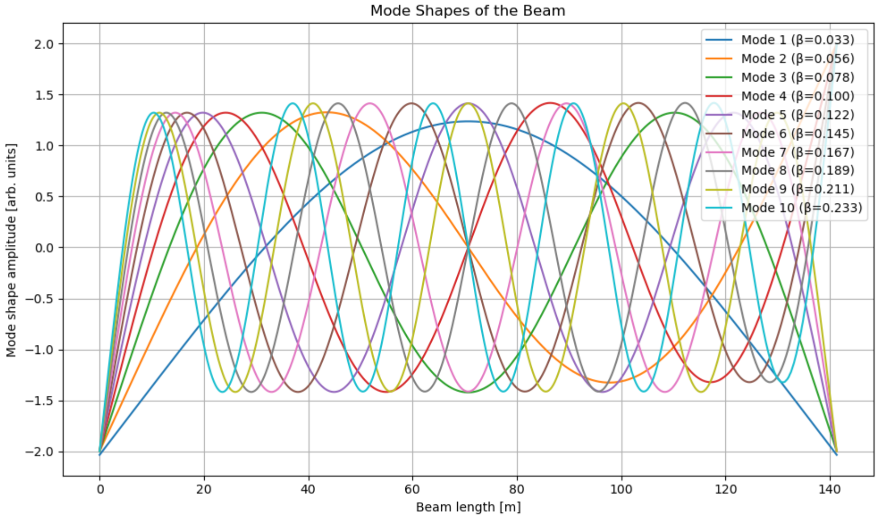

Figure 4.2: The first ten mode shapes of a free-free Euler-Bernoulli beam with corresponding β values calculated using the given properties of the beam.

With the equations for the mode shapes known, properties of the beam can be calculated in the modal space. Based on the first term in equation (4.1), the equation for the structural stiffness in the modal space is shown in equation (4.7). From the second term in equation (4.1), the modal mass equation can be derived and is shown in equation (4.8).

$$K_n = EI\beta_n^4 \int_0^L \psi_n^2(x), dx \tag{4.7}$$

$$M_n = \mu_{eff} \int_0^L \psi_n^2(x), dx \tag{4.8}$$

Since the cross-sectional area of the actual hull is not certain, the ρA term in equation (4.1) is calculated using the mass per unit length of the hull. Next to that, since the beam represents a vessel, added mass needs to be considered. This is calculated using strip theory and projected on the modes using equation (4.20). μ_{eff} is calculated using the following equation.

$$\mu_{eff} = \frac{LWT}{L} \tag{4.9}$$

The external force acting on the beam also needs to be projected onto the modes of the beam. To do that the following equation is applied.

$$F_n(t) = \int_{L_{p(x,t),min}}^{L_{p(x,t),max}} \psi_n(x)P(x,t), dx \tag{4.10}$$

In this equation the transient force is given by $P(x,t)$. Also the integral has an upper and lower bound related to where the distributed load is placed along the length of the beam.

4.2. Duhamel Convolution

There are multiple ways to solve the equations in modal space to get the deflections of a beam. An alternative approach to solving the dynamic beam response is based on Duhamel's integral, which allows for an analytical expression of the time-domain solution assuming linearity and time-invariant properties. This integral determines the displacement response for each mode and for an arbitrary force over time. The general equation for this integral can be given as follows.

$$q_n(t) = \int_0^t h_n(t-\tau)F_n(\tau), d\tau \tag{4.11}$$

In this equation F_n is the modal force as a function of time. h_n is the impulse response function for the damped oscillator with n modes. This function looks as follows.

$$h_n(t) = \frac{1}{M_n \omega_{d,n}} e^{-\zeta_n \omega_n t} \sin(\omega_{d,n} t) \tag{4.12}$$

In this equation $\omega_{d,n}$ is the damped natural frequency for each mode. This formulation avoids solving differential equations and instead uses convolution to get the deflections. By applying the damped natural frequency, the equation takes damping into consideration. The damped natural frequency is calculated using the following.

$$\omega_{d,n} = \omega_n \sqrt{1-\zeta_n^2} \quad \text{, where} \quad \omega_n = \sqrt{\frac{K_n}{M_n + A_n}} \tag{4.13}$$

ζ_n is calculated using the following equation:

$$\zeta_n = \frac{b_n(\omega)}{2\sqrt{(M_n + A_n) \cdot K_n}} + b_{struc} \tag{4.14}$$

In this equation $b_n(\omega)$ is the damping value for the specific wet natural frequency for each mode calculated using equation (4.21). The same is done for the added mass and the superposition is taken to get the final output. b_{struc} is the structural damping which is set at 1 % which is a typical value for vessels.

By applying equation equation (4.2) with the results from the Duhamel convolution the deflection along the length and at each timestep can be determined. Since the deflections are assumed to be small, velocity and acceleration are better values to determine whether the vessel is excited by the slamming pressures. This can be done by taking the first and second derivatives of $w(x,t)$ with respect to time, respectively.

4.3. Cummins Equation

A frequency domain calculation assumes that a steady-state response is always guaranteed, but in real problems this is often not the case. Due to non-linear forces acting on a vessel, a more accurate approach is needed to analyse the dynamic behaviour of a rigid body. For a time domain calculation, the Cummins equation can be used. This follows a different approach as the Duhamel integral and is applied to a hydrodynamic differential equation. The equation can be found below [14].

$$(M + A) \cdot \ddot{x}(t) + \int_0^\infty B(\tau) \cdot \dot{x}(t-\tau)\, d\tau + C \cdot x(t) = X(t) \tag{4.15}$$

From equation (4.15) it can be observed that the damping of the model is dependent on the time lag (τ). The integral goes to infinity so the equation needs to be capped to ensure a stable and fast numerical solution. $B(\tau)$ is called the retardation function. To calculate this function, an inverse Fourier transform is applied on the following equations. These are derived from the frequency domain equations.

$$a(\omega) = A - \frac{1}{\omega} \int_0^\infty B(\tau) \sin(\omega\tau)\, d\tau \tag{4.16}$$

$$b(\omega) = \int_0^\infty B(\tau) \cos(\omega\tau)\, d\tau \tag{4.17}$$

The inverse Fourier transform yields the following:

$$B(\tau) = \frac{2}{\pi} \int_0^\infty b(\omega) \cos(\omega\tau)\, d\omega \tag{4.18}$$

$$A = a(\omega) + \frac{1}{\omega}\int_0^{\infty} B(\tau)\sin(\omega\tau)\,d\tau \tag{4.19}$$

In these equations, $b(\omega)$ and $a(\omega)$ are frequency-dependent added mass and damping which are calculated for the vessel using strip theory software. The integrals need to be capped for these functions as well to ensure numerical stability. When applied correctly, the retardation function should decay quickly and could then be neglected in the rest of the time domain for faster calculations.

4.3.1. Converting Cummins to Hydro Elasticity

The Cummins equation shown in equation (4.15) is based on the assumption that the vessel is a rigid body. Since a hydro-elastic approach is needed for slamming, the Cummins equation needs to be converted. By using modal analysis, the model can be converted to a hydro-elastic model. This means projecting the variable onto the mode shapes. For the mass and the stiffness equations (4.7) and (4.8) can be used to calculate the modal mass and stiffness. However, the added mass and damping must be calculated differently. With an elastic model, the added mass and damping vary along the length of the model due to the flexure. To take this into account, the added mass and damping must be calculated for each section which is applied in the strip theory. This creates a spatial dependency for the added mass and damping. With this applied, the modal damping and added mass can be calculated using the following equations.

$$a_n(\omega) = \int_0^L a_{33}(x,\omega)\,\psi_n^2(x)\,dx \tag{4.20}$$

$$b_n(\omega) = \int_0^L b_{33}(x,\omega)\,\psi_n^2(x)\,dx \tag{4.21}$$

In the equations, only the heave damping and added mass are considered for the modal space. This is because the model only considers the vertical deflection of the model. Because strip theory discretises the hull into smaller sections, the total deflection of the beam can be seen as the individual heave components of each section. Pitch is needed to model the rotation of the hull which is ignored so the pitch coefficients and their coupling terms are neglected in this case. The results of this can be found in figures 4.3 and 4.4.

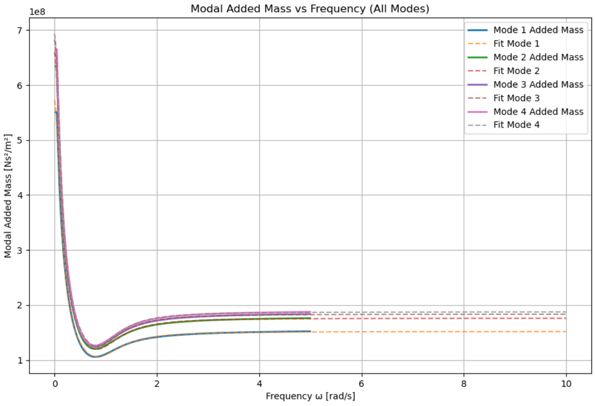

Figure 4.3: The modal added mass for each mode with the fit used in the structural model. These are based on the equations in appendix B.

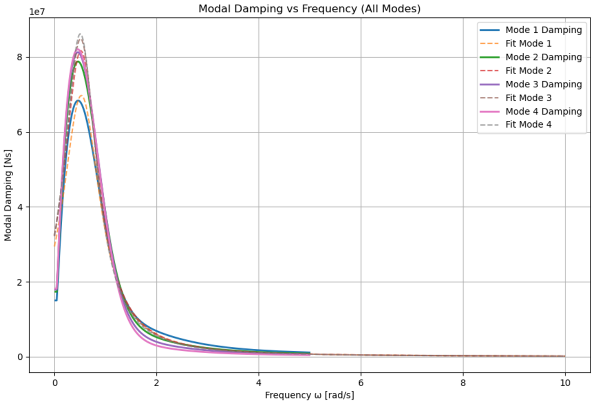

Figure 4.4: The modal hydrodynamic damping for each mode with the fit used in the structural model. These are based on the equations in appendix B.

Shipmo only returns the individual hydrodynamic coefficients for each section of the hull. So these coefficients need to be converted to the true sectional added mass and damping of the vessel. To do that, the hydrodynamic coefficients should be multiplied by the sectional length. To validate if the sectional added mass and damping are correct, the sum of the individual components should match the total damping and added mass output of the hull via Shipmo. When the sum of the sectional hydrodynamic damping and added mass is compared to the total hydrodynamic output of Shipmo, they are exactly the same. This means the sectional damping and added mass values are calculated correctly and can be used for the modal analysis.

The added mass, $a_{33}(x, \omega)$, and damping, $b_{33}(x, \omega)$, in equations (4.20) and (4.21) are calculated in strip theory. This method works well for slender bodies like the hull of a vessel and assuming that the body is also rigid. However, the hull is assumed to be hydro-elastic to analyse the responses of slamming. This creates some uncertainty regarding the added mass of the vessel. This value is dependent on how the fluid moves around the body in a certain motion. To take account for 3D-fluid effects a J-factor is introduced. J-factors are needed to account for the three-dimensional (3D) effects of fluid motion on a ship's response, which are not fully captured by traditional two-dimensional (2D) strip theory. These effects are particularly important for elastic body motions, as the 2D strip theory cannot accurately reflect the boundary conditions of an elastic body or the 3D fluid motion at the front and end of the ship. The J-factor compensates for these limitations by adjusting the added mass coefficients calculated using 2D strip theory. The J-factor can be calculated using the following experimental equation developed by Townsin.[41, 12]

$$J_n = 1.02 - 3\left(1.2 - \frac{1}{n}\right)\frac{B}{L} \tag{4.22}$$

As can be seen from the equation, the J-factor is dependent on the mode, length and width of the vessel. The corrected added mass can be calculated by simply multiplying by the J-factor.

$$a_{n,corr}(\omega) = J_n \cdot a_n(\omega) \tag{4.23}$$

Time Integration Scheme for Cummins

With the components all in modal space the differential equation of Cummins, which can be seen in equation (4.15) in appendix B, can be solved. To prevent numerical instability, the Runge-Kutta method is chosen to solve the problem numerically. The equations regarding this method are shown below.

$$\frac{dy}{dt} = f(t, y), \quad y(t_0) = y_0, \tag{4.24}$$

or, in the context of the modal analysis, a system of equations:

$$\frac{d\mathbf{y}}{dt} = \mathbf{f}(t, \mathbf{y}), \quad \mathbf{y}(t_0) = \mathbf{y}_0, \tag{4.25}$$

where $\mathbf{y}(t)$ contains the modal displacements and the derivative the modal velocities.

The fourth-order Runge-Kutta algorithm advances the solution from t_i to $t_{i+1} = t_i + h$, where $h = \Delta t$ using the following intermediate calculations:

$$k_1 = f(t_i, y_i), \tag{4.26}$$

$$k_2 = f\left(t_i + \frac{h}{2}, y_n + \frac{h}{2}k_1\right), \tag{4.27}$$

$$k_3 = f\left(t_i + \frac{h}{2}, y_n + \frac{h}{2}k_2\right), \tag{4.28}$$

$$k_4 = f(t_i + h, y_i + hk_3), \tag{4.29}$$

with the solution updated as:

$$y_{i+1} = y_i + \frac{h}{6}\left(k_1 + 2k_2 + 2k_3 + k_4\right). \tag{4.30}$$

This approach works by estimating the slope at several points within the interval and forming a weighted average. The use of multiple evaluations of $f(t, y)$, which is the reduced order model of equation (4.15), within each time-step dramatically improves the accuracy over simpler methods like the Euler scheme. These were tried first, but turned out to be incapable of showing convergence for the hydro-elastic beam model. In the RK4 method a value of 0.003 was chosen for h. Values below 0.005 seconds of h did not show significant differences between the results so it is assumed to be converged.

In the context of the hydro-elastic model, the added mass and damping vary along the hull length due to flexural effects. By discretising the hull into smaller elements (via strip theory), the modal transformations introduce spatially-dependent coefficients into the governing equations. The Runge-Kutta method is robust enough so that the time integration remains stable, even when the modal masses, stiffness and the distributed hydrodynamic effects have complex behaviour in time and space.

Moreover, the potential for adaptive step-size control further enhances the accuracy of the solution when the modal response exhibits rapid changes. This is especially useful during transient events where the dynamic excitation or changes in the hydrodynamic environment demand a finer temporal resolution.

By applying this numerical integration scheme, a reliable estimate of the system's dynamic response can be calculated without the numerical model diverging from steady-state solutions.

5

Results of ComFLOW

5.1. General Behaviour

In the upcoming paragraph, 2D snapshots of the free surface elevation and slamming behaviour will be examined in both space and time domain. These simulations were performed with the modelling settings as described in chapter 3. The images show a 2D intersection of the hull with the surrounding water, where blue colours indicates the fluid and grey indicates air. Later on, the results of the monitoring points will be elaborated, which follow from the shown fluid behaviour.

For convenience, only one simulation is shown in this section. This is done for the simulation with a H_s of 1.65 meters and a draft of 7 meters since the behaviour is well visible. The results of the other simulations show more or less the same fluid behaviour at the stern.

5.1.1. Fluid Behaviour at the Stern

When looking at the fluid behaviour underneath the stern some clear conclusions can be drawn on what causes slamming at the stern of the vessel. From the snapshots of the domain it is clear that the biggest peak pressure on the stern is caused by water hitting the stern almost flat. Instead of waves travelling under the stern and causing pressure to build up, it is clear that waves interact with each other. This is likely caused by the interaction of the incoming waves and the reflected waves by the vessel. It seems that waves have an influence on each other determining whether a wave will turn into a slam event or not. This interaction of multiple waves is called clustering and an example of it can be seen in the series of snapshots below. [5]

Snapshot at t=67.2

Figure 5.1: The start of a cluster at $t = 67.2s$ event where a breaking wave leads to a big slamming event.

In the snapshot below, the state at the time is equal to 67.2 seconds in the simulation. In front of the hull of the vessel, a breaking wave is visible with a maximum height of 1.5 meters. The vessel is moving according to the simulated run of irregular waves in the CFD. This is the start of a build-up towards a big slam event. Although this starts with a breaking wave, other cluster events also happen with normal types of waves which did not created higher pressures than the local hydrostatic at the stern when the wave passes.

Snapshot at t=68.2

Figure 5.2: At $t = 68.2s$ the wave reaches the stern. It creates a small pressure pulse, but most energy is dissipated by the breaking wave event.

After one second from the starting snapshot, the wave has lost most of its energy due to the breaking event. The stern has gradually been submerged and the wave hits the transom. This does not cause on average high pressures on the stern. This can be seen in the results in appendix A. A small spike around 70 seconds is observed, but well below the 100 kPa. This is the breaking wave moving underneath the stern.

Snapshot at t=71.4

Figure 5.3: A snapshot of the ComFLOW results at $t = 71.4s$ where the next wave moves towards the stern of the vessel. Water is sucked from underneath the stern.

In the snapshot taken at 71.4 seconds into the simulation, the next wave starts building up and moves towards the hull. What is clearly visible is that water underneath the hull from the previous wave is partly reflected back and partly pulled back by the next incoming wave. This will cause the stern to get locally above the free surface. This can be seen in the next snapshot more clearly.

Snapshot at t=72.6

Figure 5.4: A snapshot of the ComFLOW results at $t = 72.6s$. The wave is starting to break and moves into the positive z-direction.

In the snapshot at 72.6 seconds into the simulation, it is visible that the water is pulled from underneath the stern. This imbalance leads to water not only moving in the positive x-direction by the wave, but also in the positive z-direction. This will cause the water to hit the stern much like a flat plate. This is clearly visible since the impact does not create big splashes. Water is not able to dissipate its energy very well due to this effect and pressure can quickly be built up.

Snapshot at t=73.6

Figure 5.5: A snapshot of the ComFLOW results at $t = 73.6s$. The wave hits the stern flat and the energy is contained beneath the stern. This causes severe pressure pulses.

At around 73 seconds in the simulation, the wave hits the stern of the vessel. This slam created a maximum peak pressure of 500 kPa at the stern at the impact location. Other sensors on the stern showed a peak pressure of around 300 kPa. The next incoming wave in the figure also will hit the stern with pressures arising to 300 kPa, resulting in a cluster of slams.

5.2. Effect of Vessel Draft

An important variable for the vessel when operating on dynamic positioning is the change of draft during load-out. When the vessel supplies pipe sections to pipe layers, the vessel draft will change from design draft to a ballast draft, which is the minimum draft of the vessel. The draft can thus vary between a minimum of 6 meters and a maximum of 8 meters. To study the effect of the change in draft, five unique vessel drafts are chosen. These can be found in table 5.1.

Table 5.1: The selected drafts of the vessel for this study.

T_{ballast}	T	T	T_{sps}	T_{design}
6.0	6.5	7.0	7.5	8.0

In the table the draft of 7.5 meters is marked as T_{sps}. This draft falls within the interpolation, but is also an important draft for offshore installation works. Regulations prohibit the vessel from a draft deeper than 7.5 meters when the vessel is sailing with an open top or has special personnel on board. This is always the case during offshore installation work.

5.2.1. Simulations for H_s = 1.1 m and T_p = 4.6 s

For both weather conditions described in section 2.2 the effect of the change in vessel draft is analysed. For the simulations with a H_s of 1.1 meters and a T_p of 4.6 seconds, the results can be found in figures 5.6 and 5.7.

The Effect of Loading Conditions of the Vessel on the Peak Pressure and Number of Slams

When looking at the average peak pressures for different drafts in figure 5.6, a clear downwards trend can be observed. An increase in draft results in fewer violent slam events. For a draft of 6 meters, the average peak pressure is ±400 kPa. This reduces towards 230 kPa for a draft of 6.5 meters. For a draft of 7 meters, the average increases compared to a draft of 6.5 meters. This is mainly due to a single slam event where the pressure is way higher than in other slam events. This is probably a perfect scenario where a slam event is built up very well in order to get a slamming pressure of ±1750 kPa. At the design draft of 8 meters, the value is around 80 kPa, so the vessel does not encounter excessive slamming on the stern.

It can be seen in figure 5.6 that at a draft of 6 and 7 meters, the standard deviation band is wider for the upper boundary compared to the other loading conditions. This is due to the spread of the average peak pressure at that loading condition. In figure 5.7, a boxplot is shown of the data from the CFD simulation with the data spread of the identified peak pressures. For the draft of 6 meters, the data is much more spread out between high-pressure peaks and low-pressure peaks, resulting in a bigger uncertainty. It can be seen that there is a group of slam data that is very high compared to the other data for the draft of 7 meters. Even though the data is filtered for numerical errors, it still shows a very high slamming pressure. This is likely the perfect condition for a slam in terms of the position of the stern, motions of the vessel and the characteristics of the incoming wave. For a draft of 7.5 and 8 meters, the data of the pressure peak is much more concentrated and does not show any really big outliers.

When the number of slams in each simulation is counted, an interesting trend can be observed which is shown in figure 5.6. The pressure decreases almost linearly for a sea state related to Beaufort 4 wind conditions. However, the number of slams stays the same across the different drafts of the vessel except for the design draft. All loading conditions up to 7 meters show 14 unique slamming events with a draft of 7.5 meters showing 13 unique slams. At a draft of 8 meters, the waves are not able to get under the stern to hit the vessel so only three slams are observed. Also, the waves do not contain enough energy to create high-impact velocities. From both graphs in figure 5.6, it can be concluded that the loading condition of the vessel is responsible for how big of an impact load can develop and that slam events themselves are less influenced by the loading conditions of the vessel.

Although the number of slams in the simulation gives interesting results, the probability of occurrence cannot be defined. The simulations are only 100 seconds long and a random selection of wave phases is selected so that the total wave elevation is only a small snapshot of what a ship encounters at sea. To say something about the probability, a much longer simulation is required. The number of slams can only say something about how easy it is for a slam event to develop on the vessel.

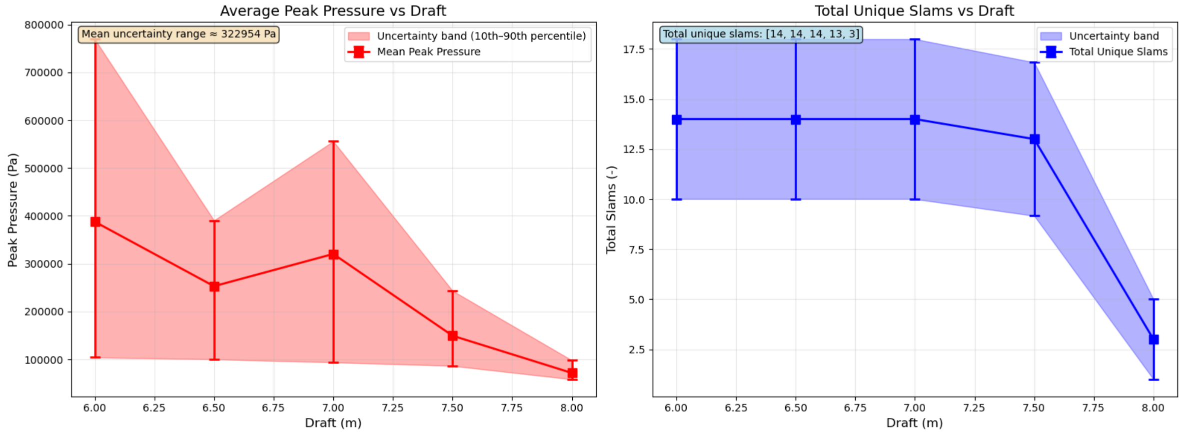

Figure 5.6: The average peak pressure for each loading condition of the vessel on the left and the number of slams for each loading condition on the right for Beaufort 4 wind condition with a standard deviation uncertainty over the data.

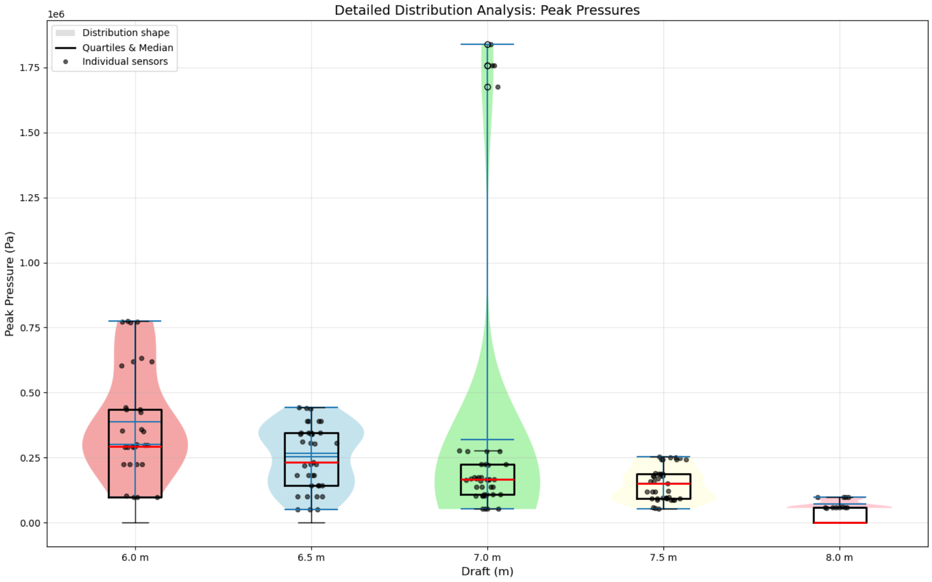

Figure 5.7: A boxplot of all data for the simulations related to the Beaufort 4 weather conditions with a H_s = 1.1 meters and a T_p = 4.6 seconds. It shows the statistics for each loading condition as well as the data spread of each loading condition.

5.2.2. Simulations for H_s = 1.65 m and T_p = 5.1 s

The Effect of Loading Conditions of the Vessel on the Peak Pressure and Number of Slams

The results of the simulations with a H_s of 1.65 meters and a T_p of 5.1 seconds, the results can be found in figure 5.8. In contrast to the results of the other weather condition, the average peak pressure on the stern decreases significantly when the draft of the vessel increases. What can be seen from the CFD simulation is that the waves are too high and cannot fully develop a slamming event underneath the stern. An increase in draft results in less space between the bottom plate of the stern and the free surface of the water. A draft of 6 meters seems to have the space for the higher waves to hit the stern harder. What can also be seen is that the design draft in this case is not enough to prevent slamming altogether. An average peak pressure of around 250 kPa is still a significantly high value.

The red area represents the standard deviation of the data from the CFD simulations. As can be seen, the deviation of the results at a draft of six meters is much higher. This is because the peak pressures of the slam events in this simulation are more spread out compared to the other loading conditions.

This can be better seen in the boxplot of the data from the simulations. In figure 5.9, it can be seen that the data of the peak pressures of every slam for the simulation of 6 meters is spread out a lot. Higher drafts show a cluster of peak pressures with no outliers.

The number of slams in each simulation also shows an interesting trend. Till a draft of 7 meters the number of slams stays around the same number, but for a bigger draft it gradually decreases. The number of slams at a draft of 8 meters is half of that for a draft of 7 meters, but the average peak pressure is more or less the same. Clustering has more of an effect on the design draft. Not every wave builds up to a slam event, but it creates circumstances for the next wave to line up perfectly for a slam event.

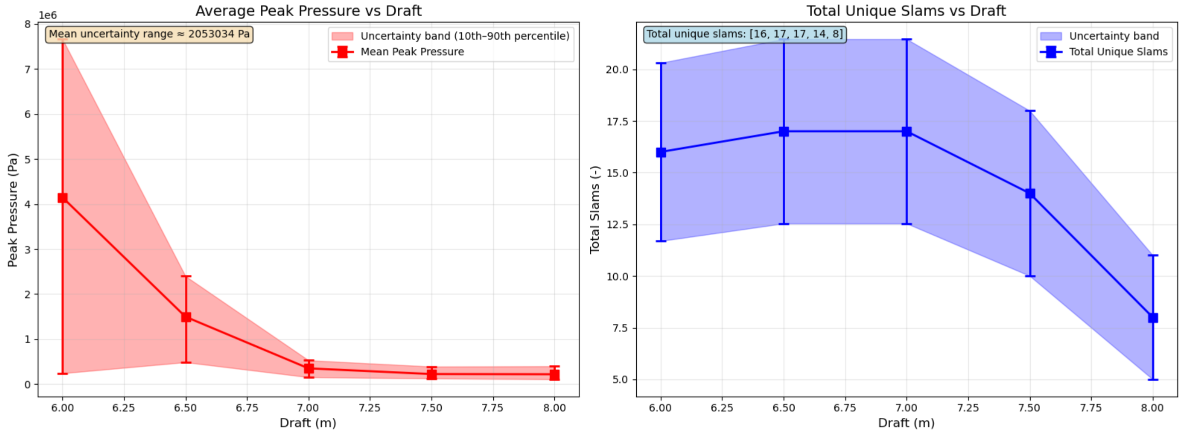

Figure 5.8: The average peak pressure for each loading condition of the vessel on the left and the number of slams for each loading condition on the right for Beaufort 5 wind condition with a standard deviation uncertainty over the data.

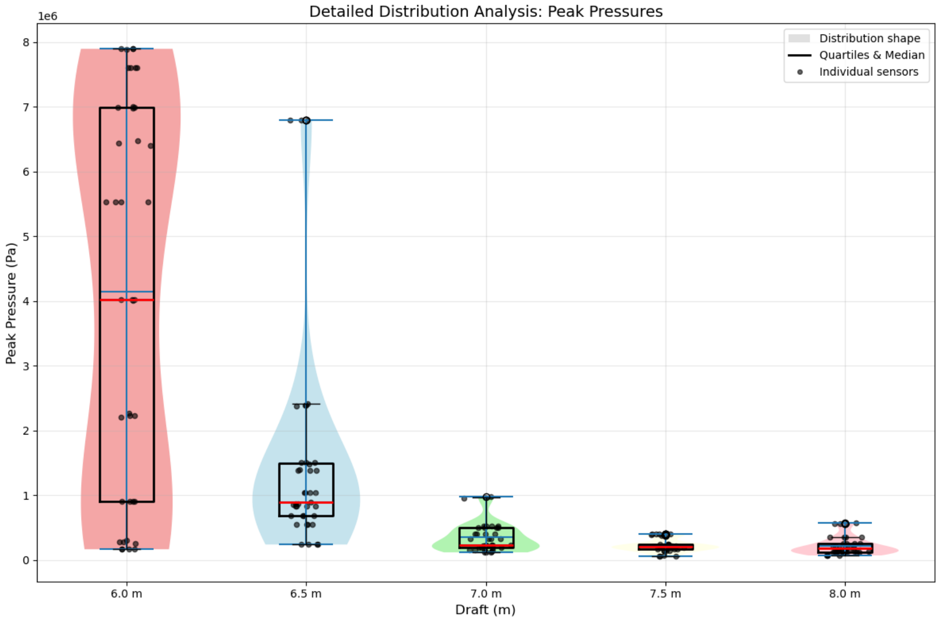

Figure 5.9: A boxplot of all data for the simulations related to the Beaufort 5 weather conditions with a H_s = 1.65 meters and a T_p = 5.1 seconds. It shows the statistics for each loading conditions as well as the data spread of each loading condition.

5.3. Effect of Vessel Trim on Slamming

Like the draft of the vessel, the trim of the vessel can also be altered by ballasting for a specific project. A change in trim is expected to change the behaviour of stern slamming. To identify the effect of trim, the limits of the trim of the vessel must be known first. Stability guidelines of the vessel prohibit the vessel from exceeding a trim of 1.683 meters above draft at the stern and 0.683 meters at the bow compared to the midship. The maximum angle of trim can be calculated using the following equation.

$$\theta = \arcsin \frac{max(T_{trim})}{LCG} \tag{5.1}$$

By filling in the values of the vessel in equation (5.1), it can be calculated that the maximum value of θ is equal to a maximum of 1.33 degrees. This change does not change the geometry of the stern as much so that significant changes in slamming behaviour can be detected due to the uncertainty of the CFD model. Therefore, it is assumed that the effect of trim on slamming is the same as the change in draft. Trim at the stern results in a locally bigger draft and trim at the bow results in a lower local draft at the stern, so depending on the trim of the vessel, it follows the same trend as shown in **??** and figure 5.8.

5.4. Effect of the Wave Period

In section 3.2 it is explained and shown how the motions of the vessel are determined. However, the motions of the vessel are very low. This is due to the fact that the peak of the JONSWAP spectrum is way outside the peak of the RAOs of the pitch and heave motion. Still, the ComFLOW results show considerable slam events. The slamming events are more dependent on the waves encountered by the vessel. To further analyse the effects of waves on stern slamming, wave parameters are altered and the motion of the vessel itself.

The only real wave parameters that can be changed are the significant wave height and wave period. Since changing wave height is not logical due to the operational limits of the vessel laying on dynamic positioning, the only wave parameter that is varied is the wave period. In table 3.2 two different wave periods are given for the wind conditions. The values are both chosen for a simulation. Next, there are three other wave periods chosen, separated by the same delta as the wave periods in table 3.2. In the table below an overview of the different wave periods is given.

Table 5.2: The different peak wave periods used to test the effect of wave period on slamming pressures.

$T_{p,1}$	$T_{p,2}$	$T_{p,3}$	$T_{p,4}$	$T_{p,4}$
4.4	4.75	5.1	5.45	5.8

When the simulations have been performed for every wave period, it can be observed in figure 5.10 that for low and high wave periods, the average peak pressure is significantly higher than the wave periods in the middle. For the lowest wave period, the average pressure is ±290 kPa and the highest wave period is ±250 kPa. This is higher than the base (middle) wave period, where the average pressure is 220 kPa. A possible explanation is that for higher wave periods, the vessel motions are higher due to the peak of the spectrum shifting more towards the peak of the RAOs. The higher value for lower wave period could be explained by the increase in wave steepness.

In order to analyse the hypotheses, the same simulations are performed again without any vessel motions added to ComFLOW. The vessel is now static and slamming can only occur due to the incoming waves. When the simulations are performed and laid over the results with vessel motions, it is clear that the average peak pressure across all wave periods is higher for the static case compared to the dynamic case. The difference lies between the 25.7% and 46.1% compared to the dynamic case. The reason for the lower peak pressures for the dynamic case is that in this sea state, the motions are mostly in phase with the wave elevation. This can result in a lower relative velocity resulting in a damping effect. During more extreme weather conditions, motions will add to the slamming pressures.
What can also be seen from the static case is that, again, the same trend can be observed as in the

dynamic case, where low and high wave periods result in bigger averages. This confirms that this behaviour is in some way caused by the waves themselves encountered by the vessel.

When looking at the number of slams for each simulation, there is not a lot of difference. The higher wave periods give a lower number of slams, but there are also fewer waves in total during the simulation, so the difference is negligible. The wave period does not have an influence on the number of slams encountered by the vessel, so it can be concluded that for this part of the spectrum, wave period does not increase or decrease the number of slams.

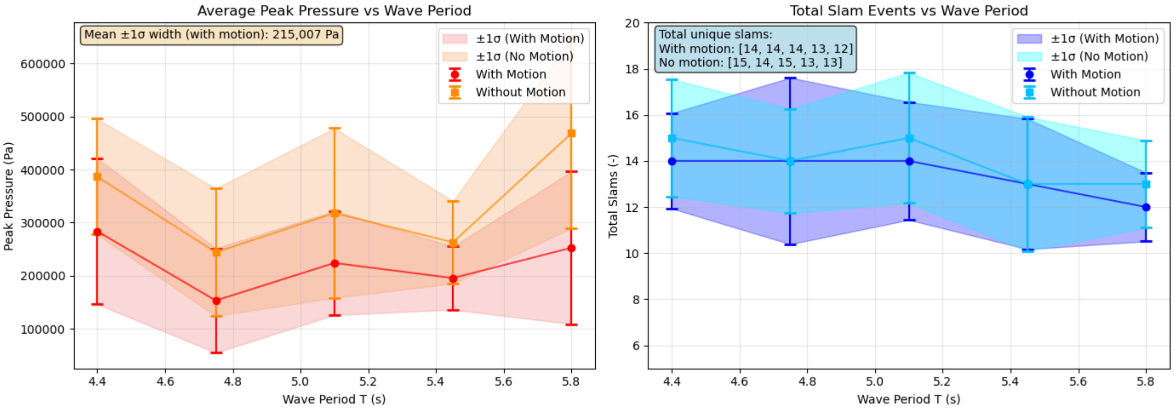

Figure 5.10: This figure represents the influence of the peak wave period of the spectrum on the slamming pressure. The orange data represents the results based on the simulation without any vessel motion and the red data represents the results of the simulation with vessel motions. On the right is the number of slams plotted. The light blue is the data without any motions and the dark blue is for simulations with motions.

5.5. Identifying Optimal Loading Condition

It is clear from the previous CFD simulations that a deeper draft is beneficial for reducing the slamming responses. This is due to the fact that the overhang of the stern is partly to fully submerged. However, regulations prohibit the vessel from reaching a bigger average draft of 7.5 meters so the stern is always above the waterline.

To tackle this, trim can be used to get the stern submerged without going deeper than a draft of 7.5 meters. In the following simulation, the draft is set at around 7.5 meters on average and a trim of one meter on the stern of the vessel. The results of this simulation can be seen in figure 5.11.

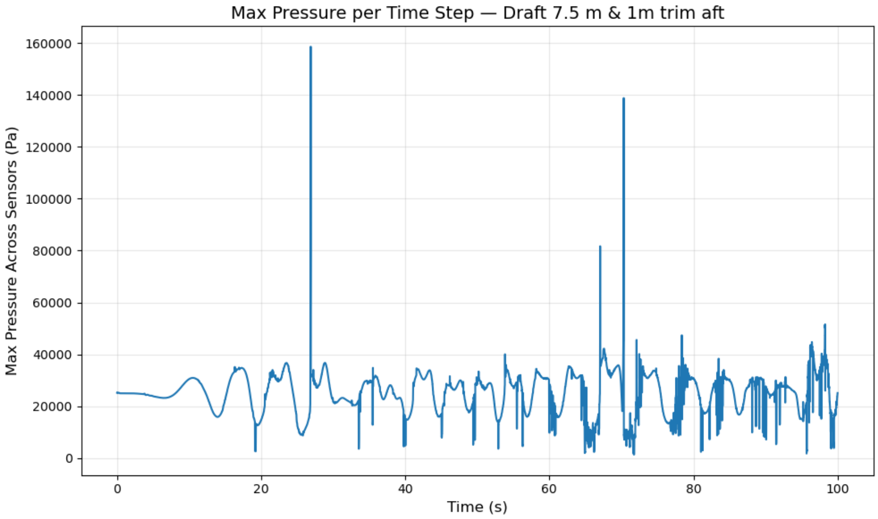

Figure 5.11: The pressure readings of the simulation with an average draft of 7.5 meters and a trim of one meter on the aft of the vessel.

From figure 5.11 it can be observed that this loading condition does not create a lot of slamming on the stern. This case is performed with a sea state of 1.65 meters and a period of 5.1 seconds. It can be seen that one real slam is observed with a maximum of 160 kPa highlghting the fact that slamming can still occur with this loading condition. The other peaks can be neglected since the duration is too small and are probably single error events. The reduction of the total number of observed slams compared to the even keel simulation with a draft of 7.5 meters is 93% and 87.5% compared to an even keel with a draft of 8 meters. During operations this loading condition is best for reducing slamming in general thus results in less vibrational responses.

5.6. Verification of the Model

Because a CFD model is used to analyse the fluid behaviour, it must be validated in order to see if this model solves the problem at hand correctly. However, verifying the results will not be possible. This CFD simulation is made on true vessel scale with a pre-described wave and motion input. There are no model tests or real-life experiments performed on this problem to compare the results of both methods to see if they correlate. Therefore, the results can not be verified properly.

However, the method can be validated by performing a convergence study. In this study, three different grid sizes are used and run. The difference in the values of the results can indicate whether the grid size was sufficiently defined to capture slamming. For this convergence study, three different grid sizes were used for the simulation with a draft of 7 meters. These are displayed in table 5.3. It can be observed that the medium grid does not have a lot of extra grid cells compared to the coarse simulation. This is because they are the same simulation, but the course simulation has no refinement around the stern and free surface where the monitoring points are.

Table 5.3: Three simulations with different grid sizes used for a simulation with a H_s = 1.65 meter and a T_p = 5.1 seconds.

	At slam location		Whole domain
Simulation refinement	Relative grid size	True grid size	Number of cells
Course	1.0	0.197	102000
Medium	0.5	0.0985	139872
fine	0.25	0.0493	555825

All three simulations are run with the computation time varying from a few hours for the coarse simulation to a whole week for the fine simulation.

In order to analyse the convergence of the CFD, the Richardson extrapolation method is used to determine the exact solution of the CFD based on the grid sizes. This exact solution is based on what the result will be for an infinitely small grid size and can be calculated using equations (5.2) and (5.3) [33].

$$p = \ln \frac{F_{x,c} - F_{x,m}}{F_{x,m} - F_{x,f}} / \ln(r) \tag{5.2}$$

$$f_{exact} = F_{x,f} + \frac{F_{x,f} + F_{x,m}}{r^p - 1} \tag{5.3}$$

This extrapolation is applied to the average peak pressure, the maximum observed peak pressure, and the number of slams. The results can be seen below. In this figure, the value of the Richardson extrapolation, grid convergence index and the order of convergence, p, can be seen.

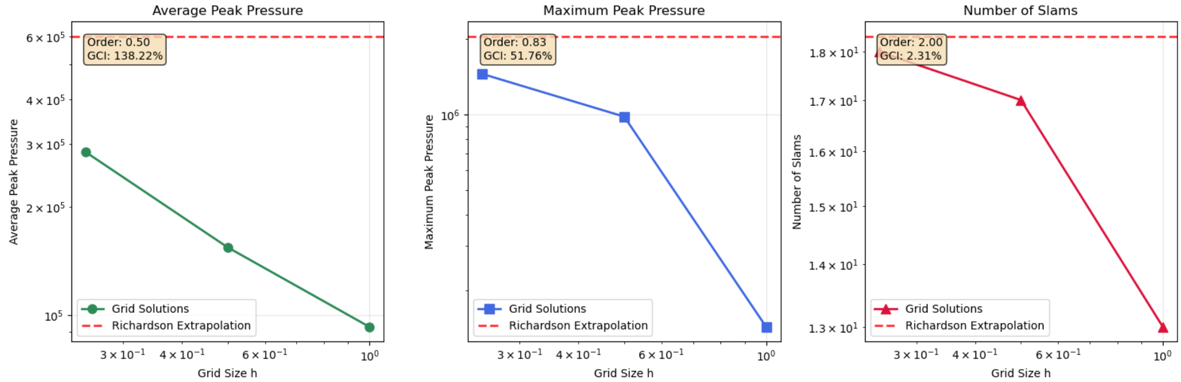

Figure 5.12: The convergence results with the Richardson extrapolation given as the red dotted line. On the left the average peak pressure calculated for every simulation, in the middle the maximum detected peak pressure and on the right the counted number of slams.

From figure 5.12 it can be concluded that the average peak pressure and the number of slams do not show any convergence. The Richard extrapolation is also plotted in each study and shows that the grid sizes are not close to that value. To put that in more context, the Grid Convergence Index, or GCI, can be calculated for the change in grid size with the equation below.

$$GCI_{f,m} = 100\% \cdot 1.25 \frac{\left| \frac{(F_{x,f} - F_{x,m})}{F_{x,f}} \right|}{(r^p - 1)} \tag{5.4}$$

$$GCI_{m,c} = 100\% \cdot 1.25 \frac{\left| \frac{(F_{x,m} - F_{x,c})}{F_{x,m}} \right|}{(r^p - 1)} \tag{5.5}$$

When these equations are used, the following results are in figure 5.13. It is clear that for the change from the medium grid to the fine grid, higher values are obtained for the average peak pressure compared to the change from a coarse grid to the medium grid. This is not optimal and shows that values do not converge yet. The maximum peak pressure does converge, but it is still way above the threshold of 5% to prove that the CFD simulation is converged. The number of slams is fully converged. The fine grid only has one extra counted slam compared to the medium grid and the GCI value is for the change from medium to fine 2.31%. This is below the 5% threshold, so this value is converged.

For the hydrodynamic results, the medium grid was chosen. As this convergence study shows, the results are not converged and the value of the pressure impulses needs to be considered as higher values in real life. However, the main goal was to identify the influence of loading conditions of the vessel on the slamming behaviour. This is still valid because the error related to convergence is applicable to all simulations and the number of slams is converged, meaning that the basic interaction between vessel and fluid does not change. Also, the fluid behaviour of what causes the slamming is still valid. For the input into the structural model, the error due to the model not being converged needs to be considered, since in that part, the values of the pressures on the hull start to matter much more.

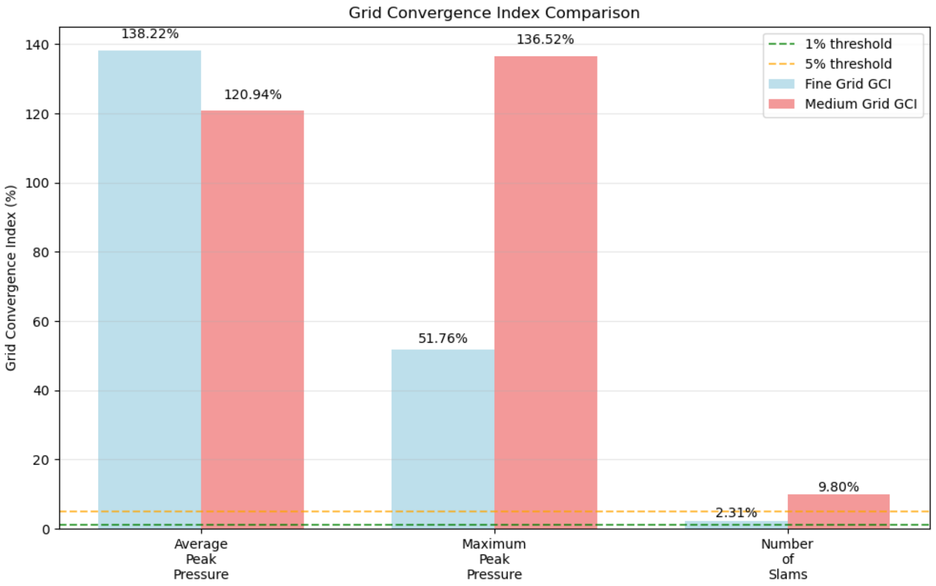

Figure 5.13: The grid convergence index for each calculated value. As can be seen all except the number of slams are well above the threshold for convergence meaning the CFD simulations are not converged.

Table 5.4: Overview of the results from the convergence study

Quantity	Fine Grid	Richardson	GCI (%)	Status
Average Pressure	251780.0	506069.9	126.25	Not converged
Maximum Pressure	1454418.0	2056700.7	51.76	Not converged
Number of Slams	18.0	18.3	2.31	Converged

6

Results of Structural model

By using the theory explained in chapter 4 and the simulated and fitted input values of the slam and hydrodynamic coefficients of the vessel which are explained in appendix B, the responses can be calculated. In this chapter, the responses of the vessel, using a simulated slam based on the results from ComFLOW, are calculated and analysed. These results are used to see if these weather conditions could lead to global vibrational responses big enough to cause mechanical failure or discomfort.

6.1. Modal Results

For this study, the first four non-rigid modes were chosen to analyse the vibrations of the vessel due to slamming. To test if this choice is sufficient, a modal analysis is performed to see the results for each mode individually.

Figure 6.1 illustrates the modal displacement contributions over time, calculated using both Duhamel and Cummins methods. Mode 1 exhibits the largest displacement amplitude and a relatively slow decay, indicating its dominant contribution to the overall transient response. The second and third modes also show significant oscillatory behaviour with smaller amplitudes and faster decay rates compared to the first mode shape. The contribution of Mode 4 to the displacement is notably small, suggesting its limited influence on the system's dynamic behaviour under the given conditions.
Figure 6.2 displays the frequency response for both displacement and velocity. These plots reveal the system's resonant frequencies, where the largest magnitudes of response occur. It can be observed that the frequency is mainly lower than the first mode, but it peaks at the second mode, suggesting the second mode is excited better than the first mode shape. While the shapes of the displacement and velocity FFTs are similar, their magnitudes differ as expected due to the derivative relationship between velocity and displacement in the frequency domain, with velocity generally showing proportionally larger magnitudes at higher frequencies.

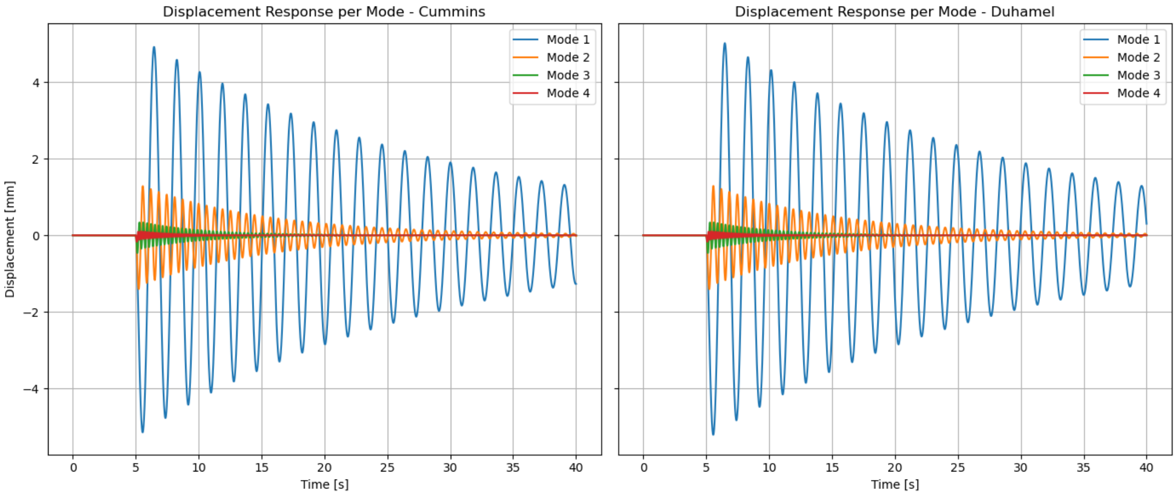

Figure 6.1: The displacement calculated for each mode individually. As can be seen is the contribution of mode four is very small.

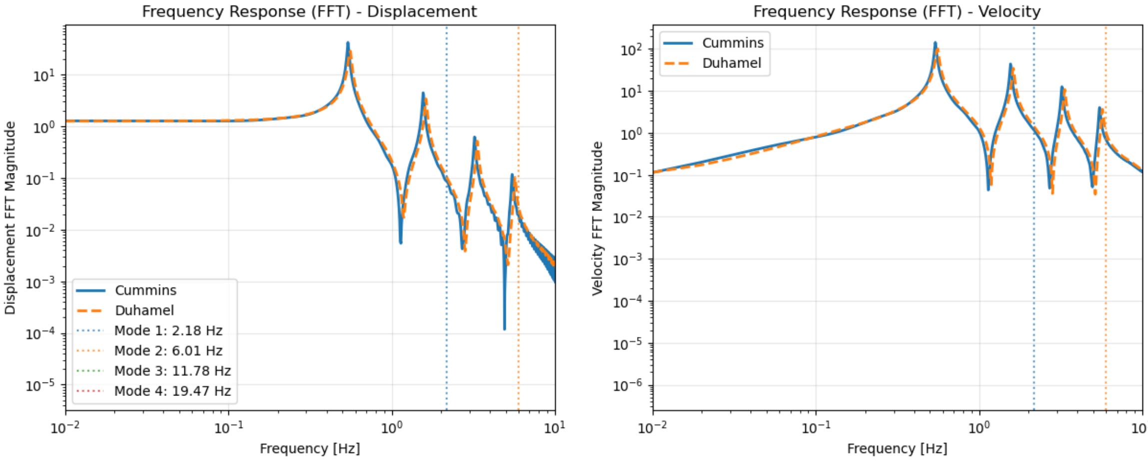

Figure 6.2: The frequency response spectrum of the displacement on the left and velocity on the right. The content is mainly low-frequency-based in the region of the first two modes.

6.2. Effect of Weather Conditions on Responses

From ComFLOW, a picture is drawn on how the weather and sea state conditions play a crucial role on the maximum pressure a wave load can excite on the vessel. To see the effect of the loads on the vessel, a simulated slamming pulse is placed on the stern of the vessel for each loading condition. This simulated load is modelled using a rise equation and a decay equation and is further described in appendix B. The rise time of the slam is 0.02 seconds and the decay time is 0.1 seconds which is common with the observed slam behaviour in ComFLOW. The peak pressure is chosen according to the output of ComFLOW for the different sea state conditions.

6.2.1. Response Over Time

Response of H_s = 1.1 m and T_p = 4.6 s

For the simulations related to the sea state where the significant wave height is 1.1 meters and the peak period is equal to 4.6 seconds, most slams were in the range of 150 kPa to 450 kPa. To analyse the vibrational responses for this sea state, a series of pressures for the slam event was chosen. These are equal to 150 kPa, 300 kPa and 450 kPa respectively. There were also higher slam pressures recorded, but these were more common in the other sea state. These higher pressures are analysed for the sea state with a significant wave height of 1.65 meters and a peak period of 5.1 seconds.

For the lower peak pressures, the global displacement, velocity and accelerations were calculated for the structure. The responses are calculated using both the Cummins equation and the Duhamel convolution. In figure 6.3, the displacement at the end of the beam is plotted for the Cummins equation and Duhamel convolution. figure 6.4 shows the response of the beam in the velocity for both Cummins and Duhamel. figure 6.5 shows the acceleration at the far end of the beam. These results are the sum of the first four bending modes of the free-free beam. Time domain responses for other locations can be found in appendix C.

As expected, the displacement increases with pressure amplitude, reaching around ± 3 mm for the 450 kPa case. The velocity peaks around ± 18.5 mm/s, and the maximum acceleration approaches 0.38 m/s^2 before it quickly decays to small accelerations.
The results from the Cummins and Duhamel methods show close agreement in all cases with a maximum deviation of 0.68% for the velocity and 2.43% for the displacement, validating both approaches. Minor differences in velocity and acceleration are likely due to numerical integration effects. All responses decay relatively smoothly, indicating effective damping and the dominance of the first mode in the structural response. The steps you see in the decay are caused by the J-factor applied to the modal added mass. This factor causes higher modes to have overall less significant damping which results in different transient behaviour compared to the lower modes.
Both methods need to converge towards a steady state solution since the memory kernel has not been built up yet just after the slamming loads are applied. This is also why a big peak in acceleration just after the loads is probably not caused by the load itself, but by the numerical instability. There is also a change in phase between Duhamel and Cummins observed. This is probably caused by the fact that the slam load contains multiple frequencies and both methods do not handle this well due to the hydrodynamic coefficients. Duhamel is slightly worse since damping in that model is also dependent on the input frequency. These are the wet natural frequencies per mode which are superimposed, which ensures a good approximation of the zeta values, but might underestimate non-linear effects.

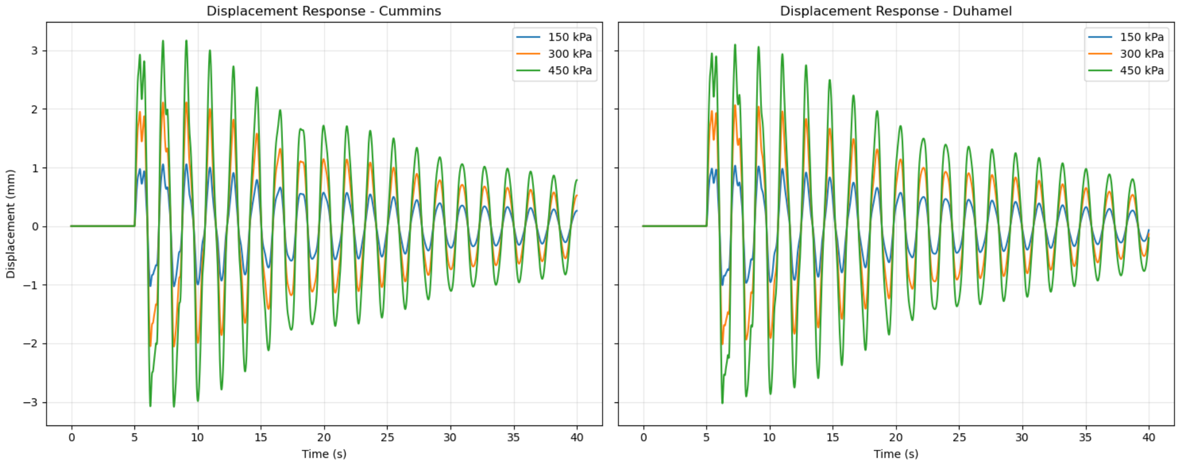

Figure 6.3: On the left is the displacement on the far end of the beam calculated using the Cummins equation. On the right is the displacement over time calculated using the Duhamel convolution.

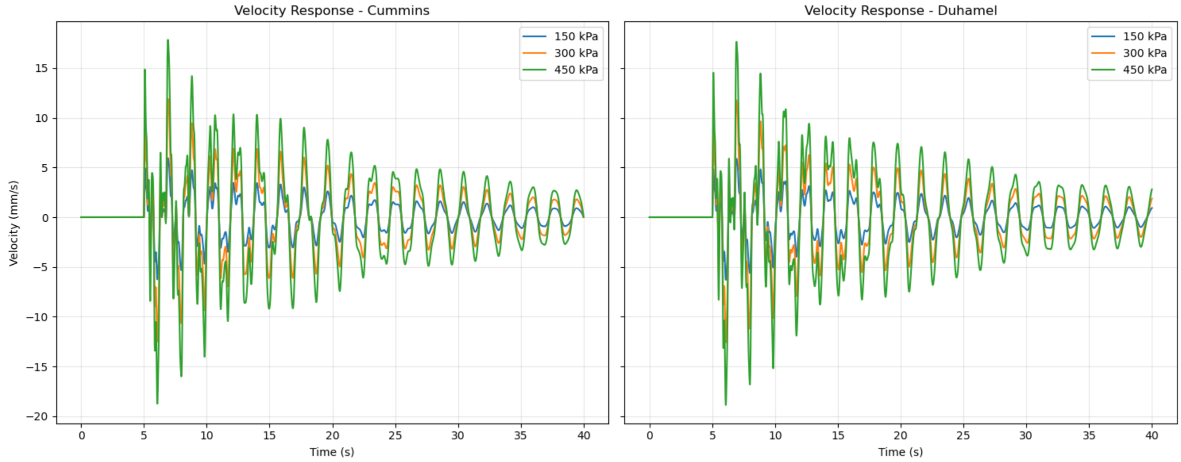

Figure 6.4: On the left is the velocity on the far end of the beam calculated using the Cummins equation. On the right is the velocity over time calculated using the Duhamel convolution.

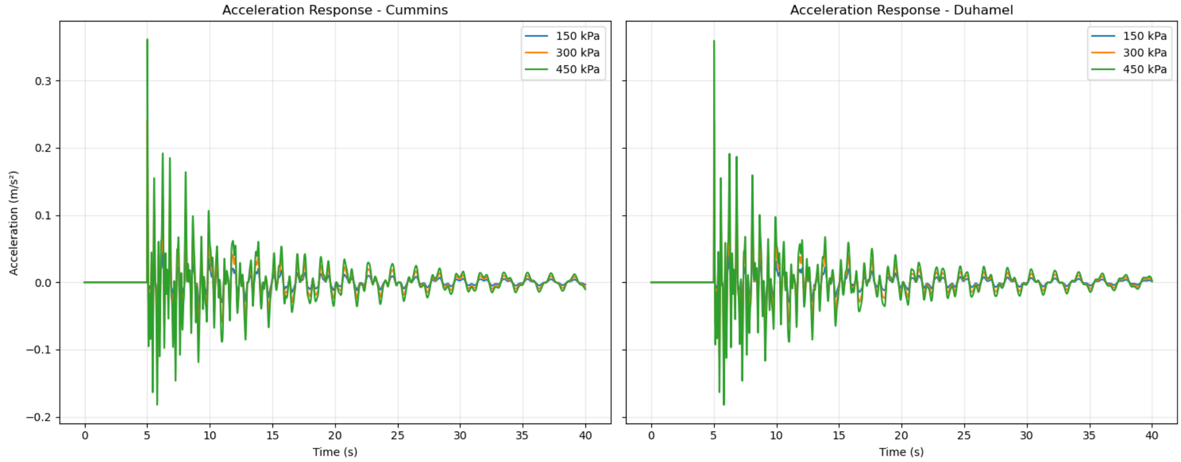

Figure 6.5: On the left is the acceleration on the far end of the beam calculated using the Cummins equation. On the right is the acceleration over time calculated using the Duhamel convolution.

Response of H_s = 1.65 m and T_p = 5.1 s

During the simulation, where the significant wave height is 1.65 meters and the peak wave period is 5.1 seconds, the number of extreme slams is much higher than in the other sea state conditions. Also, the average peak pressure is much higher than the other sea state. Because of this, the range of peak pressures for this sea state is used to analyse the vibrational response during slamming pressures in the higher end of the spectrum. For this analysis, the pressures are chosen to be 750 kPa, 1500 kPa and 4200 kPa respectively. Although 4200 kPa is really high and does not occur much in the simulation, it must be included since those slams have the biggest impact on the structure. Therefore, the results will be more critical for the vessel.

For the higher peak pressures, the global displacement, velocity and accelerations were calculated for the structure. The responses are calculated using both the Cummins equation and the Duhamel convolution. In figure 6.6, the displacement at the end of the beam is plotted for the Cummins equation and Duhamel convolution. figure 6.7 shows the response of the beam in the velocity for both Cummins and Duhamel for the higher pressures. figure 6.8 shows the acceleration at the far end of the beam for the higher pressures. Time domain responses for other locations can be found in appendix C.

At 750 kPa, the peak displacement reaches around ± 5 mm, increasing to roughly ± 10 mm at 1500 kPa, and up to approximately ±28 mm for the 4200 kPa slam case. These values demonstrate a linear increase in amplitude when the peak of the pressure is increased. Both Cummins and Duhamel also agree very well for the higher slamming loads with deviations again below 2.5% for the velocity. However, the further in the simulation there is some deviation between the methods. This is caused by damping in the Duhamel convolution. This does not consider non-linear damping effects like the Cummins tries to model with the retardation function, but it still shows good agreement with Cummins. In terms of velocity, the response peaks around ±35 mm/s for 750 kPa, ±50 mm/s for 1500 kPa, and reaches nearly ±155 mm/s for the 4200 kPa slam. These high velocities indicate strong inertial excitation of the structure, particularly under extreme slamming events.

The acceleration response shows even sharper scaling: approximately 1.3 m/s^2 for 750 kPa, 2.8 m/s^2 for 1500 kPa, and a peak of about 3.3 m/s^2 for the 4200 kPa case. These high accelerations are significant and may influence both structural integrity and onboard equipment performance.

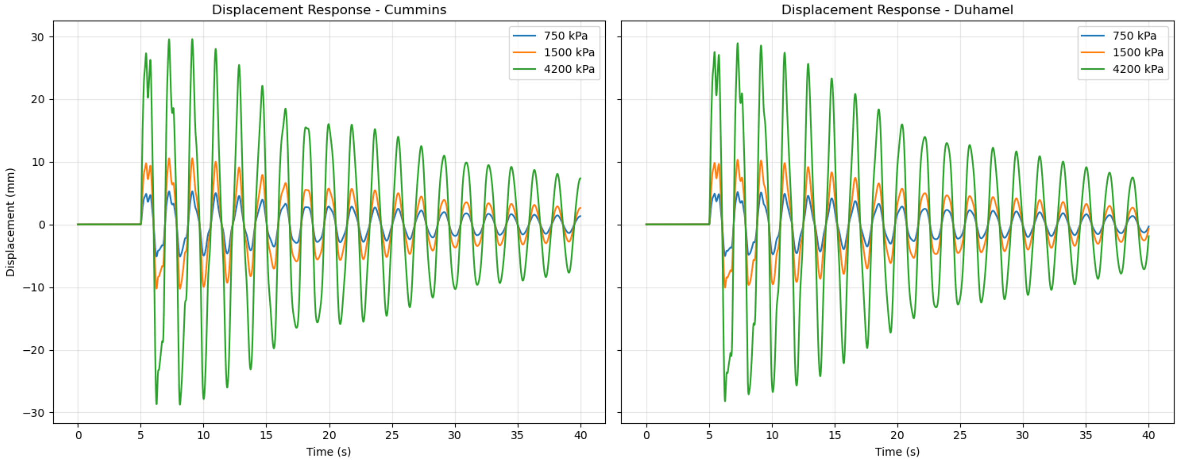

Figure 6.6: On the left is the displacement on the far end of the beam calculated using the Cummins equation. On the right is the displacement over time calculated using the Duhamel convolution.

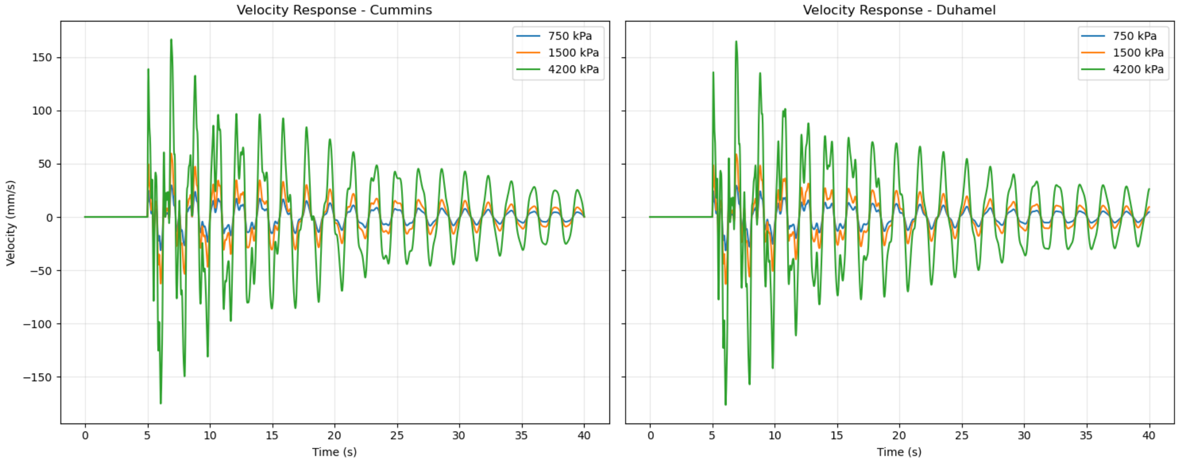

Figure 6.7: On the left is the velocity on the far end of the beam calculated using the Cummins equation. On the right is the velocity over time calculated using the Duhamel convolution.

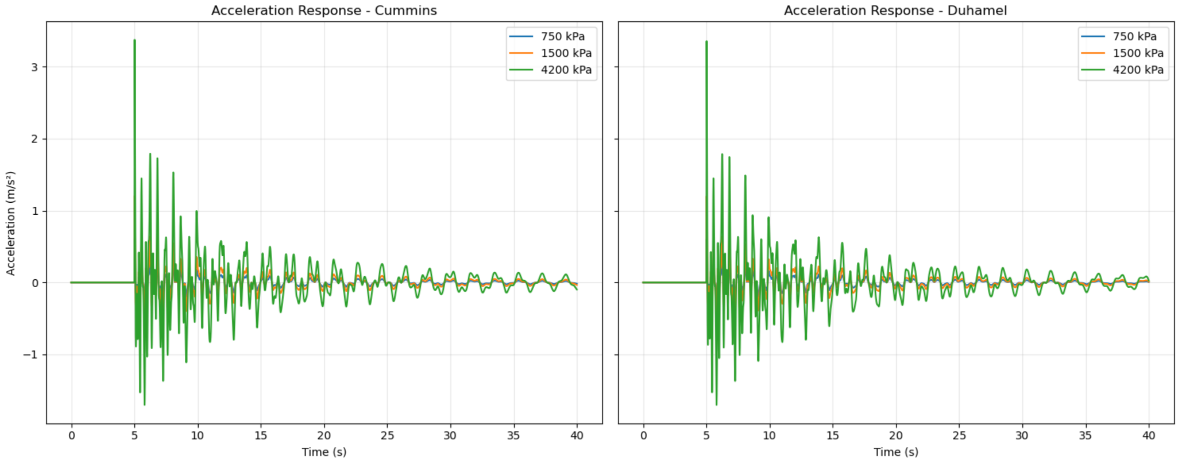

Figure 6.8: On the left is the acceleration on the far end of the beam calculated using the Cummins equation. On the right is the acceleration over time calculated using the Duhamel convolution.

6.2.2. Root Mean Square Value

In the previous figures, the true responses at the end of the beam are shown. This results in sinusoidal responses after both methods are converged. For vibrations, the best response to analyse is the velocity. This is because vibrations are caused by the flexural modes and therefore the local displacements are very low. Since the first modes where the vessel is most excited are not high enough to create high-frequency responses, the accelerations will be relatively low. This can be seen in figures 6.5 and 6.8. Therefore, the vibrational response will be underestimated and velocity provides a better picture of the bending vibrations. Also, regulations related to the vibrations on board a vessel are always given in mm/s For example, DNV states that RMS values for vibrations should not exceed 4.5 to 6 mm/s in accommodation and work spaces. DNV also states that the equipment of the thruster should not endure values higher than 18 mm/s for a longer period of time to minimise the risk of failure. [2]

Since the vibrations always result in an oscillating behaviour, the root mean square value provides a better indication of how hard the vessel vibrates. These values are also better to compare to regulatory limits set by class societies such as DNV or Lloyds. The RMS is calculated using a sliding window approach of fixed length N, corresponding to a duration of 2 seconds in physical time.

$$\text{RMS}(t_i) = \sqrt{\frac{1}{N_i} \sum_{j=i-N_i+1}^{i} x(t_j)^2} \tag{6.1}$$

This definition applies a moving average over a squared signal and then takes the square root, effectively measuring the local response of the signal within the sliding time window. It provides a smoothed representation of the vibrational magnitude, capturing how the system responds over time while filtering out short-term oscillations. The choice of a 2-second window balances temporal resolution with stability in the RMS estimate.

RMS Response of H_s = 1.1 m and T_p = 4.6 s

At 150 kPa, the RMS displacement peaks at approximately 0.7 mm, increasing to around 1.5 mm for 300 kPa, and reaching nearly 2.4 mm at 450 kPa. These values suggest a largely linear scaling of displacement amplitude with increasing peak pressure. The results from both the Cummins equation and Duhamel convolution are in good agreement for all cases, with deviations remaining below 2.55% during the early stages of the response. As time progresses, the difference between the two methods does not change a lot for all results highlighting the good agreement between the models. There is a phase change observed which is probably caused by the fact that Duhamel is not able fully account for the non-linear responses and the added mass terms are only handled for the given frequencies.

The acceleration RMS response also exhibits a consistent increase: roughly 0.03 m/s^2 for 150 kPa, 0.065 m/s^2 for 300 kPa, and about 0.95 m/s^2 at 450 kPa. While these values are lower than in extreme slamming events, they are still indicative of considerable vibrational activity. As with displacement and velocity, the Cummins-based results consistently yield higher values, reinforcing the importance of including fluid-structure interaction in predictive simulations of vibratory response.

In terms of velocity in figure 6.10, the RMS response peaks around ±2.6 mm/s for 150 kPa, increases to approximately ±6.1 mm/s for 300 kPa, and reaches a peak just around 10 mm/s for 450 kPa. These values highlight the dynamic amplification associated with higher impact pressures. More interesting is the relation towards the limits of class rules shown via the red, orange and yellow dotted lines. It is clear that a peak pressure of 150 kPa results in a vibrational velocity below the comfort rules for both accommodation and work rooms. It is clear that a slamming pressure of around 300 kPa exceeds both comfort levels, and a pressure of 450 kPa results in RMS values well above the comfort levels by class societies. Although the RMS values quickly decay towards values below the limits, this is just one single slam event. From the CFD it is clearly visible that waves interact with each other, resulting in a period of periodic slams.

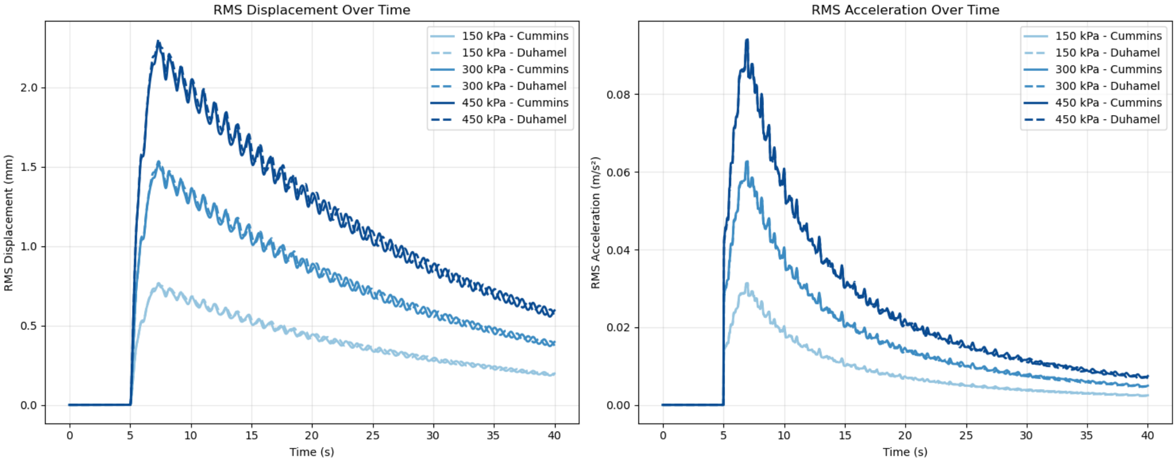

Figure 6.9: The root mean square values of the low peak pressures for the displacement on the left and for the acceleration on the right. The solid line represents the result of the Cummins equation and the dotted line the Duhamel Convolution. These are taken at the ends of the beam.

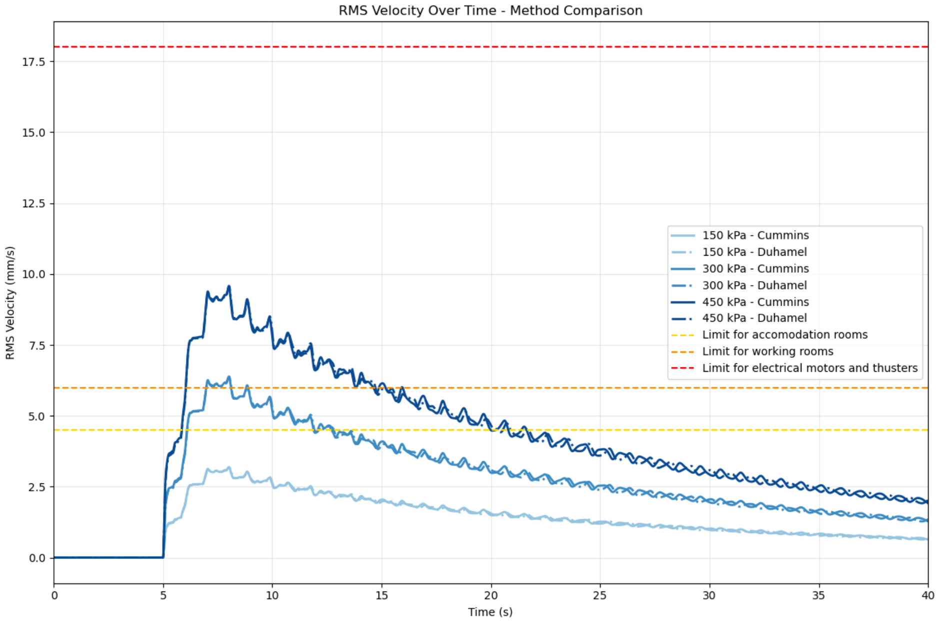

Figure 6.10: The root mean square response over time for the velocity of the low peak pressures. The dotted lines show the RMS values of the Duhamel convolution and the solid lines show the RMS results of the Cummins equation. The red, orange and yellow straight lines show vibrational limits from class rules. These are taken at the ends of the beam.

RMS Response of H_s = 1.65 m and T_p = 5.1 s

For the higher peak pressures related to a sea state with a Hs of 1.65 meters and a Tp of 5.1 seconds the same RMS values for the displacement, velocity and acceleration are calculated. The RMS displacement response shown in figure 6.11 illustrates a marked increase in amplitude as the slamming pressure intensifies. For 750 kPa, the peak RMS displacement reaches around ± 4 mm, rising to ± 7.5 mm at 1500 kPa, and for the 4200 kPa case it reaches above ± 22 mm. This relation in vibrational response remains approximately linear across the tested pressures, indicating that the structural deflection is closely governed by the intensity of the applied hydrodynamic impact.
The acceleration response mirrors this trend: the RMS acceleration climbs from approximately 0.15 m/s^2 for 750 kPa to around 0.3 m/s^2 for 1500 kPa and levelling ± 0.85 m/s^2 at 4200 kPa. Despite the high intensity of the loads, the RMS accelerations suggest that the structural vibrations do not reach high g-forces.

The RMS velocity response, presented in figure 6.12, offers further insight into the vibrational severity of these high-intensity impacts. At 750 kPa, the RMS velocity peaks around 18 mm/s, increasing to roughly 30 mm/s for 1500 kPa, and reaching values near 85 mm/s for the 4200 kPa slam. These elevated velocities are particularly significant as they exceed all vibration limits set by class rules related to the comfort for the crew on board the vessel. The curves show that more extreme slams also reach RMS velocities which could harm possible equipment related to the thrusters. While the response decays steadily, the velocity remains above critical limits for a considerable duration, underscoring the potential for accumulated fatigue or operational disturbances during sequences of repeated slams.

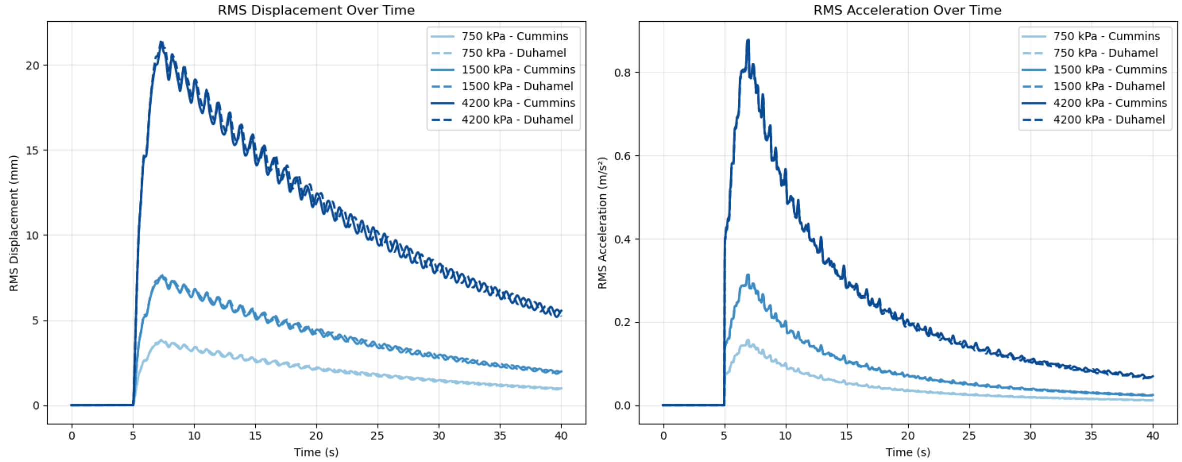

Figure 6.11: The root mean square values of the high peak pressures for the displacement on the left and for the acceleration on the right. The solid line represents the result of the Cummins equation and the dotted line the Duhamel Convolution. These are taken at the ends of the beam.

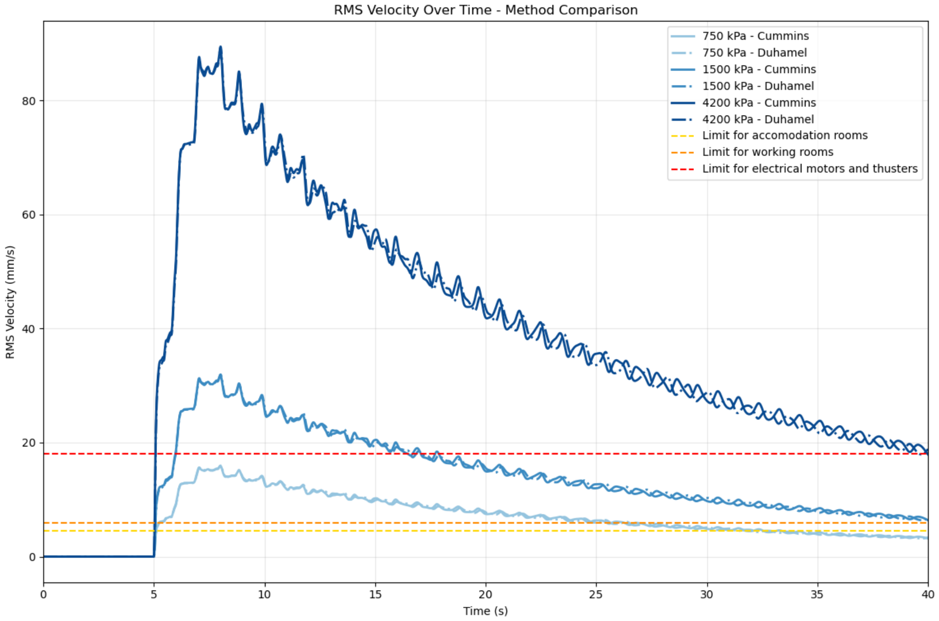

Figure 6.12: The root mean square response over time for the velocity of the high peak pressures. The dotted lines show the RMS values of the Duhamel convolution and the solid lines show the RMS results of the Cummins equation. The red, orange and yellow straight lines show vibrational limits from class rules. These are taken at the ends of the beam.

6.3. Influence of Structural Inertia

In the previous results, it is clear that the slams cause significant vibrational responses, but there is a catch. Since a simulated slam is used, the effect of the structural inertia is somewhat hidden. The pulse might be well enough to properly excite the vessel, but actual slams also have different properties with regards to the rise and decay of the pulse. Some slams might excite the vessel more and some might do the opposite. To test this, the actual CFD values of the loads are used to see how that might affect the responses. For this, the draft of 6 and 6.5 meters are chosen since both simulations contain high outliers in terms of pressure pulses which can be seen in appendix C. Only the Cummins are plotted for a better overview of the results, since the Duhamel approach yields almost identical results.

In figure 6.13, the vibrational responses are shown when the CFD results are plugged into the beam model and some interesting observations can be made. It is clear that inertia plays a big role on the output of the model. The high pressure slams in the CFD may not result in the same vibrational velocities as the simulated pulse, suggesting that some slams are short enough to prevent huge responses due to the high inertia of the hull. However, the velocities are still higher than the limits set by classification societies. This also highlights that convergence of the CFD results does not necessarily result in better estimates for the structural response of the hull since it does not react more extreme to higher pressures.

A more interesting observation is that the vibrations can be sustained by smaller slams. In both simulations, it can be seen that after a big significant slam with big responses, the vessel's vibration is sustained by the smaller slams afterwards, keeping the total response high. In the simulation of a draft of 6 meters the vibration of 20 mm/s is sustained for a longer period of time and the same applies for the simulation of 6.5 meters. After the big slam the response of 60 mm/s is sustained longer by the small slams afterwards. This is probably caused by the fact that due to the high inertia the vessel needs a large initial energy input into the system, but once it is dynamic, smaller energy inputs are enough to keep the system moving, just like a swing.

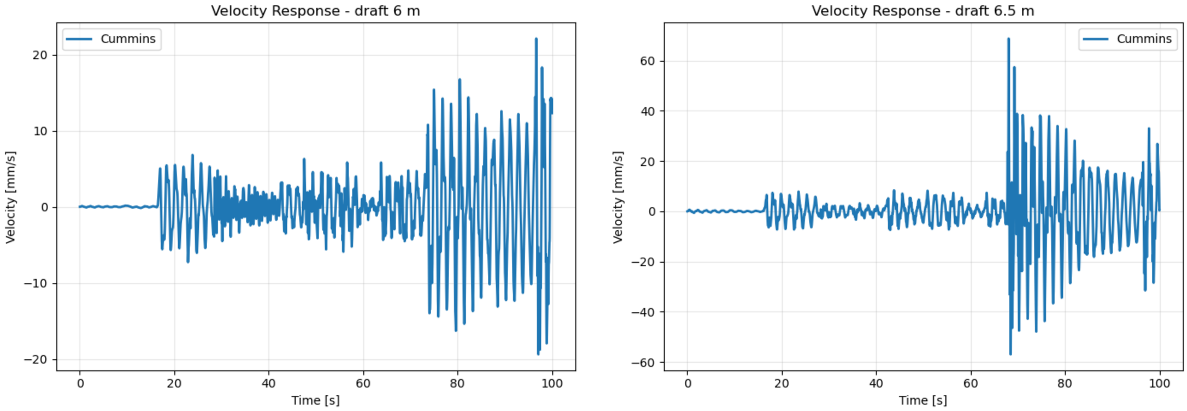

Figure 6.13: The velocity response using the Cummins equation when the CFD results of a draft of 6 meters on the left and 6.5 meters on the right are used.

6.4. Effect of Loading Conditions on Responses

When the vessel is in operation, the loading condition varies for each project, but also during the project. This has an influence on the hydrodynamic coefficients of the vessel. This will result in a different response of the hull when subjected to slamming loads on the stern. To test this, the same slamming load of 1500 kPa is applied to the vessel for each loading condition.

As can be seen in figures 6.14 to 6.16, the effect of the loading condition on the vibrations is minimal. No significant effect is observed. This is due to the minimal changes in the modal hydrodynamic coefficients used in both the Cummins equation and Duhamel convolution. Although the effect of the loading condition on the vibrations themselves is very limited, the loading condition indirectly influences the vibrational responses of the vessel. This indirect influence is caused by the difference in slamming loads due to the loading conditions.

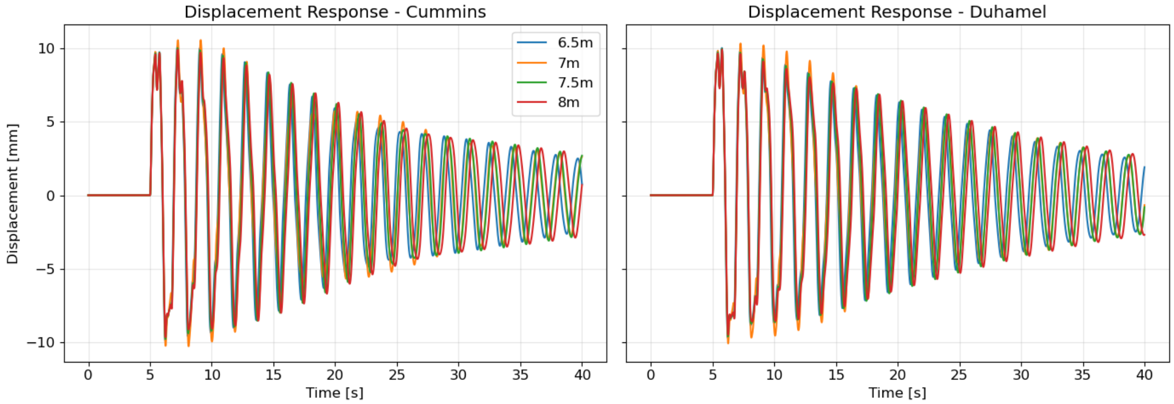

Figure 6.14: The displacement for different loading conditions. On the left via the Cummins equation and on the right via the Duhamel convolution.

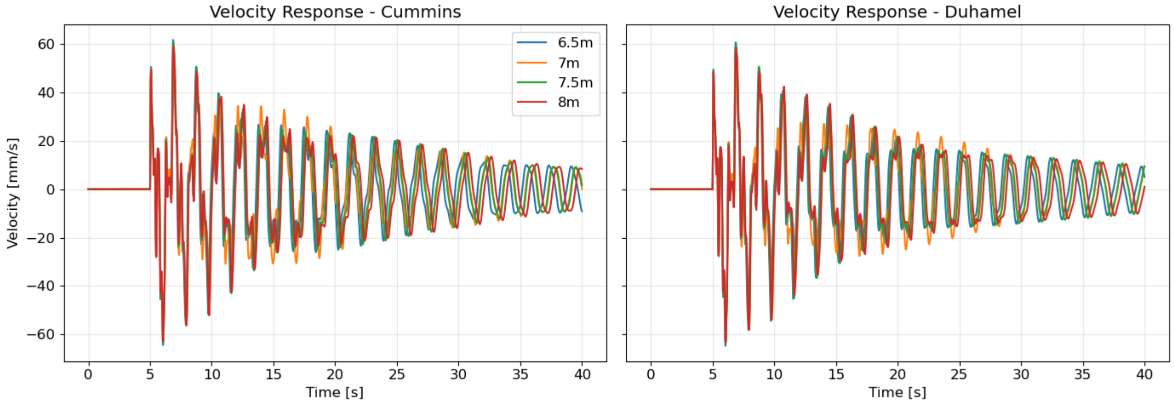

Figure 6.15: The velocity for different loading conditions. On the left via the Cummins equation and on the right via the Duhamel convolution.

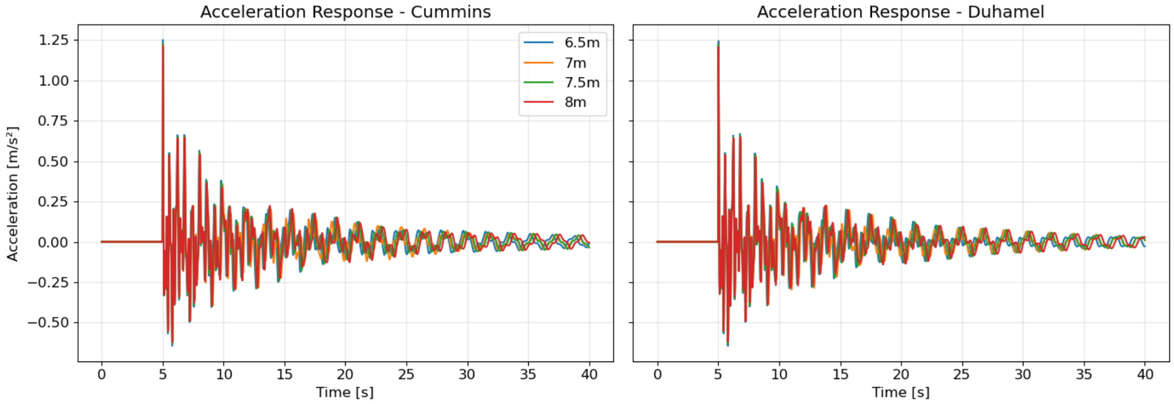

Figure 6.16: The acceleration for different loading conditions. On the left via the Cummins equation and on the right via the Duhamel convolution.

6.5. Response at Different Locations

All of the above results regarding the vibrational responses are based on the variation over time for a certain location. In this case, everything is plotted for the far end of the beam, where like the beginning

of the beam the vibrations are largest. However, the vibrational responses also vary spatially. To see how the responses vary along the length of the beam, a spatial analysis is performed.
In figure 6.17 the velocity is plotted for four different locations on the beam. These locations represent in reality where the engine room, the cranes and the accommodation of the vessel are located. It is clear that the engine room and the accommodation encounter the biggest vibrational responses with peaks of around 40 and 30 mm/s respectively. The cranes are more located in the middle which encounters less vibrations due to dominant mode shapes. It is observed that the cranes encounter a vibrational response of around 25 mm/s just after the load. Results of acceleration and displacement can be found in appendix C.

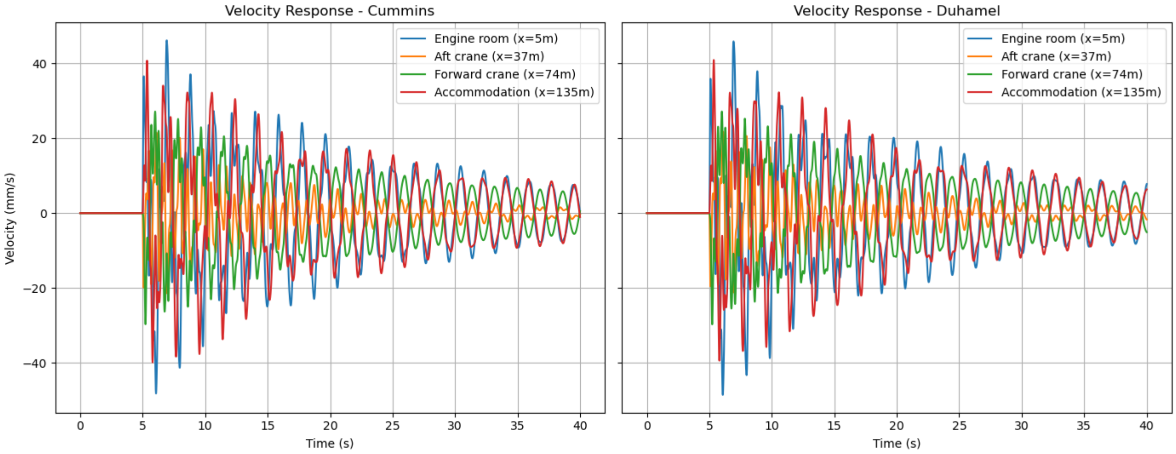

Figure 6.17: The vibrational responses at different locations of the beam. On the the responses calculated using Cummins and on the right the solution using Duhamel.

6.5.1. Distribution Along the Length of the Vessel

The biggest contributing factor to the bending vibrations is the first mode shape. The vessel deflects most in this mode and this is also reflected in the spatial distribution seen in figures 6.18 and 6.19. The stern and the bow of the vessel vibrate the most due to the first mode shape. The highest RMS values of the velocity can be found here and are equal to ±30 mm/s for a load of 1500 kPa on the stern. This is critical since most equipment and accommodations of the vessel are located. This can be seen by the side profile of the vessel plotted in the background of the histograms. The cranes encounter vibrations from 12 to 15 mm/s. The lowest RMS values are observed at around the aft bulkhead and forward bulkhead of the cargo hold. There are small differences between the maximum RMS velocities calculated by Cummins and Duhamel. This is caused by the underestimation of Duhamel of the first mode.

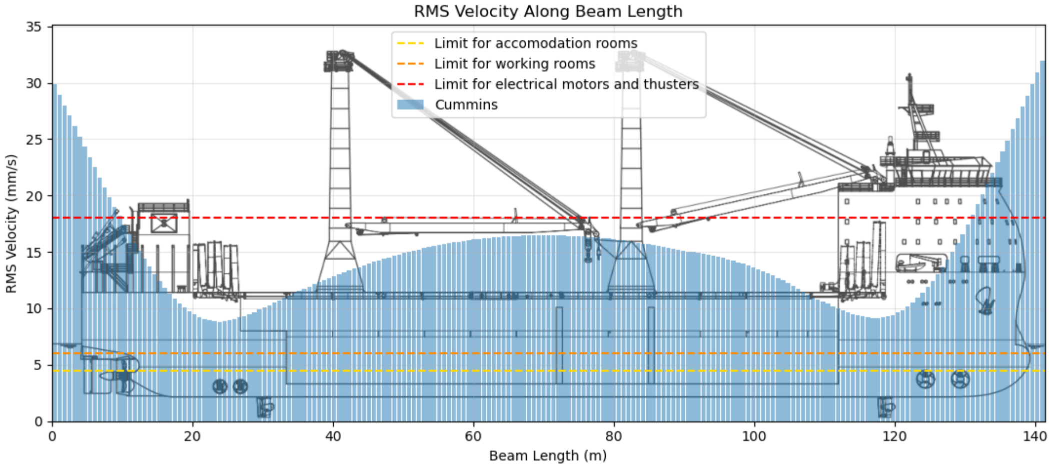

Figure 6.18: The spatial distribution of the maximum RMS velocity in mm/s using the Cummins equation.

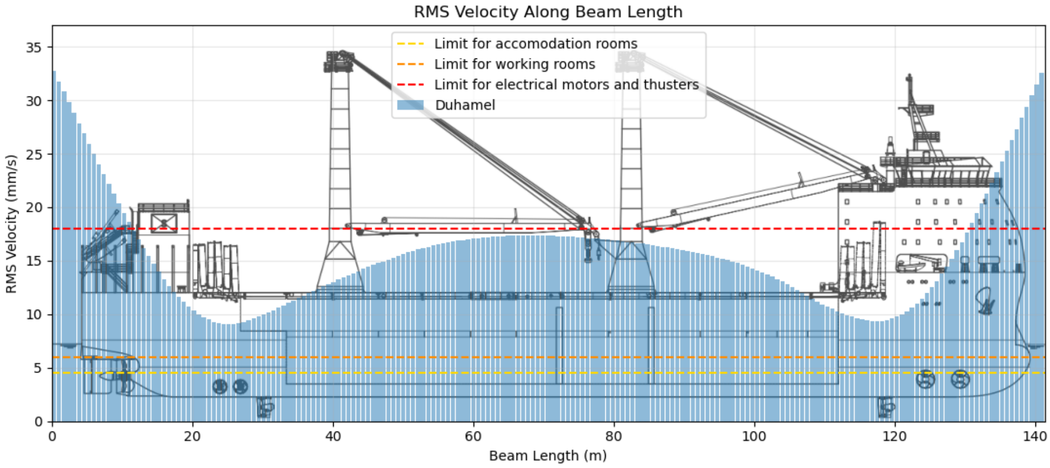

Figure 6.19: The spatial distribution of the maximum RMS velocity in mm/s using the Duhamel convolution.

What can also be observed is that along the length of the vessel, there is always a vibrational response. This is caused by the higher modes, which still play a role in the response. If we separate the spatial responses by mode, the following results in figure 6.20 are observed for a slam with a pressure of 1500 kPa. Although the contribution is much smaller, these modes are also excited by the slamming force. In the plots of the individual modes, the nodes are clearly visible. It also shows the multiple node bending in the higher modes.
The plots of each mode show that apart from the first mode, the second and third modes still show high maximum vibration levels. The second mode shows velocities up to 16 mm/s around the edges of the hull and values up to 11 mm/s between the nodes. The third mode shows velocities up to 9 mm/s at the ends and $\pm$ 6 mm/s between the nodes. The fourth mode shows that the maximum vibrations are lower than the limits set by the class societies.

Even though the higher modes still show significant vibrational responses, it is not reflected in the sum seen in figures 6.18 and 6.19. This is caused by the difference in frequency between the modes. Higher modes are excited at higher frequencies. Therefore, for most of the time, the different modes are out of phase or only slightly in phase with each other. The result shown in figure 6.20 only shows the maximum RMS value at that location for a particular mode. Also, the higher modes are quickly dampened out, showing that the only contributing mode after a certain amount of time after the slamming event is the first mode.

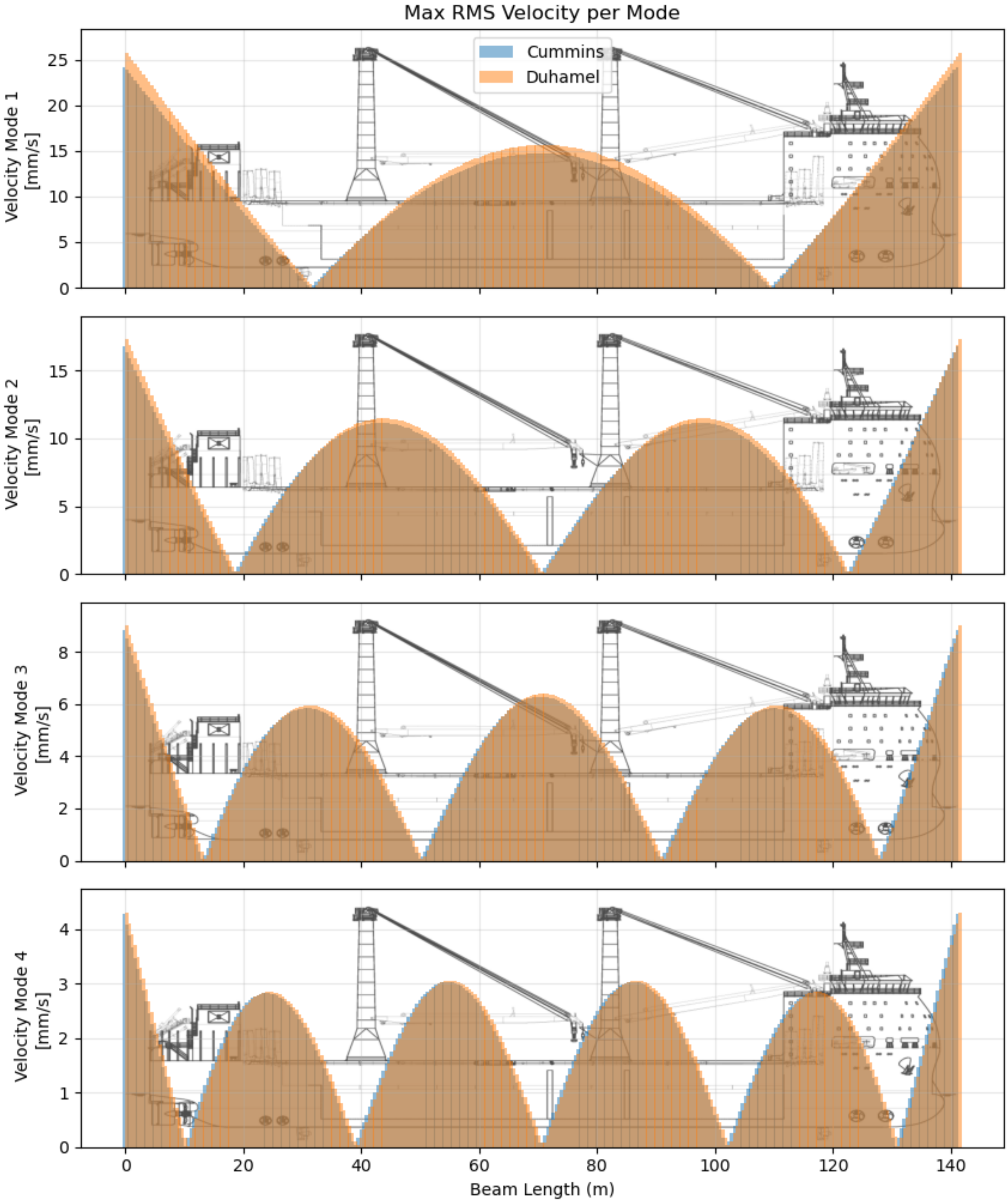

Figure 6.20: The spatial distribution of the RMS velocity of the first four modes. The orange shows the response calculated using Duhamel. The blue, or darker part, shows the response calculated using Cummins.

7

Discussion of the results

While this research provides valuable insights, it is important to acknowledge certain limitations. The CFD model, despite offering high-fidelity hydrodynamic data, exhibited non-convergence for the average and maximum peak pressures with grid convergence index values well above 5% threshold. While this suggests that the absolute pressure values might be underestimated compared to real-world scenarios, the observed trends regarding the influence of loading conditions and wave parameters are considered valid, as the error related to convergence applies consistently across all simulations. The number of slams did show convergence, highlighting even more that the behaviour of the slamming is captured. Also, the study of the actual CFD data in the structural models suggests that the vessel does not always react as violently for all high pressures pulses.

The use of a 2D CFD model inherently simplifies the problem by preventing energy dissipation in the y-direction, potentially leading to an overestimation of pressures by approximately 10 to 20%. Furthermore, the model employed a one-way coupling approach, assuming a rigid hull for hydrodynamic calculations. This simplification means that the structural response does not feed back into and influence the hydrodynamic loads in the CFD model. This is a factor that could affect the overall accuracy of the coupled analysis. However, these effects can be neglected since the CFD did not show any sign of convergence so the results will probably be more of an understatement rather than an overstatement.

Comparison between the Duhamel convolution and the Cummins method for the vibrational analysis revealed generally good agreement. However, observed deviations, particularly in damping characteristics and phase, can be attributed to Duhamel's simpler damping model and the explicit inclusion of fluid memory effects in the Cummins method. The J-factor accounts for this in a way, but the added mass term in Cummins still does not provide a fully accurate answer. This term also needs to work for a spectrum of excitation frequencies, which is not the case at the moment.

From a practical perspective, the findings underscore the significant risk stern slamming poses to DP heavy lift vessels. The identified potential for RMS values of the velocity to exceed comfort limits for crew members of 4.5 to 6 mm/s and operational limits for sensitive equipment like the thruster on board the vessel of 18 mm/s, highlights the importance of considering slamming-induced vibrations. This is more evident in what might be considered relatively calm weather conditions in which the vessel can operate. This research provides a foundational understanding that can inform operational strategies and future design considerations for mitigating the adverse effects of stern slamming on these specialised vessels.

8

Conclusion

With the results of the CFD model and the beam model known and explained in chapter 5 and chapter 6, the questions defined in the introduction can be answered. Below are the sub-questions and the main research question noted and answered below. Next to the conclusion, the research is also discussed based on the methodology and results.

8.1. Answering Sub-research Questions

What is the general behaviour of water hitting the stern from underneath?

From the CFD simulations, it can be observed that the incoming waves influence each other. This determines how heavy the slam event of a wave can be. The general behaviour of water hitting the stern from underneath is characterised by clustering of the waves. This involves the interaction between incoming and reflected waves. This leads to the stern becoming temporarily exposed, followed by an upwards motion of the fluid. This results in the water hitting the stern flat-on like a plate. This impact mechanism is inefficient in dissipating energy, resulting in severe and transient pressure pulses on the stern of the vessel.

What is the influence of vessel motions and waves on slamming?

From the CFD simulations, it is clear that the waves play a crucial role in the development of slamming on the stern. The larger the wave height the more energy is contained within the wave and thus the higher the slamming pressures. It is also clear that the wave period affects the slamming pressures created by the wave. Lower and higher periods with respect to the base case did show higher averages in terms of the pressure output. The number of slams did not affect so much. From the results, a wave period of 4.4 seconds resulted in an average peak pressure of ±390 kPa for a draft of 7 meters and a significant wave height of 1.65 meters. The base case with a wave period of 5.1 seconds showed a reduced average peak pressure of ±320 kPa. The highest pressure was observed in the simulation with a wave period of 5.8 seconds. This resulted in an average peak pressure of around 480 kPa.

In this study, the vessel motions were also investigated. The vessel motions were small based on the fact that the peak of the JONSWAP spectrum was not in line with the peak of the heave and pitch RAO of the vessel. However, when the vessel motions were turned off in the CFD a clear trend started to emerge. All simulations showed higher average peak pressure on the stern than with vessel motions. The motions of the vessel have a dampening effect on slamming. This is likely due to the vessel motions being mostly in phase with the incoming waves. On average, the peak pressure during the simulations without any vessel motions considered was between 25.7% and 46.1% higher. The same effect related to the effect of the wave period was observed, highlighting the significance of wave parameters on the slamming loads.

How do different loading conditions of the vessel affect the slamming on the stern?

In this research, the goal was to identify which drafts were critical for slamming in the selected weather conditions. A range of vessel drafts was selected based on the ballast draft of 6 meters and the maximum design draft of 8 meters. All drafts were used in simulations with an H_s of 1.1 and 1.65 meters and a T_p of 4.6 and 5.1 seconds respectively. From the output and the data based on the sensor output, it can be observed that for both weather conditions, the highest average peak pressure occurs at the lowest drafts. In these conditions, the vessel will most likely encounter slamming the easiest and heaviest. In both weather conditions, higher drafts result in less peak pressure, but in the simulation with an H_s of 1.65 meters, the pressure converges to around 250 kPa. This means that the vessel can always encounter slamming on the stern during operation and load-out under these weather conditions. For an H_s of 1.1 meters, the pressure drops almost linearly. At the design draft, the average peak pressure is around 80 kPa.

In terms of the number of slams during the simulations, it can be observed that all drafts encounter a high number of slams. These are peak pressures which have a peak higher than at least 50 kPa. For all drafts, the number of slams remains approximately the same in both sea states. Only at the design draft of 8 meters, the number of slams in the simulation at both sea states starts to drop significantly. Therefore, the best way to reduce slamming is by staying on the design draft locally at the stern. This can be done by ballasting and trimming as much as regulations allow. However, it is noteworthy to say that even at the design draft slamming still can occur, albeit less clustered and less significant.

What responses are created by slamming on the stern and how does it transmit through the hull?

From this study, it is clear that the stern is subjected to a variety of different pressure loads where the average pressure is dependent on the loading condition and sea state. It is clear that for the sea state of Beaufort 5 more extreme slamming pressure was observed than for the sea state of Beaufort 4. Therefore, a series of slamming pressures was chosen to cover a spectrum of slamming responses. The study showed that in terms of the responses, the first four bending modes play a significant role in creating high velocities. Higher modes would not contribute too much since the damping of the fourth mode is so significant that it quickly decays after the initialisation of the slamming event. Slamming pressures up to 450 kPa showed that only comfort limitations are exceeded by the whipping of the vessel with 300 kPa being the threshold for comfort limits set by class societies.

For the upper end of the spectrum, it is clear that the responses of the vessel are much bigger and also start to exceed limits regarding the operability of systems related to the thruster on board the vessel. Slamming pressure higher than 750 kPa starts to exceed the limit of 18 mm/s for the thrusters of the vessel.

Since the first mode is the biggest contributing factor in the vibrational response, the stern and bow sections of the vessel will endure the highest velocities. This is particularly bad for heavy lift vessels since the engine room and accommodations are always located at the stern or bow due to the requirement of a single unobstructed cargo hold.

The effect of the loading conditions on the vibrational response itself is also analysed. A change in draft does not lead to significant changes in the responses created by the same slamming force. For the velocities, the difference between the response for each loading condition was on average less than 2%. Therefore, the only effect the loading condition has is on the pressure created by the slamming events.

To what extent can stern slamming be mitigated or the responses of slamming be reduced during operations?

The primary operational parameter identified for mitigating stern slamming intensity is the draft of the vessel. Increasing the draft reduces the severity of slamming, with the vessel experiencing less severe impacts as it approaches its design draft of 8 meters. However, practical limitations such as regulatory constraints or project cargo weight often prevent the vessel from achieving the design draft, leaving the stern vulnerable to wave slamming. While increasing draft helps, it is important to note that slamming can still occur even at higher drafts. Especially in more severe sea states the pressure converged towards a peak pressure of 250 kPa, indicating that full mitigation through draft alone may not be feasible. The study with a draft of 7.5 meters and a trim of one meter at the stern however, proved that high drafts in combination with maximum trim at the stern reduced the slams significantly. A combination of these measures, if possible, can mitigate slamming.

8.2. Answering the Main Research Question

What is the behaviour of stern slamming and what parameters have an influence on the occurrence and how does this load translate to vibrational responses on a heavy lift vessel during offshore operations?

Stern slamming is characterized by the sudden, high-intensity, short-duration pressure pulses resulting from the interaction of incoming and reflected waves. This interaction is leading to a flat-plate-like impact on the vessel's stern.

The key parameters influencing the responses of stern slamming are:

- **Vessel Draft/Loading Condition:** This is the most significant parameter affecting slamming intensity. Smaller drafts lead to substantially higher peak pressures, while increasing the draft reduces them. However, even at deeper drafts, particularly in rougher sea states, the risk of significant slamming persists. The number of slamming events in the CFD simulations is less sensitive to draft variations.
- **Wave Parameters:** Both wave height and wave period play critical roles. Higher wave heights directly correspond to increased slamming pressure intensity in all loading conditions. The wave period exhibits a non-linear influence, with both shorter and longer periods contributing to elevated peak pressures.
- **Vessel Motions:** Contrary to initial assumptions, in the simulated sea states, the vessel's heave and pitch motions had a dampening effect on slamming pressures. This is because the motions are largely in phase with the incoming waves, reducing the relative impact velocity.

These loads, found in the CFD simulations, also showed considerable vibrational responses in the structural model of the vessel. The vibrations are primarily driven by the first few mode shapes. of the hull. In both the Duhamel convolution and the Cummins equation, the same behaviour and response were observed. The vibrational responses were also compared to the limits set by class societies showing that loads higher than 300 kPa result in RMS values which can exceed the comfort limits and loads higher than 750 kPa exceed limits for components related to the thrusters.

8.3. Counteracting Stern Slamming

This study provides an inside on how stern slamming develops and how such loads can excite the vessel. From the CFD simulations it is clear that loading conditions play a big role on the loads created by slamming on the stern. It is beneficial to try and keep the vessel as close to the design conditions as possible which trim helping the local draft at the stern. This ensures that the stern is submerged properly and significant slamming can not fully develop.

What is also clear is that the vessel cannot comply with this advice every time and that shows the biggest challenge. The vessel is basically designed as a cargo vessel, but is equipped to also be able to stay on dynamic positioning. However, design criteria related to sailing between ports is much different to the criteria for staying on dynamic positioning. It is beneficial for future vessels which might also use dynamic positioning to make sure that the design conditions of the vessel are also easily met on DP.

9

Recommendations

This research provides a preliminary method to analyse the slamming on the stern of a vessel which is stationary and how this relates to the excitation of the hull. Because of the preliminary nature of this research, there are multiple possibilities to conduct further research on this topic. Below are some recommendations for further research on stern slamming.

9.1. Hydrodynamic model

The majority of the hydrodynamic model is done in ComFLOW. For computational reasons, it is chosen that for now a 2D simulation will suffice. However, 3D effects are not taken into account and will play a role in the pressure build-up underneath the stern. Follow-up research could consider performing a 3D simulation to see the effects of energy dissipation to the sides and the effect of additional motions.

Also, from the convergence study of the CFD model, it was clear that the model was not properly converged yet. Due to the number of simulations and the computational time of the smaller grid size, it was not possible to run at those smaller grid sizes. Future work should perform simulations at the smaller grid sizes to capture the force of slamming in the stern more accurately.

Another thing that can not be concluded in this research is the probability of the occurrence of stern slamming. The model only simulates 100 seconds with a randomly selected phase for each wave component of the spectrum. For future research, a longer simulation could be performed with a broader energy spectrum to say something about the probability of occurrence.
Regarding the probability of occurrence, in future work, an experimental study may be performed to analyse and compare the loads of the CFD model. Also, experimental studies could better implement the spread of the incoming waves relative to the vessel.

Due to time limitations, a parameter study was not performed to see if a change in the geometry of the stern has an effect on the reduction of stern slamming. Future research could implement this to look at whether newbuild designs of heavy lift vessels could be optimised for a reduction in slamming.

9.2. Structural beam model

Regarding the structural model, an Euler-Bernoulli selected as the model to analyse the global responses of the hull due to the slamming load on the stern. This model can predict vibrations, but in future work, the model could be enhanced to capture the response more accurately. Future studies could implement a Timoshenko beam or a finite element analysis of a free-free beam to yield better results.

To analyse the vibrations at a certain location of the vessel, the Euler-Bernoulli beam is a 2D representation and therefore only capable of looking at a location along the length of the beam. For more accurate responses at a more precise location, for example, at the location of a component, a CFD-FEM coupling could be implemented. This will better match the results of the CFD to a structural model.

Also in the future, an effort should be made to directly place the CFD loads onto a numerical model. Now, the Cummins equation could not model the added mass term very accurately since it is dependent on the excitation frequency. The results from CFD have a broad frequency spectrum, resulting in the added mass term being approximated by a single frequency.

References

[1] *2. Mathematics and numerics — ComFLOW 4.2.0-alpha documentation*. URL: `https://poseidon.housing.rug.nl/sphinx/mathnum.html`.

[2] Det Norske Veritas AS. *RULES FOR CLASSIFICATION OF DET NORSKE VERITAS AS*. Tech. rep. Jan. 2011.

[3] J.R. Banerjee, D. Kennedy, and I. Elishakoff. “Further Insights Into the Timoshenko–Ehrenfest Beam Theory”. In: *Journal of vibration and acoustics* 144.6 (Oct. 2022). DOI: `10.1115/1.4055974`. URL: `https://doi.org/10.1115/1.4055974`.

[4] Richard Evelyn Donohue Bishop and William Geraint Price. *Hydroelasticity of Ships*. Feb. 1980. URL: `http://ci.nii.ac.jp/ncid/BA27729519`.

[5] Anna D Boon and Peter R Wellens. “The Effect of Surge on Extreme Wave Impacts and an Insight into Clustering.” In: *Journal of Ship Research* 68.2 (2024).

[6] H. Cheng et al. “Ship hull slamming analysis with smoothed particle hydrodynamics method”. In: *Applied Ocean Research* 101 (July 2020), p. 102268. DOI: `10.1016/j.apor.2020.102268`. URL: `https://doi.org/10.1016/j.apor.2020.102268`.

[7] H-BLIX Consultancy. *Offshore Wind Vessel Availability Until 2030: Baltic Sea and Polish Perspective*. Tech. rep. Prepared with input from WindEurope and industry sponsors. Polish Wind Energy Association (PWEA), June 2022. URL: `https://www.h-blix.com.pl`.

[8] Frédéric Dias and Jean-Michel Ghidaglia. “Slamming: Recent Progress in the Evaluation of Impact Pressures”. In: *Annual Review of Fluid Mechanics* 50.1 (Oct. 2017), pp. 243–273. DOI: `10.1146/annurev-fluid-010816-060121`. URL: `https://doi.org/10.1146/annurev-fluid-010816-060121`.

[9] Milton C. Lopes Filho et al. “Approximation of 2D Euler Equations by the Second-Grade Fluid Equations with Dirichlet Boundary Conditions”. In: *Journal of Mathematical Fluid Mechanics* 17.2 (Apr. 2015), pp. 327–340. DOI: `10.1007/s00021-015-0207-8`. URL: `https://doi.org/10.1007/s00021-015-0207-8`.

[10] Gung-Min Gie et al. *The Navier-Stokes Equations in a Periodic Channel*. Jan. 2018, pp. 251–305. DOI: `10.1007/978-3-030-00638-9\{_}6`. URL: `https://doi.org/10.1007/978-3-030-00638-9_6`.

[11] K. Hasselmann et al. “Measurements of wind-wave growth and swell decay during the Joint North Sea Wave Project (JONSWAP)”. In: *Wikiwaves* 12 (Jan. 1973), pp. 1–95. URL: `http://repository.tudelft.nl/assets/uuid:f204e188-13b9-49d8-a6dc-4fb7c20562fc/Jonswap-Hasselmann1973.pdf`.

[12] Kyeong-uk Heo et al. “Quadratic strip theory for high-order dynamic behavior of a large container ship with 3D flow effects”. In: *International Journal of Naval Architecture and Ocean Engineering* 8.2 (2016), pp. 127–136.

[13] Ning Ji and Jinkun Liu. *Basic Boundary Control of a Flexible Three-Dimensional Euler–Bernoulli Beam Based on Disturbance Observers*. Jan. 2022, pp. 37–64. DOI: `10.1007/978-981-19-0079-2\{_}3`. URL: `https://doi.org/10.1007/978-981-19-0079-2_3`.

[14] J.M.J. Journée and W.W. Massie. *Offshore Hydromechanics*. First Edition. Delft, Netherlands: Delft University of Technology, 2001. Chap. 5.

[15] G. K. Kapsenberg. *Slamming of Ships: Where Are We Now?* Tech. rep. 1788-P. Published in: Philosophical Transactions of the Royal Society, A 2011 369, 2892-2919, doi:10.1098/rsta.2011.0118. Delft, Netherlands: Delft University of Technology, Ship Hydromechanics Laboratory, 2011.

[16] Geert Kees Kapsenberg. “On the Slamming of Ships: Development of an Approximate Slamming Prediction Method”. Promoter: Prof. dr. ir. R.H.M. Huijsmans. PhD Thesis. Delft University of Technology, June 2018. ISBN: 978-94-92679-47-5. DOI: `10.4233/uuid:14eac2bb-63ee-47e4-8218-1ba3830a97b4`. URL: `https://doi.org/10.4233/uuid:14eac2bb-63ee-47e4-8218-1ba3830a97b4`.

[17] Theodore von Karman. *The Impact on Seaplane Floats During Landing*. Tech. rep. Technical Note 321. Translated by Frank L. Wattendorf from the original report by the Aerodynamical Institute of Aachen Technical High School. Washington, D.C.: National Advisory Committee for Aeronautics (NACA), 1929.

[18] Jung-Hyun Kim and Yonghwan Kim. “Numerical analysis on springing and whipping using fully-coupled FSI models”. In: *Ocean Engineering* 91 (Sept. 2014), pp. 28–50. DOI: `10.1016/j.oceaneng.2014.08.001`. URL: `https://doi.org/10.1016/j.oceaneng.2014.08.001`.

[19] K.M.T. Kleefsman et al. “A Volume-of-Fluid based simulation method for wave impact problems”. In: *Journal of Computational Physics* 206.1 (Jan. 2005), pp. 363–393. DOI: `10.1016/j.jcp.2004.12.007`. URL: `https://doi.org/10.1016/j.jcp.2004.12.007`.

[20] Santosh Konangi, Nikhil K. Palakurthi, and Urmila Ghia. “von Neumann Stability Analysis of a Segregated Pressure-Based Solution Scheme for One-Dimensional and Two-Dimensional Flow Equations”. In: *Journal of Fluids Engineering* 138.10 (June 2016). DOI: `10.1115/1.4033958`. URL: `https://doi.org/10.1115/1.4033958`.

[21] Santosh Konangi, Nikhil K. Palakurthi, and Urmila Ghia. “von Neumann stability analysis of first-order accurate discretization schemes for one-dimensional (1D) and two-dimensional (2D) fluid flow equations”. In: *Computers Mathematics with Applications* 75.2 (Nov. 2017), pp. 643–665. DOI: `10.1016/j.camwa.2017.09.040`. URL: `https://doi.org/10.1016/j.camwa.2017.09.040`.

[22] W. Lafeber, H. Bogaert, and L. Brosset. “Elementary Loading Processes (ELP) Involved In Breaking Wave Impacts: Findings From the Sloshel Project”. In: *MARIN* (Jan. 2012).

[23] M.C. Lin and T.Y. Ho. “Water-entry for a wedge in arbitrary water depth”. In: *Engineering Analysis with Boundary Elements* 14.2 (Jan. 1994), pp. 179–185. DOI: `10.1016/0955-7997(94)90094-9`. URL: `https://doi.org/10.1016/0955-7997(94)90094-9`.

[24] M. B. Liu and G. R. Liu. “Smoothed Particle Hydrodynamics (SPH): an Overview and Recent Developments”. In: *Archives of Computational Methods in Engineering* 17.1 (Feb. 2010), pp. 25–76. DOI: `10.1007/s11831-010-9040-7`. URL: `https://doi.org/10.1007/s11831-010-9040-7`.

[25] Xinyu Liu et al. “Experimental investigation on the slamming loads of a truncated 3D stern model entering into water”. In: *Ocean Engineering* 252 (2022). URL: `https://www.sciencedirect.com/science/article/pii/S0029801822003134`.

[26] Ananthan Mohan and Gaurav Tomar. “Volume of Fluid Method: A Brief Review”. In: *Journal of the Indian Institute of Science* (Jan. 2024). DOI: `10.1007/s41745-024-00424-w`. URL: `https://doi.org/10.1007/s41745-024-00424-w`.

[27] Lionel Moskowitz. “Estimates of the power spectrums for fully developed seas for wind speeds of 20 to 40 knots”. In: *Journal of Geophysical Research Atmospheres* 69.24 (Dec. 1964), pp. 5161–5179. DOI: `10.1029/jz069i024p05161`. URL: `https://doi.org/10.1029/jz069i024p05161`.

[28] Hidemi Mutsuda et al. “Occurrence of stern slamming pressure and its characteristics in following irregular waves”. In: *Ocean Engineering* 170 (Oct. 2018), pp. 222–236. DOI: `10.1016/j.oceaneng.2018.10.018`. URL: `https://doi.org/10.1016/j.oceaneng.2018.10.018`.

[29] P. Naaijen. “Motions and Loading of Structures in Waves”. In: (2023), pp. 1–18.

[30] Akemi Nishida. “Effect of Timoshenko Coefficient in Wave Propagation Analysis of a Three-Dimensional Frame Structure”. In: *Theoretical and applied mechanics Japan* 56 (Jan. 2008), pp. 57–65. DOI: `10.11345/nctam.56.57`. URL: `http://ci.nii.ac.jp/naid/130004463663`.

[31] T.F. Ogilvie. *Compressibility effects in ship slamming*. Oct. 1963. URL: `https://ntnuopen.ntnu.no/ntnu-xmlui/handle/11250/237627`.

[32] Antonina Pirrotta, Stefano Cutrona, and Salvatore Di Lorenzo. "Fractional visco-elastic Timoshenko beam from elastic Euler–Bernoulli beam". In: *Acta Mechanica* 226.1 (June 2014), pp. 179–189. DOI: `10.1007/s00707-014-1144-y`. URL: `https://doi.org/10.1007/s00707-014-1144-y`.

[33] Patrick J Roache. *Verification and validation in computational science and engineering*. Vol. 895. Hermosa Albuquerque, NM, 1998.

[34] Tony Saad and Joe Majdalani. "Pressure Integration Rules and Restrictions for the Navier-Stokes Equations". In: *38th Fluid Dynamics Conference and Exhibit* (June 2010). DOI: `10.2514/6.2010-4288`. URL: `https://doi.org/10.2514/6.2010-4288`.

[35] Tony Saad and Joseph Majdalani. "Some thoughts on the pressure integration requirements of the Navier–Stokes equations". In: *Fluid Dynamics Research* 44.6 (Oct. 2012), p. 065508. DOI: `10.1088/0169-5983/44/6/065508`. URL: `https://doi.org/10.1088/0169-5983/44/6/065508`.

[36] M. S. Shadloo, G. Oger, and D. Le Touzé. "Smoothed particle hydrodynamics method for fluid flows, towards industrial applications: Motivations, current state, and challenges". In: *Computers Fluids* 136 (May 2016), pp. 11–34. DOI: `10.1016/j.compfluid.2016.05.029`. URL: `https://doi.org/10.1016/j.compfluid.2016.05.029`.

[37] Rajesh A. Shetty et al. *Bending Deflection Solutions of Thick Beams Using a Third-Order Simple Single Variable Beam Theory*. Sept. 2022, pp. 233–246. DOI: `10.1007/978-981-19-4040-8\{_}20`. URL: `https://doi.org/10.1007/978-981-19-4040-8_20`.

[38] Stergios – Alexandros Sideris and Charalampos Tsakmakis. "Consistent Euler – Bernoulli beam theories in statics for classical and explicit gradient elasticities". In: *Composite Structures* 282 (Dec. 2021), p. 115026. DOI: `10.1016/j.compstruct.2021.115026`. URL: `https://doi.org/10.1016/j.compstruct.2021.115026`.

[39] Hui Sun. *A Boundary Element Method Applied to Strongly Nonlinear Wave-Body Interaction Problems*. Jan. 2007. URL: `https://ntnuopen.ntnu.no/ntnu-xmlui/handle/11250/237627`.

[40] Hui Sun and Odd M. Faltinsen. "Water entry of a bow-flare ship section with roll angle". In: *Journal of Marine Science and Technology* 14.1 (Aug. 2008), pp. 69–79. DOI: `10.1007/s00773-008-0026-1`. URL: `https://doi.org/10.1007/s00773-008-0026-1`.

[41] RL Townsin. "Virtual Mass Reduction Factors JValues for Ship Vibration Calculations Derived from Tests with Beams Includind Ellipsoids and Ship Models". In: *Trans RINA* 111.3 (1969), pp. 385–97.

[42] Johannes Tewes Tuitman. "Hydro-elastic Response of Ship Structures to Slamming Induced Whipping". Promotor: Prof.dr.ir. R.H.M. Huijsmans. PhD Thesis. Delft, Netherlands: Delft University of Technology, Feb. 2010. ISBN: 978-90-9025031-1.

[43] Martin Van Der Eijk and Peter Wellens. "Two-phase free-surface flow interaction with moving bodies using a consistent, momentum preserving method". In: *Journal of Computational Physics* 474 (Nov. 2022), p. 111796. DOI: `10.1016/j.jcp.2022.111796`. URL: `https://doi.org/10.1016/j.jcp.2022.111796`.

[44] H. Wagner. "Uber Stoss-und Gleitvorgange an der Oberflache von Flussigkeiten". In: *ZAMM Journal of applied mathematics and mechanical engineering* 12 (1932), pp. 193–215.

[45] Shan Wang and C. Guedes Soares. "Experimental and numerical study of the slamming load on the bow of a chemical tanker in irregular waves". In: *Ocean Engineering* 111 (Dec. 2015), pp. 369–383. DOI: `10.1016/j.oceaneng.2015.11.012`. URL: `https://doi.org/10.1016/j.oceaneng.2015.11.012`.

[46] Shan Wang and C. Guedes Soares. "Stern slamming of a chemical tanker in irregular head waves". In: *Ocean Engineering* 122 (May 2016), pp. 322–332. DOI: `10.1016/j.oceaneng.2016.05.013`. URL: `https://doi.org/10.1016/j.oceaneng.2016.05.013`.

[47] J. Xiao and R. Batra. "Local water slamming of curved rigid hulls". In: *The International Journal of Multiphysics* 6.3 (Sept. 2012), pp. 305–340. DOI: `10.1260/1750-9548.6.3.305`. URL: `https://doi.org/10.1260/1750-9548.6.3.305`.

[48] Hang Xie et al. “Methodology of evaluating local dynamic response of a hull structure subjected to slamming loads in extreme sea”. In: *Ocean Engineering* 239 (Sept. 2021), p. 109763. DOI: `10.1016/j.oceaneng.2021.109763`. URL: `https://doi.org/10.1016/j.oceaneng.2021.109763`.

[49] Zhao-Fei Zhang, Ning Liu, and Chong Zhang. “Investigation on whipping characteristics of a container ship in irregular waves considering the effect of structural damping”. In: *Ocean Engineering* 313 (Oct. 2024), p. 119418. DOI: `10.1016/j.oceaneng.2024.119418`. URL: `https://doi.org/10.1016/j.oceaneng.2024.119418`.

[50] R. Zhao and O. Faltinsen. “Water entry of two-dimensional bodies”. In: *Journal of Fluid Mechanics* 246 (Jan. 1993), pp. 593–612. DOI: `10.1017/s002211209300028x`. URL: `https://doi.org/10.1017/s002211209300028x`.

A

Addtional information ComFLOW model

A.1. Raw Data and Filtered Data

To analyse the pressures acting on the stern of the hull, a series of pressure sensors is placed on the complete stern. The sensors are placed from the far end of the hull in the ComFLOW domain at x equals 44.254 meters to x equals 51.929 meters. Because the hull has a meter width, the sensors are also varied along the y-axis with a spacing of 0.25 meters between each sensor, varying from y equals -0.5 meters to 0.5 meters. Because the sensors at the boundary edges may result in inconclusive data, it is chosen to only consider the middle three rows of sensors along the y-axis. When the simulations are run, the following results can be found.

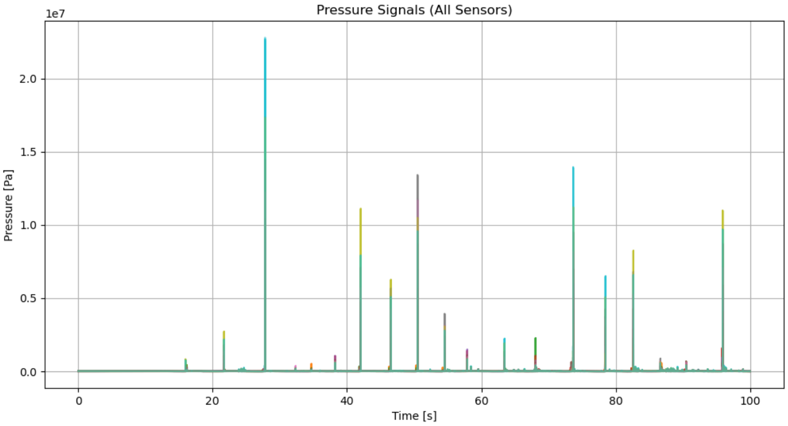

Figure A.1: The results of the pressure sensors when the data is not filtered.

As can be seen from figure A.1, the pressure peaks do not follow a logical trend for slamming pressures. The peaks are too narrow and do not have a clear "tail" which represents the hydrostatic pressure of the water that can be seen in figure A.3. Looking more closely at the peak, it can be observed that these values are generated by a single timestep in most cases. This is probably due to numerical errors within the CFD simulation.

Results do need to be filtered to filter out the single-timestep errors. There are multiple filters which can be used to filter that data. A commonly used filter is the Butterworth filter which is able to filter with non-linear impulsive loads like slamming. However, tuning the model turned out to be difficult and the results were not satisfactory, as the results were too smoothed out. A simpler mean filter turned out to be a better option which could filter local errors while retaining the rawness of the data. For the mean filter a size must be defined at which the filter will locally look at the average. A size too low will result in the filter being unable to get all of the errors out. A size too high means the results are averaged too much which will lower the peak pressures. To find this, a parameter sweep is performed to identify the optimal size for the filter. This sweep is done for every CFD simulation and can be seen in figure A.2.

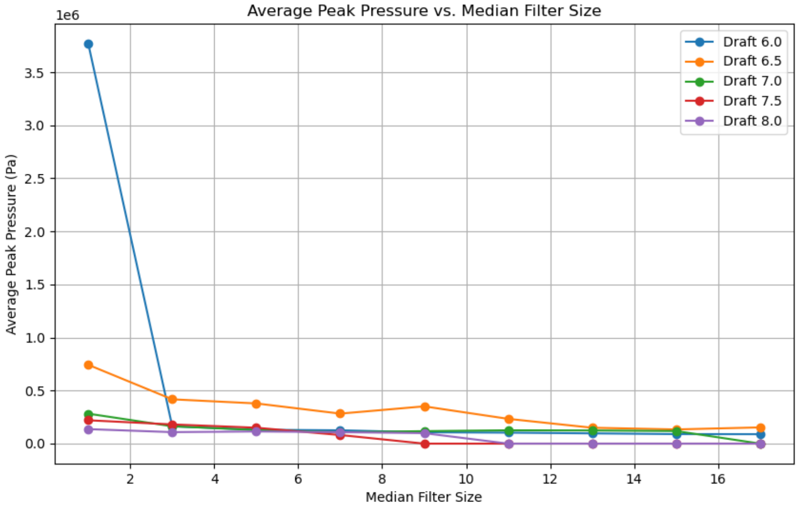

Figure A.2: Results of the parameters sweep for every CFD simulation of the H_s = 1.1 m and T_p = 4.6 s.

As can be seen in the results of the parameter sweep, a minimum size of three must be chosen for the simulation at a draft of six meters. However, looking at the reading from the pressure sensors with a mean filter of size three, there are still some errors left. A size of five turns out to be the first filter size where there are no big enough errors left while still retaining the best slamming characteristics.

A.2. Identification of Peaks and Slams

In order to say something about the slamming events in the simulations, simply looking at averages does not say a lot in this simulation. This is due to the fact that for most timesteps the pressure measured by the sensors is either very low or even zero. Only for short amounts of time does the pressure rise significantly. This creates very low averages so it is best to identify the slamming peaks of the simulation output. With these values a better analysis can be done to say something about the slamming events in each simulation.

To do that a script is written which looks at the data of every sensor output and finds the highest values that fall in the given interval. In this study, a slamming event is characterised when the value exceeds a minimum of 50 kPa. A distance of 500 is set to prevent the code from taking a series of values from multiple slam events. Because the results of every sensor are taken into account a better estimate can be given can just looking at a single sensor or a row at a certain x-value since that might result in much higher or lower values depending on the distribution of the slam on the stern.
With the peak values of each simulation known, the number of slams can also be defined by counting the peak values. However, since the peaks are found for every sensor output of the number of values is way higher than the number of slams in the simulation. Therefore, a cluster of peak values which fall within a time interval is considered to be a single slam event on the stern of the vessel. It turned out that a time interval of 0.5 seconds is enough to cluster all peak values in the slamming events. A representation of a cluster with the identified peaks can be found in figure A.3.

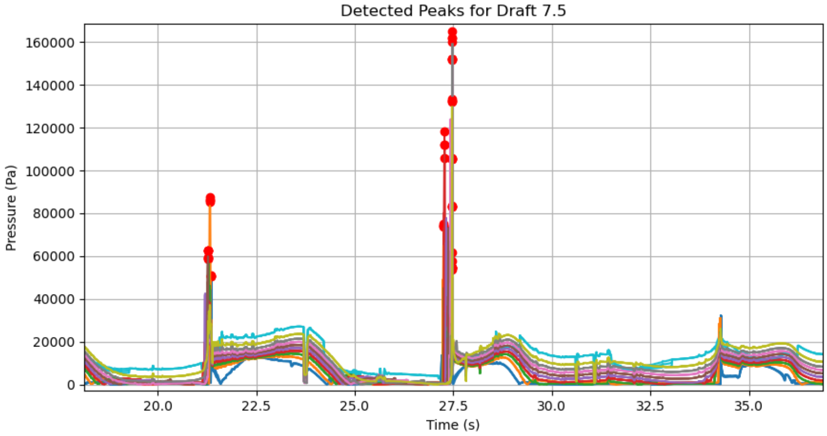

Figure A.3: A snapshot of two identified slamming events for the simulation with a draft of 7.5 meters and a H_s of 1.65 meters. The red dots represent all the identified peaks of the simulation output.

A.3. Pressure Distribution on the Stern

With the readings of the sensors and the location of each sensor, a map of the pressure distribution along the stern can be made. This is important for the input into the beam model to analyse the possible whipping effect of the hull due to slamming. By applying a linear interpolation fit over the data and locations of the monitoring points, a 3D map of the transient slamming distribution can be made. In the below figure, a series of snapshots can be found of a slamming event since this is a transient response.

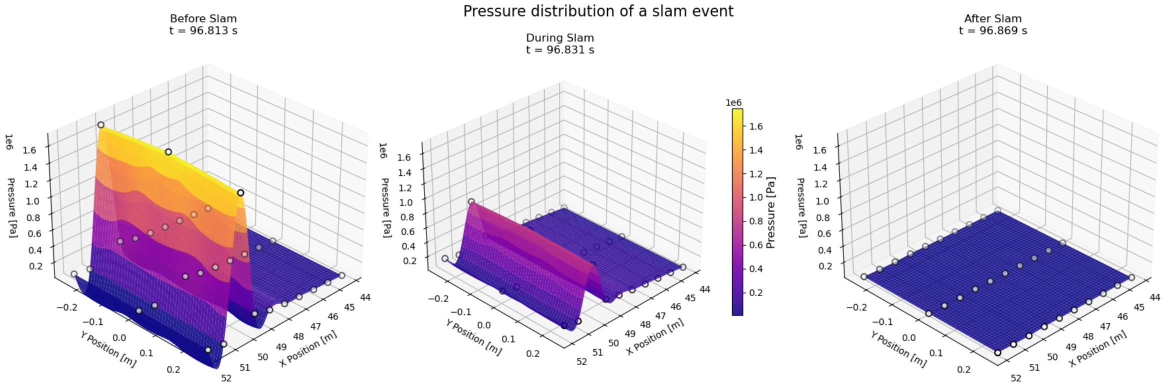

Figure A.4: A series of the pressure distribution according to the sensors located on the stern. The yellow dots are the sensors.

It can be observed in figure A.4 that for the output the pressure is equal along the unit width of the vessel. Therefore, the pressure can be transformed into a 2D distributed force along the length of the stern. This data can later be used in the beam model to analyse the responses of the hull due to the slamming on the stern.

B

Addtional information beam model

B.1. Rigid Body Motions

In order to get a feeling of the numerical method that will be used in the beam model to analyse the vibrational responses due to slamming loads, first a rigid body model is used to analyse the heave motion via a frequency domain calculation and via the Cummins equation.

B.1.1. Frequency Domain Calculation

In order to derive the expression for x_0 and the corresponding phase and amplitude of the system, first the general equation of motion needs to be derived. The general equation of motion if the barge looks like the following.

$$(m + a_\infty) \cdot x_{3,tt} + b(\omega) \cdot x_{3,t} + c \cdot x_3 = F \tag{B.1}$$

In equation (B.1) the m and a_∞ are the values for the mass and added mass respectively. The added mass is in reality a function of the excitation frequency, but is constant for high frequencies, so in practice it is most common to take that constant value. The $b(\omega)$ is the damping value as a function of the excitation frequency due to the hydrodynamic effects. c is the hydrodynamic stiffness value. F and x are the excitation force and the motion respectively and both can be written in the following form.

$$x = x_a \cdot e^{i(\omega_\zeta t + \epsilon_{\zeta x})} = x_a \cdot e^{i\omega_\zeta t} e^{i\epsilon_{\zeta x}} \tag{B.2}$$

$$F = F_a \cdot e^{i(\omega_\zeta t + \epsilon_{\zeta F})} = F_a \cdot e^{i\omega_\zeta t} e^{i\epsilon_{\zeta F}} \tag{B.3}$$

The forms shown in equation (B.2) and equation (B.3) can be differentiated and substituted in the general equation of motion. This yields the following form.

$$(-(m + a_\infty) \cdot \omega^2 x_a e^{i\epsilon_{\zeta x}} + b(\omega) \cdot i\omega x_a e^{i\epsilon_{\zeta x}} + c \cdot x_a e^{i\epsilon_{\zeta x}} = F_a e^{i\epsilon_{\zeta F}}) e^{i\omega_\zeta t} \tag{B.4}$$

Equation (B.4) can be rewritten in a form that shows the expression for $x_a e^{i\epsilon_{\zeta x}}$. This expression is shown in the following equation.

$$x_a e^{i\epsilon_{\zeta x}} = (-(m + a_\infty)]\omega^2 + b(\omega) i\omega + c)^{-1} F_a e^{i\epsilon_{\zeta F}} \tag{B.5}$$

With the expression for $x_a e^{i\epsilon_{\zeta x}}$ now known, the amplitude and phase can be determined. As can be seen in equation (B.5), the equation consists of a real part and a complex part. In order to find the phase the arctan of the complex part divided by the real part needs to be derived. This is shown below.

$$\epsilon_{\zeta x} = tan^{-1} \frac{\Im(x_a)}{\Re(x_a)} = \frac{(b(\omega) i\omega)^{-1} F_a e^{i\epsilon_{\zeta F}}}{(-(m + a_\infty)\omega^2 + c)^{-1} F_a e^{i\epsilon_{\zeta F}}} \tag{B.6}$$

The amplitude of the expression can be calculated using the absolute value of x_a. This is shown in the equation below.

$$a_x = \sqrt{\Re^2 + \Im^2} = \sqrt{((-[M + A]\omega^2 + [K + C])^{-1} F_a e^{i\epsilon_{\zeta F}})^2 + (([D] i\omega)^{-1} F_a e^{i\epsilon_{\zeta F}})^2} \tag{B.7}$$

B.2. Validating the Cummins Equation

B.2.1. Rigid Body

For rigid bodies which are excited by simple external forces like a sinusoidal force, the Cummins equation should yield the exact same result as a frequency domain calculation. When both methods are applied to the rigid vessel, the following results can be obtained for the heave motion.

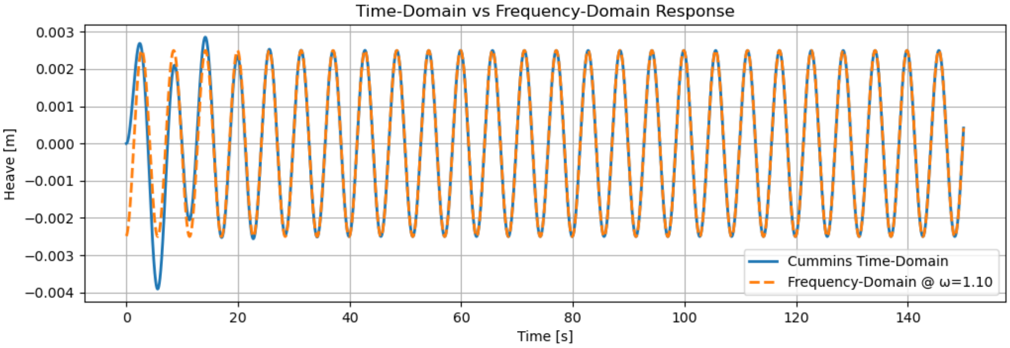

Figure B.1: The results of the heave motions of a rigid vessel using a frequency domain calculation and the Cummins equation for an excitation frequency of $\omega = 1.1$ rad/s.

As can be seen from the two graphs, the Cummins equation eventually settles toward the steady solution which can be found using the frequency domain calculation. The reason why the Cummins equation needs to settle is because of the time lag. The damping in the Cummins equation takes into account the history of the time domain calculation. In the first few seconds, the equation does not have any "history" and needs to converge to a steady state, while the frequency domain calculation always returns the steady state solution. Also, when looking at the retardation function, it can clearly be seen that the function decays very quickly as expected. This can be seen below.

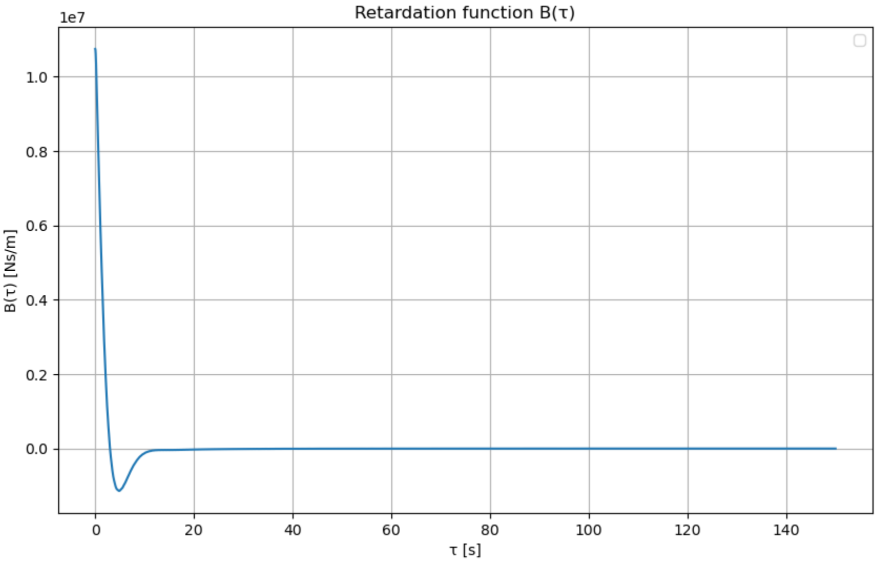

Figure B.2: The output of the retardation function for a rigid vessel. The function decays quickly over time towards zero.

B.2.2. Hydro-elastic Simply Supported Beam

For this case, a simply supported beam is chosen first with the same characteristics as the vessel. A simply distributed load which varies in time with a sine wave is applied to the beam. To convert this load to model space, equation (4.10) is used. Because the shape of the load should match the first mode of the beam, only the first non-rigid mode of the beam can be excited. A 3D plot of the force can be seen in figure B.3.

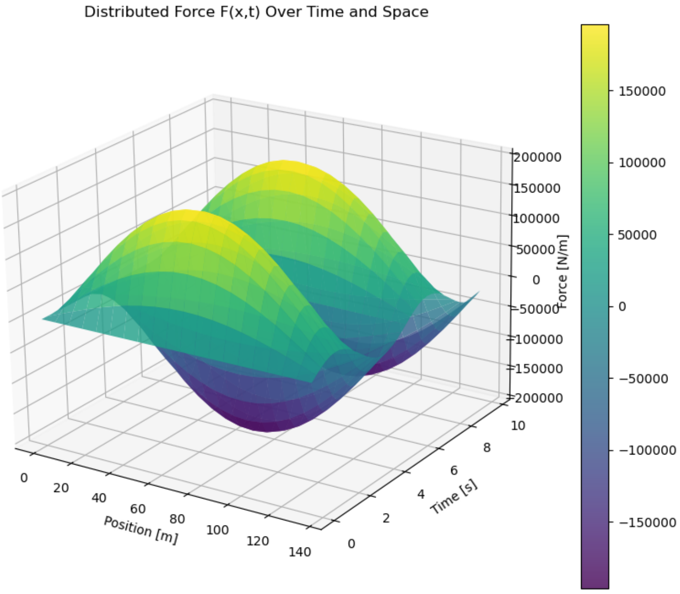

Figure B.3: A 3D representation of the distributed force over the length of the beam and over time. This force has the same form as the first mode shape of a simply supported beam.

When this force is plugged into the Duhamel integral, the deflection can be calculated. Compared to the results when this force is put into the Cummins equation, it can be observed in figure B.4 that both methods show agreeable results when the Cummins equation is converged. Both methods show the same steady-state solution for a simply supported beam under the distributed load. This confirms that both models work well for this case.

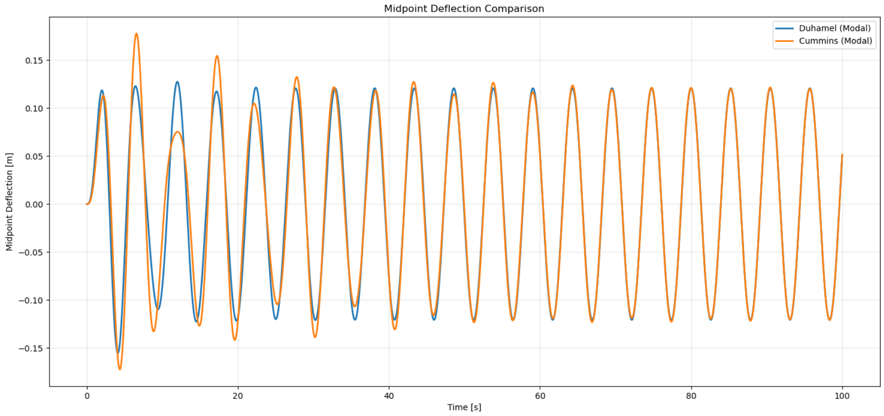

Figure B.4: The results of the deflection for a simply supported beam under a distributed load for the first mode using Cummins and Duhamel. Both converge towards the same steady state solution.

B.2.3. Hydro-elastic Free-Free Beam

A way to validate if the Cummins equation works for hydro-elastic problems is to make sure that for a beam under a simple distributed load in the shape of a mode of the beam, the response of the Duhamel integral and Cummins should be the same.

To validate the model, the free-free beam is used with the same characteristics as the vessel. A simply distributed load which has the same shape as the first mode of the beam and varies in time with a sine wave is applied to the beam. To convert this load to model space, equation (4.10) is used. Because the shape of the load should match the first mode of the beam, only the first non-rigid mode of the beam can be excited.

When this force is plugged into the Duhamel integral, the deflection can be calculated. Compared to the results when this force is put into the Cummins equation, it can be observed in figure B.5 that both methods show agreeable results when the Cummins equation is converged. Both methods show the same steady-state solution for a simply supported beam under the distributed load. This confirms that both models work well for this case.

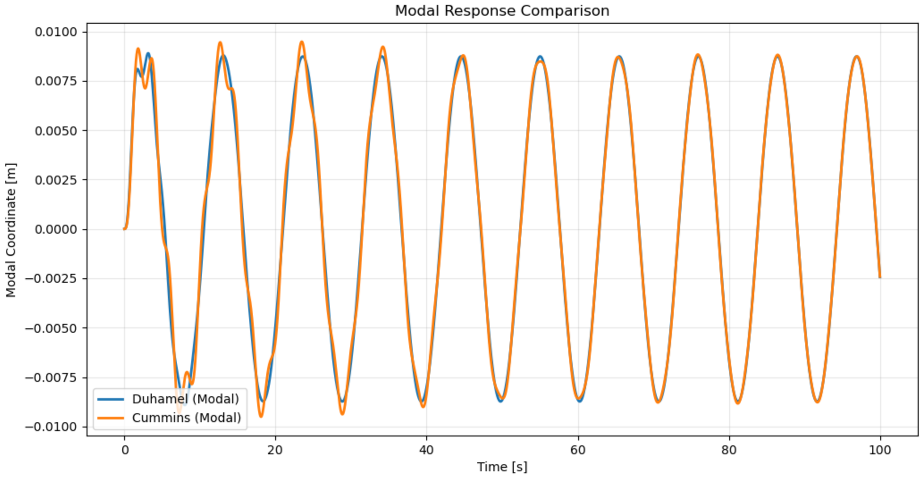

Figure B.5: The results of the deflection for a free-free beam under a distributed load for the first mode using Cummins and Duhamel. Both converge towards the same steady state solution.

B.3. Second Order Differential Equation

The Duhamel convolution is a way to prevent the need to solve the differential equations. However, this problem can also be solved using the second-order differential equations. Each mode satisfies a second-order ordinary differential equation:

$$M_{nn}\ddot{q}_n(t) + B_{nn}\dot{q}_n(t) + C_{nn}q_n(t) = F_n(t) \tag{B.8}$$

In this differential equation the mass, damping and stiffness values are matrices which are all diagonal. Each row and column represents a single mode. In order to determine the damping matrix, Rayleigh damping is applied, where the damping matrix is a linear combination of the mass and stiffness. This is shown in the following equation.

$$B_n = \alpha M_n + \beta C_n \tag{B.9}$$

The constants α and β are selected such that a target damping ratio ζ is achieved at the first two natural frequencies. Like the Duhamel convolution, the damping ratio is set at 0.03 which is a typical value for steel structures and taking into account the damping of the water [4].

$$\alpha = \frac{4\zeta\omega_1\omega_2}{\omega_1 + \omega_2} \tag{B.10}$$

$$\beta = \frac{4\zeta}{\omega_1 + \omega_2} \tag{B.11}$$

These are solved numerically to obtain the time history of modal displacements $q_n(t)$ and accelerations $\ddot{q}_n(t)$. This is done by using the model order reduction. To solve this equation numerically, it is first rewritten as a system of first-order equations by defining a state vector:

$$\mathbf{y}(t) = \begin{bmatrix} q(t) \\ \dot{q}(t) \end{bmatrix} \tag{B.12}$$

This formulation yields the following set of equations

$$\frac{d\mathbf{y}}{dt} = \begin{bmatrix} \dot{q}(t) \\ M^{-1}(F(t) - B\dot{q}(t) - Cq(t)) \end{bmatrix} \tag{B.13}$$

This system is integrated using a numerical differential solver, specifically the Backwards Differentiation Formula method. The initial conditions are set both to zero since at $t = 0$ the beam is in a static condition and no transient load is applied yet.

$$q(0) = 0, \quad \dot{q}(0) = 0 \tag{B.14}$$

Once the time integration is completed, the displacement $q(t)$ and velocity $\dot{q}(t)$ are directly obtained from the solver output. To ensure consistency, the acceleration is recomputed using the original equation of motion:

$$\ddot{q}(t) = M^{-1}(F(t) - B\dot{q}(t) - Cq(t)) \tag{B.15}$$

This approach will solve the response in the time domain, but it is not suited for the slamming and vibrational problem at hand. The reason is that the damping and added mass in this equation are constant over space and time. This works for rigid linear systems well, but applying this equation to a hydro-elastic problem in modal space will result in wrong results. The Cummins equation takes into account that the damping and added mass are dependent on space and time in non-linear systems. This results in more accurate results for non-linear problems such as slamming on an elastic model of a vessel.

B.4. Force & Hydrodynamic Input Values

B.4.1. Fitting hydrodynamic coefficients

The Cummins equation, which is explained in chapter 4, uses the retardation function where the integral is bounded till infinity. To solve this, an upper value must be chosen that captures most of the spectrum contained by the system while ensuring stability of the equation. Therefore, a high enough upper frequency limit must be chosen. Since the results from the strip theory allow values till a frequency of 5 rad/s. The hydrodynamic coefficients must be extrapolated for the retardation function. To ensure faster computations of the Cummins equation, it is chosen to develop an equation that accurately describes the hydrodynamic coefficients which can easily be filled in by the retardation function with a random frequency. These equations are shown in equations (B.16) and (B.17)

$$a_{n,fit}(\omega) = \left(A_\infty + \frac{A_0 - A_\infty}{1 + a\omega^2} \right) \left(1 - d \cdot \frac{\gamma^2}{(\omega - \omega_d)^2 + \gamma^2} \right) \tag{B.16}$$

$$b_{n,fit}(\omega) = B_\infty \cdot \frac{\gamma^2}{(\omega - \omega_{\text{peak}})^2 + \gamma^2} \tag{B.17}$$

In these equations, the A_∞ and B_∞ are the extrapolated values based on the last known value from strip theory. A_0 is the first known value from strip theory. a is a decay rate parameter. d and γ are parameters to capture the "dent" of the added mass curve. ω_{peak} is the frequency at the peak of the damping curve. The results of the fit can be seen in figure B.6, and it can be observed that there is strong agreement between the fitted curves and the original results.

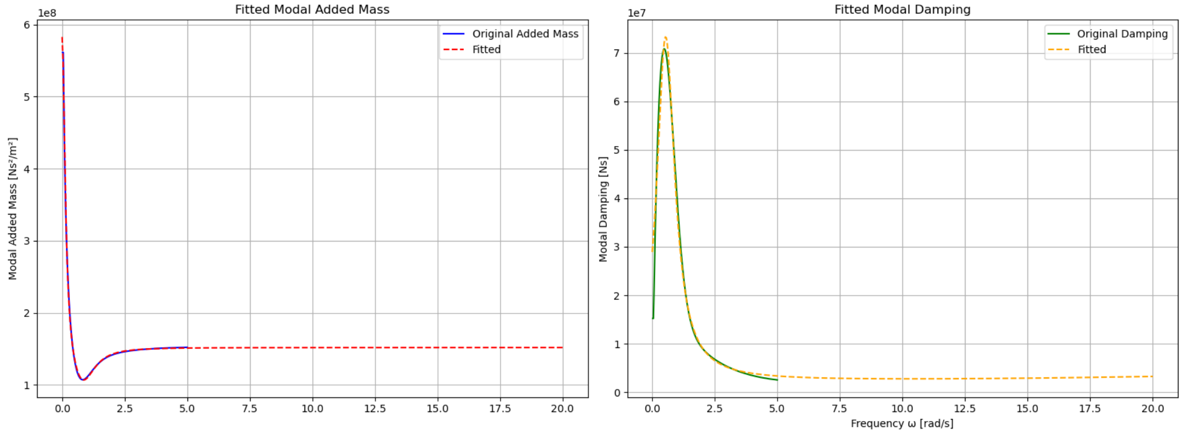

Figure B.6: The fitted equations for the modal added mass on the left and modal damping on the right to fill in the Cummins equation.

B.4.2. Simulated Slam Force

The Cummins equation has a drawback related to the function which calculates the added mass as a function of the frequency. This function is dependent on a frequency input into the system. This frequency is related to the excitation frequency of the system. For a simple load, this is simple, but the results of ComFLOW contain a whole frequency spectrum. This results in the Cummins equation not being able to accurately describe the added mass contribution in the time domain.
The same applies to the Duhamel convolution. This is based on the frequency domain and will only describe the response based on the excitation frequency that is put into the model.

In order to mitigate this error as much as possible, a simulated impulse response is modelled to analyse the response of the vessel. This impulse is based on the data from all the different CFD simulations. The benefit of a simulated slam is that the response to a single slam can be isolated to see how the response decays over time. Although this slam still contains multiple different frequency components, the error related to the added mass will be less than the high fidelity results of CFD.

The spatial component of the pulse is defined as a uniform distribution over a section of 10 meters. Mathematically, the spatial profile $f(x)$ is defined as:

$$f(x) = \begin{cases} 1, & \text{for } 0 \leq x \leq 10 \text{ m} \\ 0, & \text{otherwise} \end{cases}$$

This ensures that the pressure is applied evenly along a finite portion of the beam or hull structure. The temporal shape $g(t)$ is asymmetric, characterized by a sharp linear rise followed by an exponential decay. The full temporal function is:

$$g(t) = \begin{cases} 0, & t < t_0 \\ \frac{t-t_0}{t_r}, & t_0 \leq t < t_0 + t_r \\ \exp\left(-\frac{t-(t_0+t_r)}{\tau}\right), & t_0 + t_r \leq t \leq t_0 + t_r + 4\tau \\ 0, & t > t_0 + t_r + 4\tau \end{cases}$$

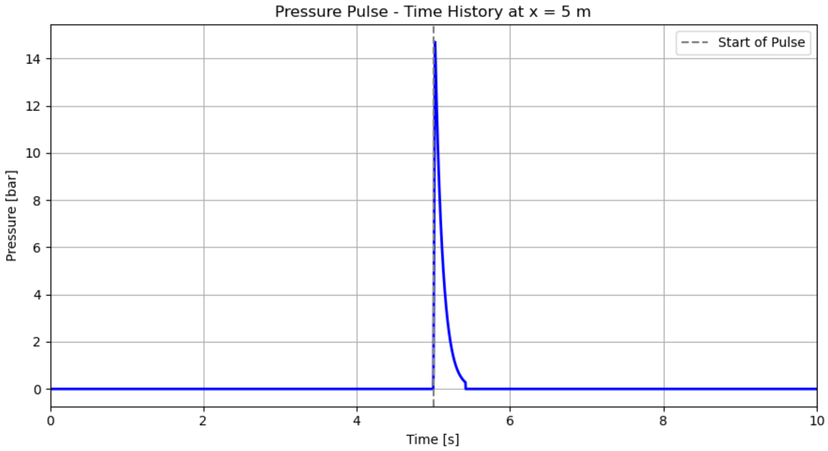

Figure B.7: A simulated pressure pulse.

C

Additional results

The rest of the results are plotted in here. Such as pressure readings of all simulations and responses of certain locations.

C.1. Results of the Simulations with H_s = 1.1 m and T_p = 4.6 s

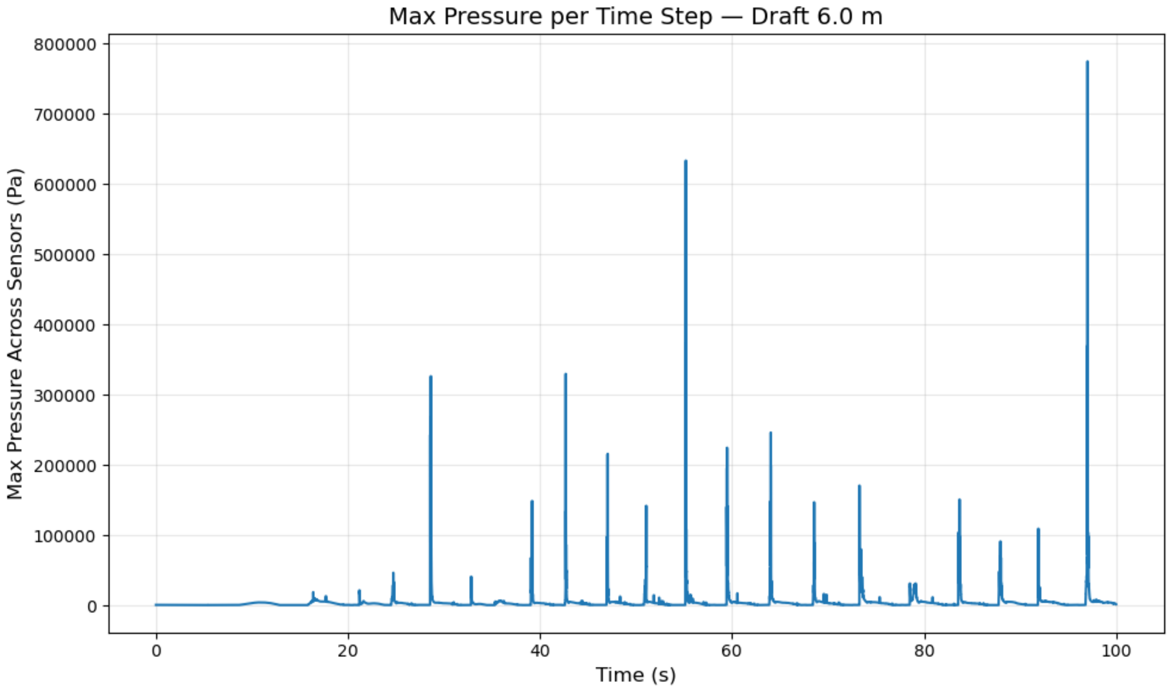

Figure C.1: The time domain results for a draft of 6 meters.

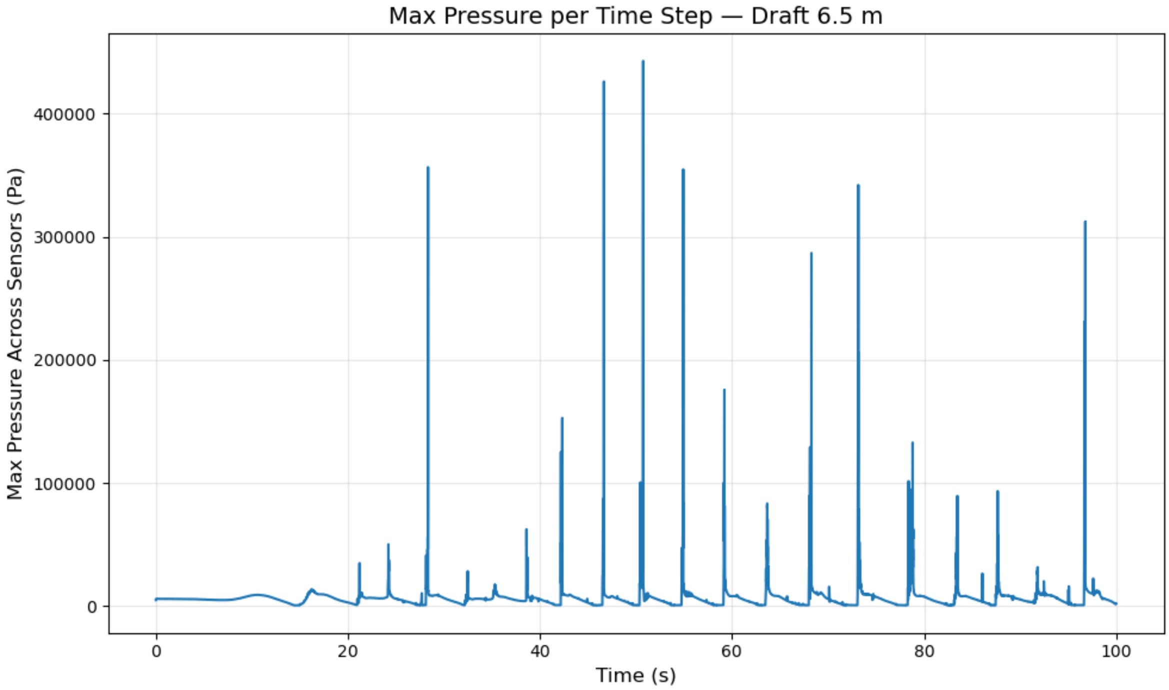

Figure C.2: The time domain results for a draft of 6.5 meters.

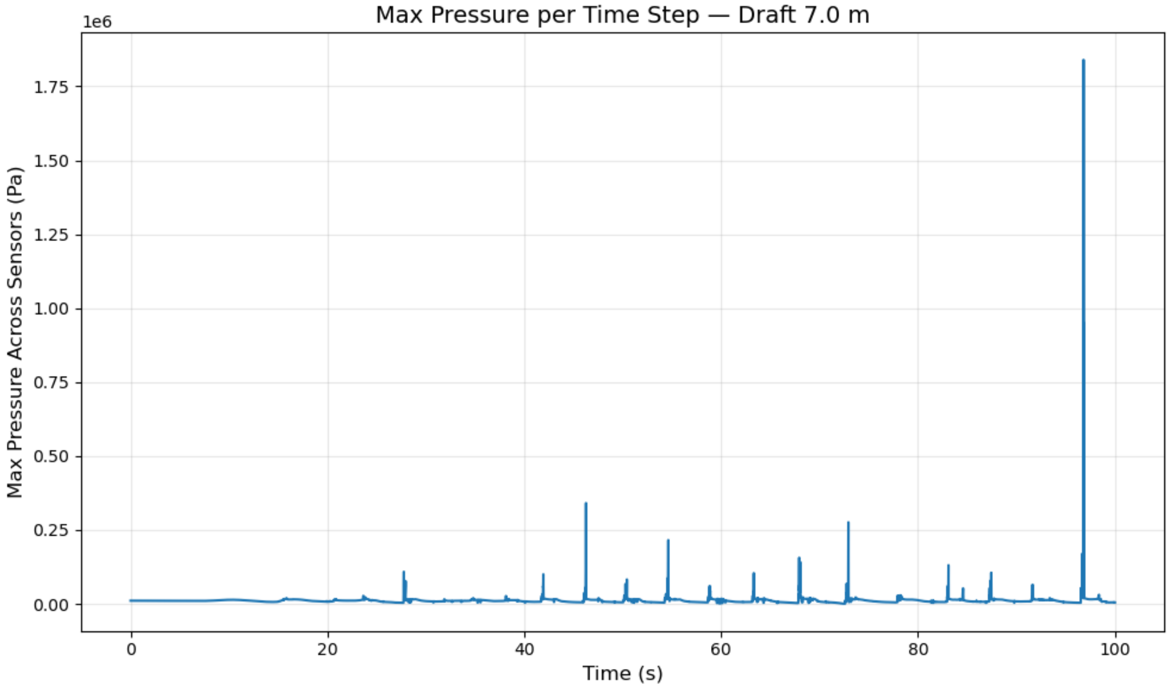

Figure C.3: The time domain results for a draft of 7 meters.

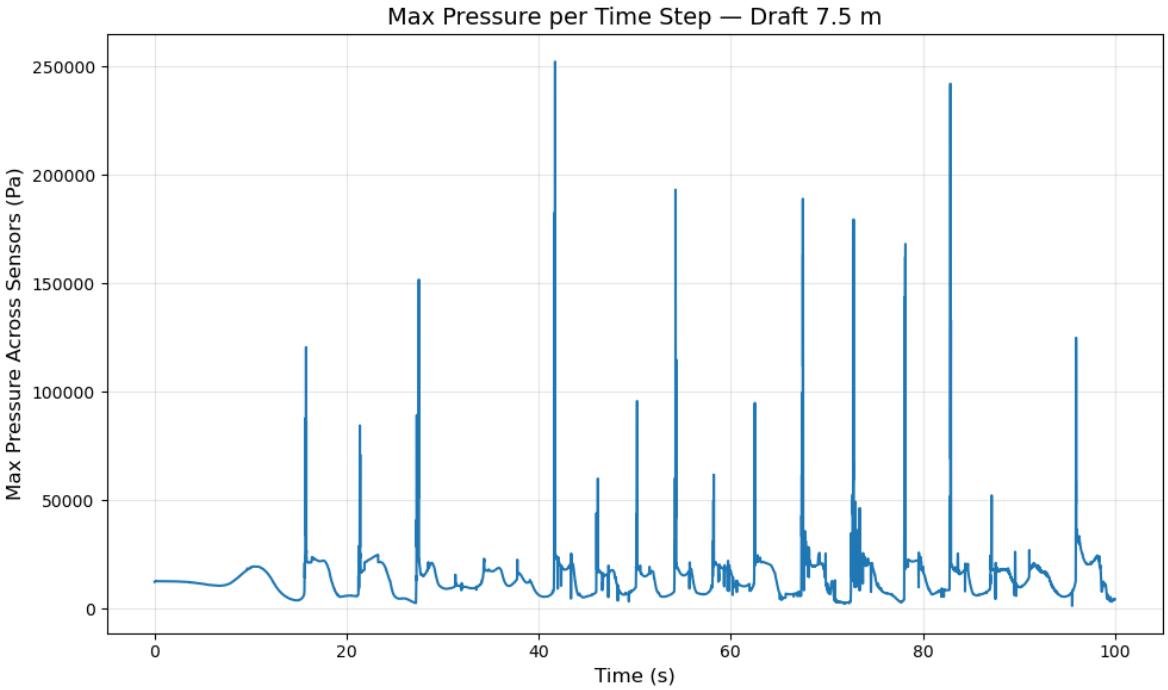

Figure C.4: The time domain results for a draft of 7.5 meters.

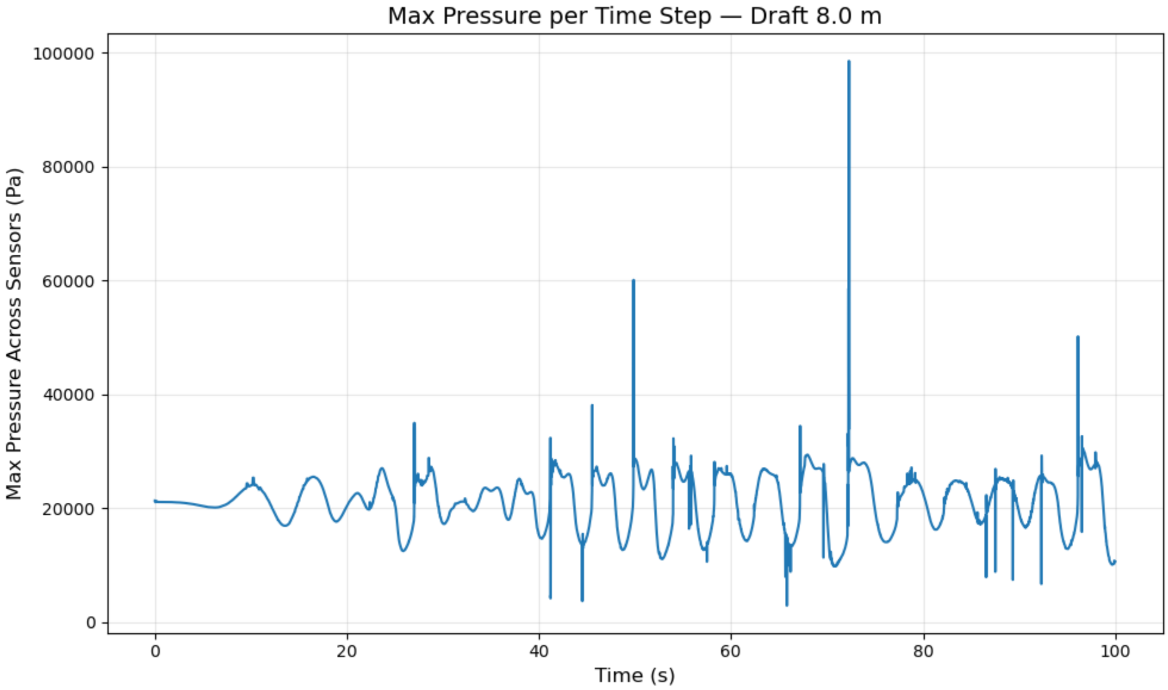

Figure C.5: The time domain results for a draft of 8 meters.

C.2. Results of the Simulations with H_s = 1.65 m and T_p = 5.1 s

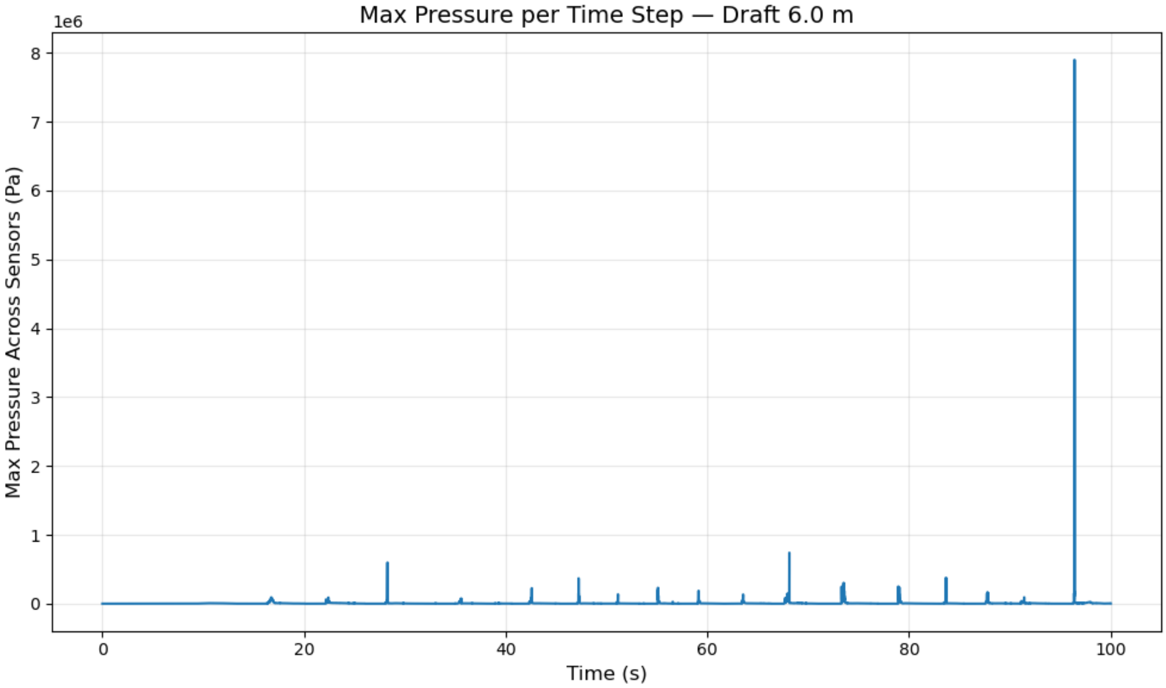

Figure C.6: The time domain results for a draft of 6 meters.

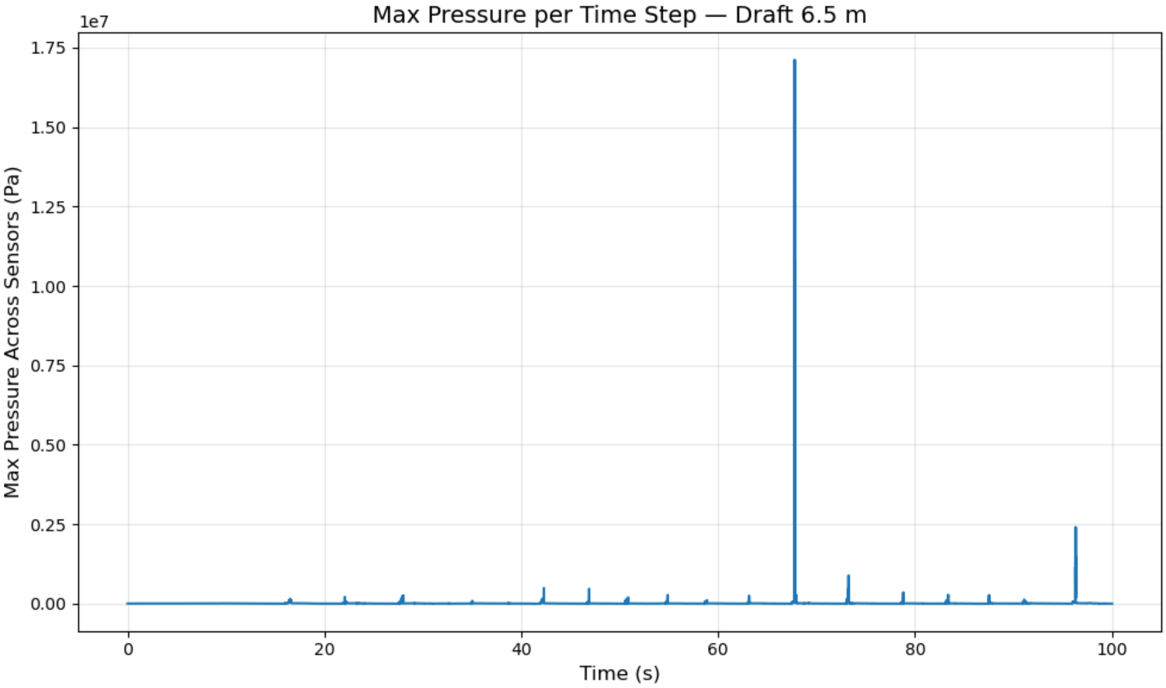

Figure C.7: The time domain results for a draft of 6.5 meters.

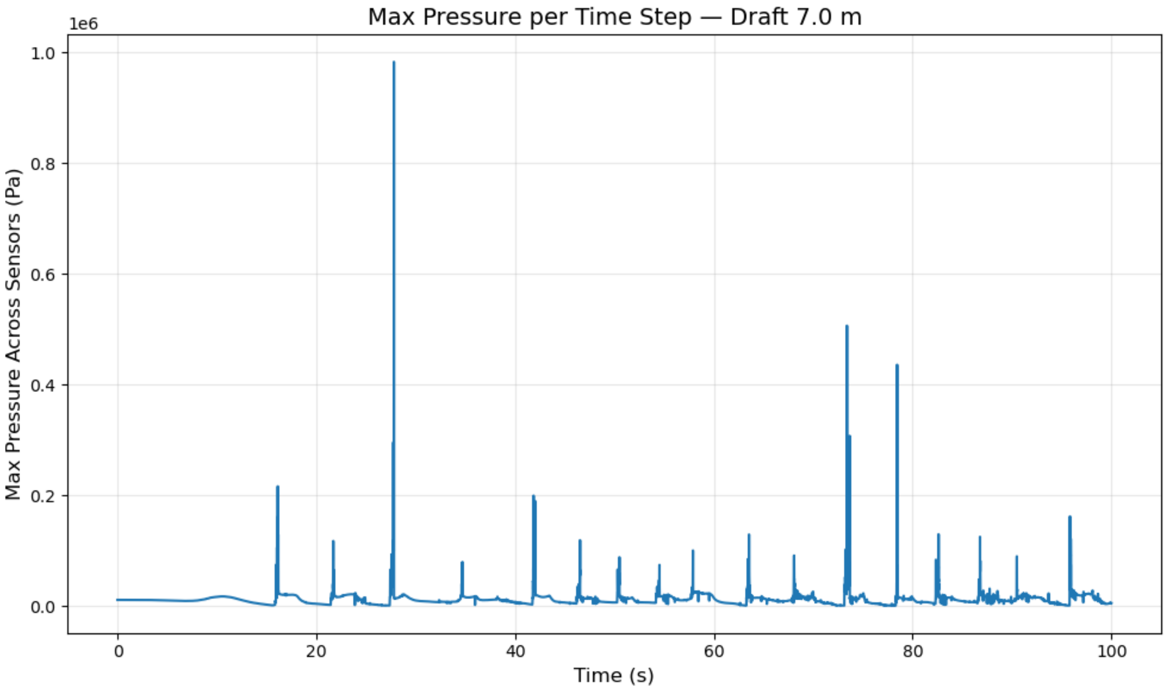

Figure C.8: The time domain results for a draft of 7 meters.

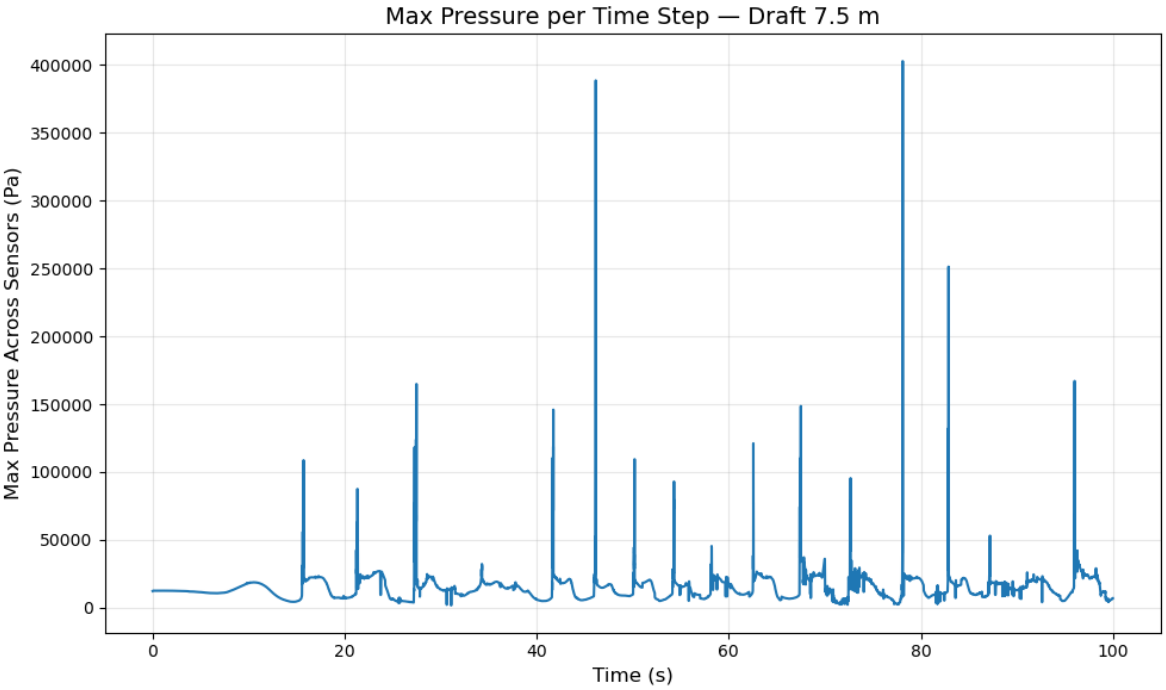

Figure C.9: The time domain results for a draft of 7.5 meters.

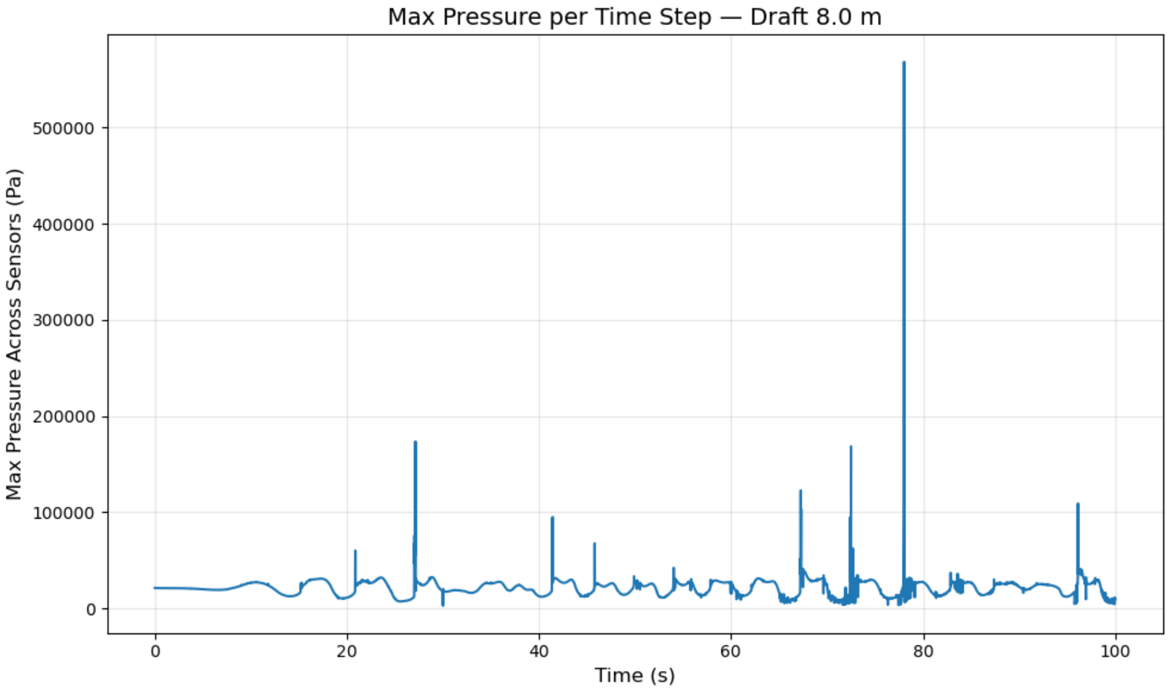

Figure C.10: The time domain results for a draft of 8 meters.

C.3. Results of Displacement and Acceleration at Different Locations

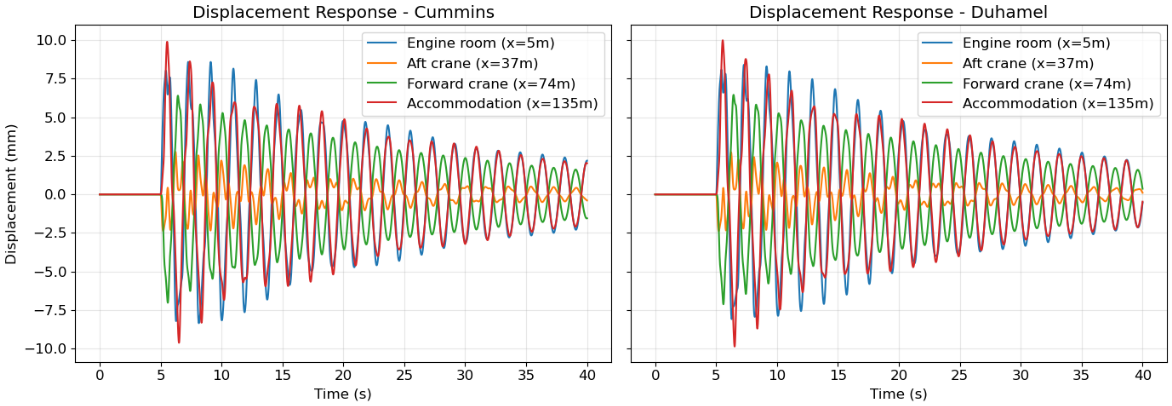

Figure C.11: The displacement response at different locations along the length of the vessel using Cummins on the left and Duhamel on the right.

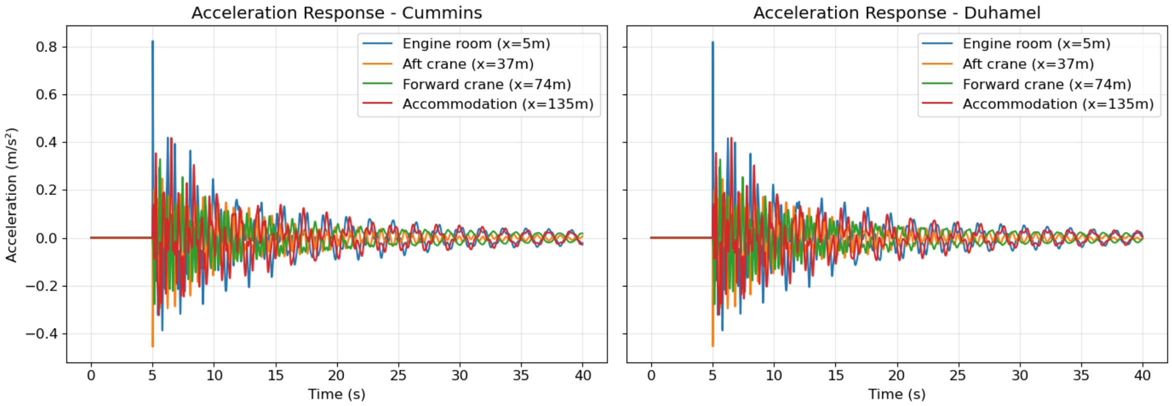

Figure C.12: The acceleration response at different location along the length of the vessel using Cummins on the left and Duhamel on the right.